ISSN 1028-8546

Azərbaycan Milli Elmlər Akademiyası
Fizika-Riyaziyyat və Texnika Elmləri Bölməsi
Fizika İnstitutu

3

Fizika

Cild
VII
2001

Bakı ✵ Elm

THE CAPTURE OF HOLES BY EDGE DISLOCATIONS WITH PARTICIPATION OF OPTICAL PHONONS IN SEMICONDUCTORS

Z.A. VELIEV, N.A. KARDASHBAYOVA
Nakhichevan State University
Azerbaijan Republic, Nakhichevan, University campus

The process of the capture of holes by edge charged dislocations accompanied with radiation of optical phonons is considered. It is shown that in the considered case the effective cross section of the capture sharplier depends on temperature compared with the coressponding processes accompanied with radiation of acoustical phonons.

It is well-known that in the temperature below indoors the main channel of loosing energy in capture of holes in n-type semiconductors with charged edge dislocations is the interaction with acoustic phonons [1] Indeed, interaction of holes with optical phonons has an exponential small probability in this case $exp(-(\hbar\omega_0-E_D)/kT)$, where E_D is the bound state energy of hole dislocations, $\hbar\omega_0$ is the energy of optical phonons if $\hbar\omega_0-E_D>>kT$. However, in capture process the levels with the energy $E_D\sim\hbar\omega_0$ can be arisen. Then in this case $\hbar\omega_0-E_D<<kT$ and the probability of transition of thermal electrons will not be exponentially small, though $\hbar\omega_0>>kT$

We shall investigate a capture process of holes by edge charged dislocations corresponding to the last situation.

For simplicity, let us suppose that the Read radius of separate dislocation is $R<<N_D^{-1/2}$ (N_D is the density of charged dislocations), i.e. the cylindrical regions arising around the edge charged dislocations do not intersect. The flux per unit of an isolated centre is determined by the expression [2]

$$j=\int d^3\vec{r}\,d\varepsilon d\varepsilon' F(\varepsilon,r)\rho(\varepsilon)w(\varepsilon,\varepsilon')P(U). \quad (1)$$

Here ε and ε' are the kinetic energies of holes before and after emission of optical phonons, $F(\varepsilon,r)$ is the distribution function of the holes with the kinetic energy ε at the distance r from the axis of dislocation

$$\rho(\varepsilon) = \frac{8\sqrt{2\pi}\,m^{\frac{3}{2}}}{(2\pi\hbar)^3}\sqrt{\varepsilon} \quad (2)$$

ρ is the density of the states, m is the effective mass of the holes, $w(\varepsilon,\varepsilon')$ is the probability of the transition of the holes per unit of time with spontaneous emission of phonons, $P(U)$ is the probability of the stick of the holes in the state with the energy U. In the case of edge charged dislocation

$$U = \frac{e^2 f}{4\pi\varepsilon\varepsilon_0 a}\ln\frac{R}{r} - \varepsilon' \quad (3)$$

where ε_0 is the electric constant, ε is the dielectric constant of the semiconductor, a is the distance between the atoms along the axis of the dislocations, f is the coefficient of filling of charged dislocation by electrons.

The life time and the cross section of capture of holes in the field of the charged dislocation are determined by the expressions:

$$\tau^{-1}=N_D j/P$$
$$\sigma=j/P<U>=1/N_D<U>\tau \ , \quad (4)$$

where P is the concentration of holes, $<U>$ is the average thermal speed of holes.

Let us consider the situation, when in the valence zone the holes are distributed equilibriously and the interaction is going on with deformative optical phonons.

The probability of such interaction is determined by the formula [1]

$$W(\varepsilon,\varepsilon') = \frac{(2m)^{\frac{3}{2}}E_{op}^2}{4\pi\rho_0\omega_0\hbar^2}\left[N(\omega_0)\sqrt{\varepsilon+\hbar\omega_0}+(N(\omega_0)+1)\sqrt{\varepsilon-\hbar\omega_0}\right]. \quad (5)$$

Here ρ_0 is the density of the crystal, $N(\omega_0)$ is the function of the distribution of optical phonons (in the considered case it is the Planck function), E_{op} is the constant of the optical potential of deformation. Putting (2)-(5) in (1) we obtain the expression for the cross section of the capture

$$\sigma_{op}=\frac{4mE_{op}^2r_D^2}{3\sqrt{\pi}\,\hbar^4\rho_0}A\alpha^2\frac{(kT)^2}{mS_0^2\hbar\omega_0}exp(-1/\alpha), \quad (6)$$

after a long but not difficult calculations.Here $r_D=(\varepsilon\varepsilon_0kT/n_d)^{1/2}$ is the Debye radius of screening, $\alpha=e^2f/8a\pi\varepsilon\varepsilon_0kT$, n_d is the density of donors in the volume, A is the numerical factor of the order of unit. Let us compare the formula (6) with the corresponding formula obtained in [3] for same conditions.

In this case

$$\sigma_{op}/\sigma_{ac} \sim (kT)^2/mS_0^2\hbar\omega_0 . \quad (7)$$

According to (7) σ_{op} is more sensitive to the change of temperature than σ_{ac}. In the end, let us estimate the characteristic temperature T_{char} when $\sigma_{op}/\sigma_{ac}\sim1$ For the value of

the parameters of the n – Ge crystal: $W=(E_{op}/E_{ac})^2 \sim 0,4$ (E_{ac} is the constant of the deformative potential), $mS^2 \sim 0{,}4K$ $\hbar\omega_0 \sim 430$ K and the characteristic temperature is $T_{char} \sim 50$ K. Thus at the temperatures $T>>T_{char}$ the emission of optical phonons plays the leading role. However at $T<T_{char}$ the emission of acoustic phonons plays the leading role.

[1] *B.K. Ridley*. Quantum processes in semiconductors, M: Mir, 1986.

[2] *V.N. Abakumov, V.I. Perel, I.N. Yassievich*. FTP, 1978, v. 12, №1, p. 3-32.

[3] *Z.A. Veliev*. FTP, 1983, v. 17, №7, p. 1351-1353.

Z.Ə. Vəliyev, N.A. Qardaşbəyova

OPTİK FONONLARIN İŞTİRAKI İLƏ YARIMKEÇİRİCİLƏRDƏ DEŞİKLƏRİN KƏNAR YÜKLÜ DİSLOKASİYALAR TƏRƏFİNDƏN ZƏBT OLUNMASI

İşdə optik fononların şüalandırılması ilə müşahidə olunan deşiklərin kənar yüklü dislokasiyalarla zəbt olunması prosesinə baxılmışdır. Göstərilmişdir ki, zəbt olunmanın effektiv kəsiyi baxılan halda, akustik fononların şüalanması ilə gedən uyğun proseslə müqayisədə temperaturdan daha kəskin asılı olur.

З.А. Велиев, Н.А. Гардашбекова

ЗАХВАТ ДЫРОК КРАЕВЫМИ ДИСЛОКАЦИЯМИ В ПОЛУПРОВОДНИКАХ С УЧАСТИЕМ ОПТИЧЕСКИХ ФОНОНОВ

В работе рассмотрен процесс захвата дырок краевыми заряженными дислокациями с излучением оптических фононов. Показано, что сечение захвата от температуры зависит сильнее, чем в процессе с излучением акустических фононов.

Received: 20.10.00

EFFECTIVE PLANAR METHOD OF DEFECTS GETTERING

F.D. KASIMOV
Azerbaijan National Aerospace Agency
159 Azadlig ave., Baku 370106

E.S. MAMEDOV
Azerbaijan Technical University
H.Javid ave., Baku 370073

It was shown that treatment of polycrystalline silicon films of small grain size in a atmosphere of oxygen leads to a decrease in their resistance owing to recrystallization of the grains, whereas during the annealing of films of large grain size the oxidation of intergrain boundaries is the dominant process resulting in an increase in the resistance.

The planar arrangement of gettering centers at close distance to active elements make process of gettering independent of duration and temperature technological processes and therefore increase their effectiveness without additional technological operation of the insertion of the gettering centers.

1. Introduction

Polycrystalline silicon (poly-Si) films are frequently used in semiconductor devices and integrated circuit (IC) elements. In particular, p-n-junctions prepared by the local deposition of poly-Si films of one conductivity type onto monocrystalline silicon (mono-Si) substrates of the opposite conductivity type have been described in [1, 2], as well as resistors for monolithic ICs [3] based on deposited poly-Si films.

The characteristics of poly-Si and mono-Si films formed simultaneously during a single process of epitaxial growth on locally oxidized silicon substrates have been reported in [4]. Similar films may be used as discrete elements of ICs, their properties being determined by the requirements of the mono-Si films which depend on the class of the circuits in which the film is used.

The constant temperature of the industrial chloride process of epitaxy as well as the homogeneous surface of the amorphous SiO_2 films which seem to be a template for the growth of the local poly-Si films do not make it possible to control the parameters of the poly-Si films to be grown. It is well known that the basic parameters which determine the electrical properties of poly-Si films are mean grain size (determined by the temperature), the film thickness and the dopant concentration which are constant for a given class of circuit. Hence the films were grown on predeposited thin films of silicon which act as nucleation layers.

The main aim of this study was to investigate the structure and electrical properties of poly-Si films grown on the nucleation layers at various deposition temperatures.

2. Sample preparation

The samples were fabricated on silicon substrate of p-type conductivity, orientation (111) and resistivity 10 Ω·cm. The substrates were oxidized to obtain a thermal oxide layer of 0.5 μm thick onto which a thin undoped nucleation layer of about 100Å thick was deposited by the low temperature process of monosilane pyrolysis (800-860°C). Using photolithography and etching we obtained the local nucleation areas onto them. Then a vertical reactor heated by high frequency power was used for the epitaxial growth of the n-type film by a high temperature chloride process (1220°C) carried out according to the technology described in [5]. The films were doped by phosphorus with the addition of phosphine to the float at a partial pressure of 6.8 Torr. The thickness of the films was 5 μm, and the dopant concentration was $10^{16}cm^{-3}$, as determined by the four-probe method on the monocrystalline substrate.

3. Experimental data

When the films were studied by scanning electron microscopy it was found that an increase in the deposition temperature of the nucleation layer from 800° to 860°C results in an increase in the grain size by a factor of 10 (fig. 1). The poly-Si films grown on a nucleation layer deposited at 800°C were fine grained, the size of the spherical grains being not more than 0.5 μm. However, the films contained rather large edge blocks 2-3 μm in size (fig. 1,a). The films grown on a nucleation layer deposited at 830°C had the most uniform structure with a grain size of 1-2 μm (fig. 1,b), while for a high deposition temperature of the nucleation layer (860°C) the poly-Si films had a grain size of 4-5 μm and their structure was non-uniform showing occasional formations and monoblocks up to 10 μm (fig. 1,c).

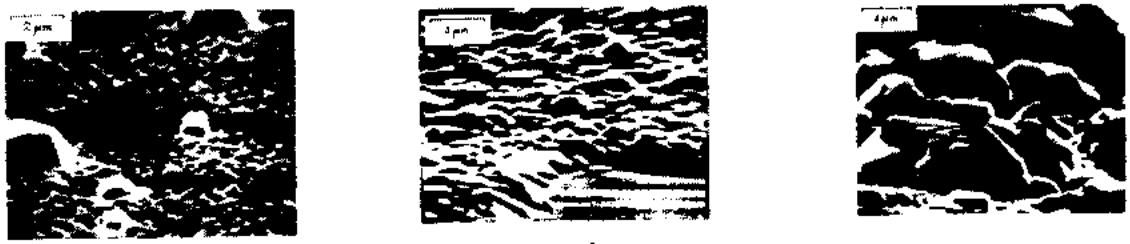

a b c

Fig. 1. The structure of poly-Si films grown on nucleation layers deposited at various temperatures: (a) 800°C; (b) 830°C; (c) 860°C

The results show that in spite of the higher film growth temperature in the chloride process the size of the grains is determined by the deposition temperature of the nucleation layer.

The electrical resistance of poly-Si films of size 200μm×20μm grown on nucleation layers deposited at different temperatures were determined from measurements of the voltage divided by the current. There was a considerable spread in the resistances of the films. It should be noted that at low applied voltages (up to 1 V) an increase in the temperature deposition of the nucleation layer results in a decrease in the resistance by a factor 10 (fig. 2,a). When the applied voltage exceeded 1V, the resistance of the fine-grained films decreased markedly, becoming lower than that of the film grown on the nucleation layer deposited at 830°C. The films grown on the nucleation layers whose deposition temperatures were 830° and 860°C showed slight changes in resistance when the voltage was increased. The films with a coarse-grained structure had the lowest resistance over the entire range of voltage.

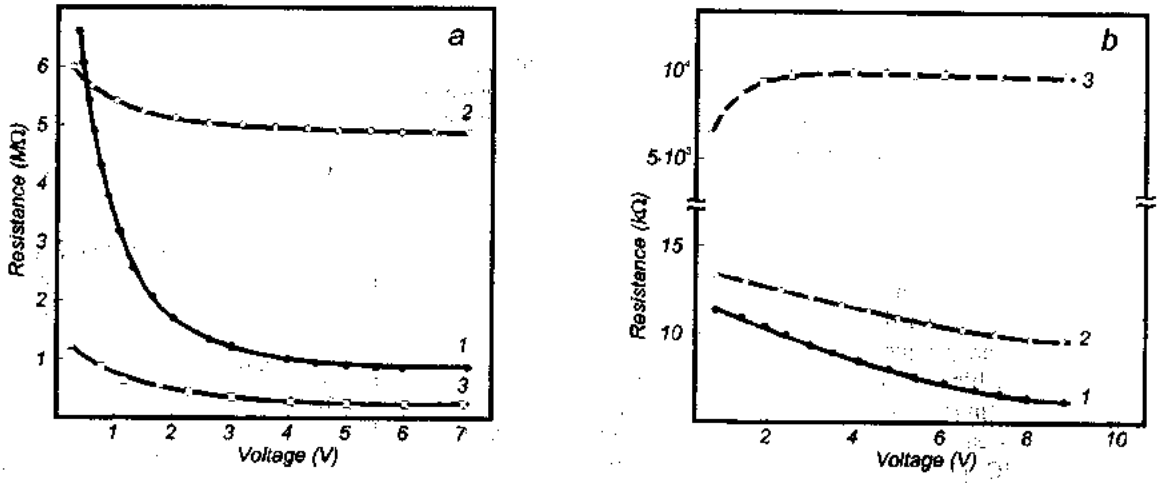

Fig. 2. Voltage-resistance characteristics of poly-Si films of different structures (a) before the heat treatment and (b) after the heat treatment: curves 1, 800° C; curves 2, 830° C; curves 3, 860° C

Since the simultaneous growth of the poly-Si and mono-Si films on a single substrate offers good possibilities for their use as IC elements, it seemed to be appropriate to study the effect of heat treatment, which conforms to the technology of the manufacture of the active elements, on the electrical characteristics of the poly-Si films. For this purpose the samples were subjected to consecutive heat treatments at a temperature of 1000°C (oxidation; 45 min) in wet oxygen, at a temperature of 1150°C (base formation; 1.5 h) in a mixture of oxygen and nitrogen and at a temperature of 1050°C (emitter formation; 50 min) in oxygen, the total time being over 3 h.

After heat treatment the size of the grains in the fine-grained samples had increased with the result that the electrical resistance of the films had decreased (fig. 2,b). The resistance of the coarse-grained films (860°C) had increased to 50-100 MΩ.

For the coarse-grained film structure consisting of two monocrystalline areas separated by a poly-Si film with an area of 10^{-5}cm^2 the breakdown voltages were 50-60 V after a complete heat treatment, the leakage current density being 10^{-2}A·mm^{-2}. This demonstrates the possibility of utilizing these films as an insulating material for IC elements.

4. Application

Increasing reliability VLSI in certain extent depends of substrate enhancement, reduction of damage and p-n-junction leakage. It is known, that bipolar transistors with narrow base are very sensitive to existence of precipitates of metallic impurity, which display itself as generation-recombination centers and circuit regions of emitter with collector [6].

There are methods of gettering which are based on previously introducing of damage into back side of substrate. This damage captures and holds impurity in during the high temperature technological operation. For this purpose additional operation is used, for example, mechanical thermal or laser treatment [7].

The problem is that gettering centers are located on the back side of substrate and during implementation of technological operations metallic impurities have to be diffused across substrate thickness, which is approximately 450 μm. However, recently there is a tendency towards reduction of temperature and duration of processing. At the same time the diffusivity of impurities atoms sharply decreases and the duration of the operation can be not sufficient for the atoms to reach the gettering centers on the rewards side substrate.

A technology of simultaneous growth of mono- and polycrystalline silicon films in the single epitaxial processing makes it possible to form local regions of the poly-Si films required configuration, which act themselves as gettering centers.

The density surface states N_{SS} are the most sensitive characteristic to the defects of devices. Therefore we fabricated the test MOS-structure, the C-V-characteristics of which was investigated. The capacitance-voltage characteristics were measured with an L2-7 impedance bridge at room temperature over frequency range 0.465-10 MHz, using an ac signal of low voltage (25 mV).

Calculation of interface Si-SiO_2 charge was done by formula

$$\left(Q_{ox} + Q_{ss}\right)^{FB} = \Delta U_g^{FB} C_o \,, \qquad (1)$$

where C_o is undergate oxide capacity; ΔU_g^{FB} is a shift of experimental curve about theoretical in the point of flat band capacity C_S^{FB}.

$$C_S^{Fb} = g\left(\varepsilon_S N_D / kT\right)^{1/2}. \quad (2)$$

For determination of surface states charge Q_{SS} required to find capacity of semiconductor in the point of inversion

$$C_S^{inv} = \left[q\varepsilon_S N_D / 2\left(U_g^{inv} - \varphi_S\right)\right]^{1/2}. \quad (3)$$

Then by the help of the formula (1) the calculate full charge interface $Si\text{-}SiO_2$ in the point of inversion and substract from full charge in the point of flat band. The calculation showed, that N_{SS} on the samples, around polysilicon films, two order less, than in the samples, around p-n-junction isolated.

The planar arrangements of gettering centers at close distance to active elements IC makes the process of gettering independent from duration and temperature technological processes and therefore increase their effectiveness without additional operation of the insertion of the gettering centers.

[1] *Zvy and B.-L.Adiz.* IEEE Trans. Electron Devices, 1977, №24, p.1025.

[2] *L.D.Lopatina, V.L.Sukhanov and V.V.Tuchkevich.* Pisma Zh. Eksp. Teor. Fiz., 1979, №5, p.11.

[3] *F.D.King and G.Shewchun.* Solid-State Electron., 1973, №16, p.701.

[4] *M.A.Garibov, F.D.Kasimov and V.M.Mamikonova.* Izv. Akad. Nauk AzSSR., Ser. Fiz-Tekh. Mat. Nauk, 1979, №4, p.91.

[5] *F.D. Kasimov and B.Kh. Mamedov.* Electron. Tekh., Ser. Materiali., 1984, №5, p.23.

[6] *C.W. Pearce, L.E. Katz and T.E. Seidel.* Considerations regarding gettering in integrated circuits., Electrochem. Soc., Pennington New Jersey, 1981.

[7] *B. Hartiti and J. Muller.* IEEE Trans. Electron. Devices, 1992, №39, p.27.

F.C. Qasımov, E.S. Məmmədov

DEFEKTLƏRİN PLANAR HETTERİRLƏNMƏSİNİN EFFEKTİV METODU

Göstərilmişdir ki, kiçik dənəcikli polikristallik silisium təbəqələrinin (PST) oksigen mühitində termik işlənməsi dənəciklərin rekristallizasiya sayəsində onların elektrik müqavimətinin azalmasına gətirib çıxarır, baxmayaraq ki, iri dənəcikli təbəqələrdə dənəciklər sərhəddinin oksidləşməsi prosesi üstünlük təşkil edir, bu da ki muqaviməti artırır.

PST-də hetterirləmə mərkəzlərinin planar yerləşməsi aktiv elementlərin yaxın məsafələrində hetterirləmə proseslərinin zamandan və texnoloji proseslərin temperaturundan qeyri asılı edir və əlavə əməliyyatlar aparmadan onun effektivliyini artirir.

Ф.Д.Касимов, Э.С.Мамедов

ЭФФЕКТИВНЫЙ МЕТОД ПЛАНАРНОГО ГЕТТЕРИРОВАНИЯ ДЕФЕКТОВ

Показано, что термообработка мелкозернистых пленок поликристаллического кремния (ППК) в атмосфере кислорода ведет к уменьшению их электрического сопротивления благоларя рекристаллизации зерен, в то время как в крупнозернистых пленках доминирующим процессом является прокисление границ зерен, что приводит к увеличению сопротивления.

Планарное расположение геттерирующих центров, каковыми являются ППК, на близких расстояниях от активных элементов делает процесс геттерирования независимым от времени и температуры технологических процессов и увеличивает его эффективность без проведения дополнительных операций.

Received: 04.07.01

MICROPLASMA BREAKDOWN OF p-n JUNCTIONS

S.G. RZAEV
Institute of Physics, Azerbaijan National Academy of Sciences
H. Javid av., 33, Baku, 370143

It is shown that the charged point defect clusters (PDC) by perturbing the electrical field E of space charge layer of the p-n junctions create large-scale traps, which decrease a voltage of breakdown. It is found that at the magnitude of E less than its critical value E_c PDC behave themselves as the generation centers and increase the leakage current of the p-n junctions, but at the magnitude of the field $E \geq E_c$ they behave themselves as the recombination centers on which microplasma arises and the breakdown of the p-n junction starts. The formula of dependence of E_c on the PDC parameters is obtained.

INTRODUCTION

It is known that in processes of fabrication of the semiconductor devices various defects, which change their electrophysical parameters appear. An influence of defects on the electron processes in active elements of integrated circuits becomes especially actual in connection with miniaturization of production of the semiconductor microelectronics.

Thus, for instance, as a result of thermotreatment of devices with space charge layer (SCL) unequilibrium own point defects which can be locally clustered under various factors appear and they may have an essential influence on the electron processes in it [1-9]. It is clear that the degree of this point defect cluster (PDC) influence on electron processes will depend on both of their size and the charge state. However, in spite of revealing of this dependence the investigation devoted to this problem is absent in a known literature.

The present paper is devoted to an investigation of the PDC influence on microplasma breakdown of p-n junction.

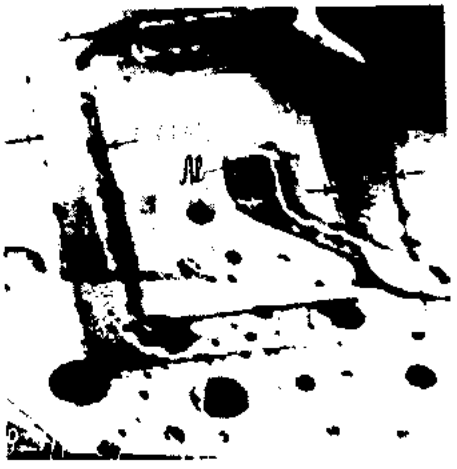

Fig.1 Microphotography of n^+-p junction, obtained in the regime of second electrons of SEM.×1400. The cluster of impurity in space charge layer on the interface of collector-base and collector-matrix are shown by pointers. Al is the aluminum contact.

The investigation was carried out on n^+-p junction of integrated circuits in which 2.1-μm - thick B-doped (111) Si epitaxial film with p~5×10^{16}cm^{-3}served as a base layer, and the collector comprised a buried n^+ (~10^{20}cm^{-3}) layer, prepared by diffusion of As into the p-type substrate, and an adjacent n^+ vertical contact layer reaching the surface.

By the methods of scanning electron microscope in the interface of base-collector and collector-matrix of space charge layer of p-n junction of the integrated circuits with increased leakage currents globe-shaped clusters which were responsible for leakage currents were discovered (fig.1). Localization of these clusters at negative poles of SCL testifies that they are positively charged and clear-cut boundaries of PDC show that defects in them are distributed by the Poisson law . The charge Q on PDC is considered as one which uniformly distributed on the surface of a good conducting sphere of a radius R.

It was shown in [4,5] that impurity clusters in SCL of p-n junction play the role of generation centers at the magnitude of electric field less than $1{,}91\cdot10^5$ V/cm through which the generation of unequilibrium carriers due to increased leakage current take place.

At field E_c of the magnitude greater than $1{,}91\cdot10^5$ V/cm as a result of collision ionization an avalanche breakdown of p-n junction take place and on SCL microplasmas appear. They appear also as a result of recombination of "hot" carriers on them. So under the strong electric field condition and growing of concentration of the carriers in PDC they transform from generation centers into recombination ones.

DISCUSSION OF THE RESULTS

As fig.1 shows the PDC has a spherical form. Therefore it can be viewed as a charged sphere put into uniform electric field of the SCL of the p-n junction. Under the action of electric field of the SCL free carriers leave the region of space charge of the p-n junction. At the strong electric field of SCL of p-n junction when the screening of PDC charge by the free carriers are impossible, the characteristic picture of a distribution of force line arises, as it shown in fig.2. As a result of a such distribution of force lines, the potential barrier appears which is a large-scale trap for carriers. Generation and recombination properties of PDC are determined by the height of the potential barrier and a capture cross section, which vary under the action of electric field. The potential of the charged globe in the uniform electric field is described by the following expression [6]:

$$\varphi(r,\theta) = -rE_c\cos\theta + E_c\frac{R^3}{r^2}\cos\theta + \frac{Q}{4\pi\varepsilon\varepsilon_c\cdot r} \qquad (1)$$

where first term is the contribution of the field E_0, the second is the contribution of polarization of the neutral part, and the third one is the contribution of the charge Q. The angle θ is counted on the direction of the field E_0.

As a consequence of screening of the field, directly after a trap there is a saddle point of the potential relief in $r=R_c$. It is necessary to note that between the saddle point and charged surface of the globe there is a potential barrier which regulates the flow of carriers from the trap.

The height of this barrier is

$$\delta\varphi = \varphi(R_c) - \varphi(R) \qquad (2)$$

where $\varphi(R_c)$ and $\varphi(R)$ are the potential magnitudes at the points R_c and R, respectively.

Putting in Eq. (2) instead of $\varphi(R_c)$ and $\varphi(R)$ their values determined by the formula (1) and making some transformations, we obtain:

$$\delta\varphi = E_0 R\left(\frac{R^2}{R_c^2} - 1\right) - \frac{R^2 N_t e}{3\varepsilon\varepsilon_0}\left(\frac{R}{R_c} - 1\right), \qquad (3)$$

where N_t is the density of ionized impurity in PDC, e is an electron charge.

Keeping in mind that for every PDC its characteristic parameters such as R_1, R_2 and N_t are constant in the stationary condition, we can rewrite the expression (3) as follows:

$$\delta\varphi = C - \alpha E_0 \qquad (3a)$$

where C and α are the positive magnitudes, which are determined by the parameters of PDC indicated above, so that they are constant under the stationary conditions.

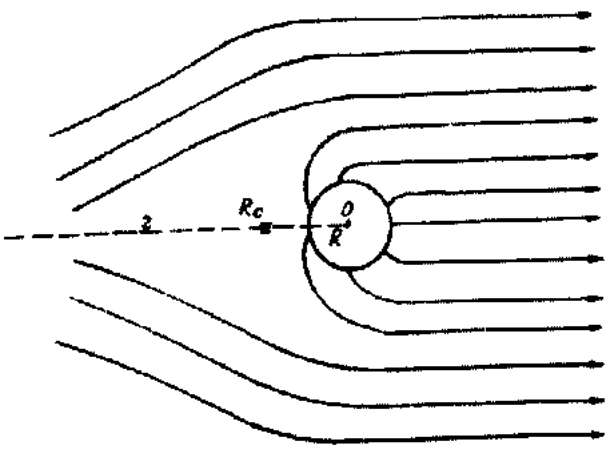

Fig.2. The perturbation of uniform electrical field of charged point defect cluster (PDC). R is the radius of (PDC). R_c is the coordinate of a saddle point, r is the current coordinate.

As it is seen from the Eq. (3a) at the small value of the field, when $\alpha E_0<C$, the height of voltage barrier will be diminished by the increasing of the field that will lead to the increase of the probability of emission of the carries from trap i.e. to the generation of free carries. At the critical value of the field E_0, when $\alpha E_0<C$, the height of potential barrier disappears ($\delta\varphi=0$) that corresponds to the equality $R=R_c$ i.e. the saddle point touches surface of PDC. This condition is implemented when the intensity of the electric field, created by the surface charges of PDC is equal to E_0. Under these conditions minority carries accelerated by the field will be reaching the surface of PDC that will lead to the recombination of "hot" carriers and appearing of microplasmas on the PDC and the local breakdown of p-n junction are takes place. At a certain value of E_0, when the energy of "hot" carriers is enough for collision ionization, there have been appeared a microplasma on the PDC surface and the local breakdown have taken place. The last one is in agreement with experimental results of [4, 5, 7].

Thus the change of $\delta\varphi$ leads to the change of carriers concentration in the trap and the capture cross-section σ. The dependence $\sigma(E_0)$ can be found from the equation for the principle of detailed balance of the rate of capture and emission of carriers from the trap:

$$G\sigma = \frac{S\Delta n}{\tau} exp\left(-\frac{e\delta\varphi}{kT}\right) \qquad (4)$$

where S is the square of that part of sphere from which emission of carriers generated by "hot" carriers, G is a rate of generation of unequilibrium carriers, Δn is concentration of unequilibrium carriers, τ is a life time of carriers.

We obtain from (3a) and (4):

$$\sigma = \frac{S\Delta n}{G\tau} exp\left[\frac{(\alpha E_0 - C)}{kT} e\right] \qquad (5)$$

According to Eq. 5) when E_0 reaches the value E_c at which the condition is fulfilled

$$\alpha E_c = C \qquad (6)$$

the height of voltage barrier $\delta\alpha=0$ and the capture cross-section does not depend on the field. It dictates, that radiation intensity of microplasma is independent of field.

Actually, it has been experimentally determined in [7,8], that the number of microplasmas increased with the increasing of field, but intensity of radiation of some microplasma have not changed till the ceasing of forming of new microplasma.

Thus, the fulfillment of the $\alpha E_0=C$ condition, the recombination of "hot" carriers on the surface of PDC and the independence of the capture cross-section on field correspond to the initial condition of arising of the microlpasma and avalanche breakdown of p-n junction.

The magnitudes of critical field E_c on which microplasma arise, as it follows from Eq. (6), depend on the PDC parameter. When fulfillment of condition Eq. (6) from Eq. (3) we obtain

$$E_c = \frac{eN_t R}{6\varepsilon\varepsilon_0} \qquad (7)$$

i.e. E_c is proportional to the radius of PDC and the density of ionized impurity in PDC.

According to Eq. (7), with the increase of the number of microplasmas with the increase of the field the electric field first reaches critical value on PDC of small size, then on large ones. The last one is agreement with experimental results of [7,8], that testifies the certainty of Eq. (7).

The certainty of obtained dependence is proved by the fact that it accurately coincides with the dependence for intensity of electrical field on surface of charged globe, which, according to the condition of the problem, is related to PDC. We must note that the obtained dependence can be used in any material, where the screening of charge PDC by free carriers is absent.

Given model completely describes the experimental results in [4,5,7,8].

The sizes of PDC which are within $(0,3\pm0,5)\cdot10^{-4}$cm, in SCL of investigated p-n junction are determined by the means of SEM (fig.1), and a magnitude of critical field at which microplasmas arise, that corresponds to the condition (6) and changes within $(1,8\pm2)\cdot10^{5}$V/cm, depending on the size of the PDC.

By using of experimental data and proceeding from the condition (6) such parameters of PDC are determined: the capture cross section ($3\cdot10^{-8}$cm^2), its charge ($2,2\cdot10^{-14}$C) density of ionized impurity ($1,7\cdot10^{16}$cm^{-3}), lifetime of unequilibrium carriers in the region of microplasma ($<10^{-15}$s).

CONCLUSIONS

It is shown that charged point defects clusters create large-scale traps, by perturbing electric field of space charge layer of p-n junction.

The dependence of the height of the potential barrier and the capture cross-section of traps are determined both from parameters of PDC and the magnitude of external electric field. We found that there is a critical value of an external electric field E_c on which microplasma on PDC arises and avalanche breakdown of p-n junction takes place.

It is found that at the magnitude of the field less than E_c PDC behave themselves as generation centers and increase the leakage current of p-n junction, but at the magnitude of field $E \geq E_c$ they behave themselves as recombination centers on which microplasmas arise and starts to breakdown of p-n junction.

The necessary conditions and mechanism of microplasma formation on PDC are presented. The dependence of E_c on the parameters of PDC is obtained. It is shown that capture cross-section of traps, depends exponentially on the electric field due to impurity cluster.

[1] *Y.V. Vizhigin, N.A. Sobolev, B.N. Geresserov, E. Shek.* J. Phys. and techn. of semicond., 1992, v.26, №11, p.1938-1944.

[2] *V.K. Eremin, N.B. Stroken, O.P. Chikalova-Luzina.* Phys. and thechn. of Semicond., 1985, v.19, №1, p.70-76.

[3] *N.M. Karelin, S.J. Kusakin, Yu.M. Litvinov, E.J. Paw, G.V. Spivak.* Microelectronica, 1980, v.9, №1, p.48-53.

[4] *S.G. Rzayev, A.H. Abdullayev.* Microelectronica, 1984, v.13, №3, p.260-263.

[5] *S.G. Rzayev.* Electron. techn., ser. "Microelectronica», 1986, №3(119), p.21-25.

[6] *V.V. Batigin, J.N. Toptigin.* Sbornic zadach po electrodinamike. Moscow. 1970, 410.

[7] *S.G. Rzayev.* Izvestiya AN Azerb. SSR, FTMN, 1984, №4, p. 69-71.

[8] *A.G. Chinoveth and K.G. Mckay.* Phys. Rev., 1956, v.102, №2, p.369-376.

[9] *S.G. Rzayev.* Inorganic mat., 1998, №12, p.1415-1419.

S.Q. Rzayev

p-n KEÇİDLƏRİN MİKROPLAZMİK DEŞİLMƏSİ

Göstərilmişdir ki, yüklənmiş nöqtəvi defektlər topaları (HDT) p-n keçidlərin fəza yük qatının sahəsini E həyəcanlandıraraq böyük ölçülü tələlər yaradır. Onlar p-n keçidin deşilmə gərginliyini azaldır. Müəyyən edilmişdir ki, elektrik sahəsinin kritik qiymətinə E_c qədər onlar qenerasiya rolunu oynayır. $E \geq E_c$ olduqda onlar rekombinasiya mərkəzlərinə çevrilirlər və onların üzərində mikroplazma yaranır, bununla adi p-n keçidin deşilməsi başlayır. E_c-nin HDT parametrlərindən asılılığının düsturu alınmışdır.

С.Г. Рзаев

МИКРОПЛАЗМЕННЫЙ ПРОБОЙ p-n ПЕРЕХОДОВ

Показано, что заряженные скопления точечных дефектов (СТД), возмущая электрическое поле E слоя объемного заряда p-n переходов, создают крупно-масштабные ловушки, которые уменьшают напряжение пробоя. Установлено, что при значениях электрического поля меньше его критической величины E_c, СТД ведут себя как генерационные центры и увеличивают токи утечки p-n переходов, а при $E \geq E_c$ они ведут себя как центры рекомбинации, на которых зарождаются микроплазмы и начинается пробой p-n перехода. Получена формула зависимости E_c от параметров СТД.

Received: 29.06.01

THE DIELECTRIC PROPERTIES OF THE ZnS FILMS

M.M. PANAHOV
Baku State University
Z. Khalilov str.23, Baku, 370148

The dielectric properties of the ZnS films obtained by magnetron sputtering on the glass and the mica are considered. Beginning from the thickness of 150 Å. the films were solid. The dependence of dielectric constant on thickness shows the decrease of ε in the range of 0.1 mkm and less. The frequence dependence of $tg\delta$ increases, and versus the electrode resistance media it decreases. The moisture effect on the dielectric loss tangent is also shown.

1. INTRODUCTION

The dielectric properties of films are of great Interest both in studies of electroconductivity of such films and their application in different devices.

The description of dielectric properties in literature refers mainly to thick films intended for preparation of condenser in microelectronics. It is clear that for the condenser with a high capacity the films of low thickness and high dielectric constant are necessary. As the solid films of a very low thickness with permanent properties are very difficult to be prepared, rather thick films (more than 500 Å for oxide films) are usually used in condensers. Thus, the study of temperature and frequency dependences of dielectric constant and dielectric tangent of the ZnS films is the purpose of the present paper. The thin films of ZnS were obtained, by the magnetron sputtering method in argon medium [1].

The mica and glass were used as the substrates. The aluminum and golden electrodes were used as the contacts. The structure and morphology of films were controlled by electron diffraction camera.

2. RESULTS AND DISCUSSION

Theoretical calculations show [2] that the dielectric constant of films is independent of the thickness up to several atomic layers. This fact was confirmed experimentally [3] with organic films of cadmium stearate with perfect structure and thickness to 24 Å. The dielectric properties of the dielectrics films are estimated according to the results of a simultaneous measurement of capacity and dielectric tangent. The dielectric loss coefficient measured is composed of the dielectric losses of different mechanisms and the dielectric loss at series connection of electrode resistance with capacity.

The contribution of electrode resistance to electroconductivity depends on frequency and this fact should be taken into account. That is, in order to decrease the dielectric loss coefficient at high frequencies, the metallic electrodes of low resistivity should be used.

When deposited from the vapor phase, the atomic accumulation takes place during the growth. As a result, the thin films (200 Å) are usually porous and the dielectric constant values of such films decrease rapidly with decrease in thickness [4]. The dielectric constant (ε) of the ZnS films is shown in fig.1. When the film porosity effect on the dielectric constant is appreciable, the film thickness depends on the way and conditions of film deposition. In the case of ZnS, this thickness decreases with decrease of the substrate temperature. For the mica substrate it is lower than for the glass. A high inner mechanical tension usually existing in deposited films does not nearly affect their properties. In the case of cracking and shelling of these films under the effect of mechanical tension, their effective dielectric constant becomes lower.

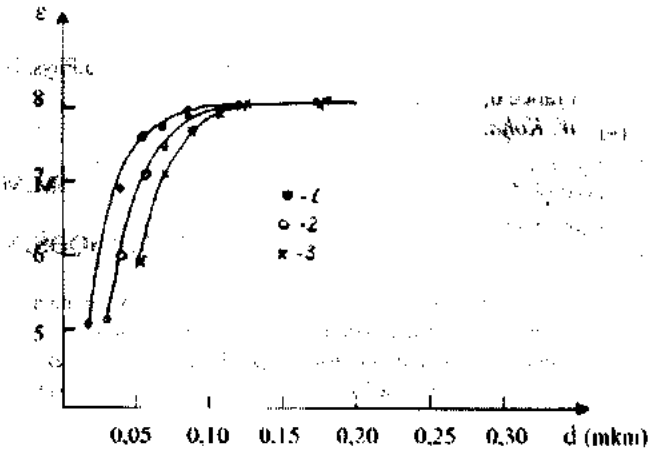

Fig.1 The dependence of dielectric constant on the ZnS film thickness: 1) Al-ZnS-Al on the mica at 25° C;
2) Al-ZnS-Al on the glass at 25° C;
3) Al-ZnS-Al on the glass at 300° C.

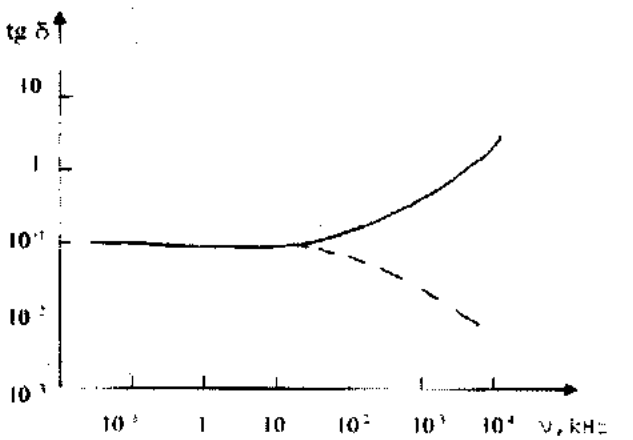

Fig.2 The frequency dependence of dielectric loss in the ZnS films: 1) The solid line – without account of the electrode resistance;
2) The dash line – with account of the electrode resistance.

The electric field applied to the thin film of the dielectric is usually of the order of 10^8 V/m that is close to the breakdown voltage value. If the polarization in the dielectric does not correspond to the change of the field, the dielectric losses, as is known, appear. Principally, the dielectric losses refer to the

bulk properties and should be independent of the thickness if the structural defects are not involved into any relaxation mechanism. If the film is not very thin, the thickness does not affect the dipole reorientation. The dielectric losses can be varied by stoichiometry, Therefore, their magnitudes strongly depend on the deposition conditions. As the temperature increases and depending on the material of electrodes that diffuse in the dielectric film, the intensive increase in losses is observed [5]. The frequency dependence of the loss coefficient measured with the ZnS condenser of 1000 pF in capacity is shown in fig.2. The increase of the losses at high frequencies is due to unaccounted electrode resistance.

The solid lines in fig.2 denote the data without account of electrode resistance, while the dash line denotes the data with account of electrode resistance. The dielectric loss in such films can be explained by excess concentration of vacancies.

The dependence of dielectric loss has the maximum at 200 and 450 K corresponding to the activation energies of 0,15 and 1,12 eV.

Subsequent to film deposition, their dielectric losses increase with the film aging. The loss coefficient and the capacity are higher, the lower the frequency. Hence, one can say that at frequencies below 100 Hz a certain relaxation mechanism takes place, while at frequencies about ~ 1 Hz the dependence of (ε) and $tg\delta$ has the form of the plateau which can be considered as the mechanism attributed to the joint action of the two mechanisms of losses, at least.

The absorbed moisture considerably increases the capacity and the dielectric loss even in the case of material insoluble in water. This increase of capacity and the dielectric losses is probably due to the effect of principal mechanisms of the change of ε and $tg\delta$.

[1] *A.A. Agasiev, M.Z. Mamedov and M.D. Muradov.* J.Phys. III France 6, 1996, p. 853-861.
[2] *W. Kohn.* Phys. Rev., 1958, 110, p. 857.
[3] *K.L. Chopra.* J.Appl. Phys. , 1965, 36, p. 655.
[4] *C. Zeldman, M. Hacskaylo.* Rev. Ici. Jnste. 1962, 33, 1459.
[5] *C. Zeldman.* Rev. Ici. Jnste., 1955, 26, 463.

M.M. Panahov

ZnS NAZİK TƏBƏQƏSİNİN DİELEKTRİK XASSƏLƏRİ

Məqalədə maqnetron tozlandırma üsulu ilə şüşə və slüda üzərində alınmış ZnS nazik təbəqəsinin dielektrik xassələrinə baxılmışdır. Qalınlığı 150 Å –dən böyük təbəqələr səlt təbəqələr idi. Təbəqələrin dielektrik nüfuzluğunun qalınlıqdan asılılığı göstərir ki, 0,1 mkm-dən kiçik qalınlıqlarda ε azalır. Dielektrik itkisi $tg\delta$ tezlik artdıqca artır, ancaq elektrodların müqavimətini nəzərə alsaq, azalır.

İşdə həmçinin su buxarlarının dielektrik itgisi $tg\delta$–ya təsiri göstərilmişdir.

М.М. Панахов

ДИЭЛЕКТРИЧЕСКИЕ СВОЙСТВА ПЛЕНОК ZnS

Рассмотрены диэлектрические свойства пленок ZnS, полученных магнетронным распылением на стекле и слюде. Пленки были сплошными, начиная с толщины 150 Å. Толщенная зависимость диэлектрической проницаемости показывает уменьшение. ε начиная с 0,1 мкм и меньше. Зависимость $tg\delta$ частоты возрастает: а с учётом сопротивления электродов, уменьшается. Показано также влияние влаги на $tg\delta$ диэлектрических потерь.

Received: 10.09.01

ACOUSTO-OPTIC METHODS AND DEVICES OF SIGNALS HANDLING IN TEMPORAL AREA

A.R. HASANOV

Institute of Physics, Azerbaijan National Academy of Sciences
H. Javid av., 33, Baku, 370143

The results of the authors investigations directed on the use of peculiarities of photoelastic effect for electronically controllable signals delay, for separation of channel signals by a temporal indication and for a pulse-width modulation of a sequence of rectangular impulses are generalized.

1. GENERAL INFORMATION

Interaction of light and acoustic waves in photoelastic media (the photoelastic effect) has a number of peculiarities representing a certain interest in the context of applicability for the solution of series of the radioelectronic problems. They include: significant regulated delay of an output response, modification of a distribution direction, intensity and frequency of diffraction order in accordance with coordinates of acousto-optic interaction, frequency and amplitude of an elastic wave being spatial analog of an input electrical signal.

The purpose of the present work is a generalization of outcomes of the authors theoretical and experimental investigations directed on handling of signals in temporal area based on the use of peculiarities of acousto-optic interaction effect in photoelastic media.

For facilitation of perception of the accepted decisions, at first we shall consider some properties of photoelastic effect.

A major unit of any acousto-optic device is an acousto-optic modulator representing a photoelastic medium, to one edge of which an electroacoustic converter is attached, it transforms a radio-frequency signal into an elastic wave spreading in a photoelastic medium with a velocity, approximately, 10^5 times less than a velocity of propogation of an electromagnetic wave. During an excitation of an elastic wave in a photoelastic medium dynamic modifications of an index of refraction (density of a medium) occur. These modifications lead to the formation of a phase lattice, with a step equal to the length of an elastic wave, and the amplitude proportional to the amplitude of an acoustic wave, as well as photoelastic constant medium. With realization of definite conditions, optical waves incident on this phase lattice deviate.

Diffractions of Raman-Nath and Bragg are distinguished. The diffraction of Raman-Nath is widely applied in acousto-optic devices of signal handling working on frequencies up to 100 MHz. Acousto-optic devices using Bragg diffraction are applied in data reduction systems working in the field of frequencies from several tens MHz up to units of GHz. The basic exterior difference of Bragg from a Raman-Nath diffractions consists of a nonsymmetric emerging of diffractional orders, with modification of the incidence angle a light stream in the aperture of acousto-optic modulator. The maximum of light intensity in a diffractional order takes place if the Bragg [1] conditions are fulfilled, i.e. if light falls on the aperture of acousto-optic modulator at the Bragg angle θ_B, defined from the relation

$$Sin\theta_B = 0,5\lambda/\Lambda , \qquad (1)$$

where λ is a wavelength of incident light; Λ- is an elastic wavelength in a photoelastic medium of acousto-optic modulator. Thus all deviating light will be concentrated in one order spreaded at the angle,

$$sin\theta_d = \lambda/\Lambda = 0,5f\lambda/\vartheta , \qquad (2)$$

where f and ϑ are frequency and velocity of elastic wave distribution, respectively.

From (2) it follows, that the modification of an elastic wave frequency is accompanied by the modification of deviating light distribution direction.

The intensity of a deviating bundle is determined by an expression [2]:

$$I_1 = BU^2 \qquad (3)$$

where U is the amplitude of the voltage on an electrical input of acousto-optic modulator; B is a constant factor.

In correspondence with (3), the intensity of deviating light is proportional to a square of input voltage.

2. VARIABLE SIGNALS DELAY

The indicated peculiarities of acousto-optic interaction can be applied to a signal delay, by extraction of a useful signal by means of elastic-optical connection on a defined distance from the electro-acoustic converter. A significant signal delay accessed by this method is determined by the run time of an elastic wave from the electro -acoustic converter up to the point of acousto-optic interaction. The device which operation is based on the indicated principle is named an acousto-optic delay line. Thus, the controlled delay of signals is got by a modification of a distance (span) from an electro-acoustic converter up to the point of acousto-optic interaction, by transition of acousto-optic modulator relative to a laser beam. However, the mechanical installation of the position of acousto-optic modulator eliminates the possibility to use the acousto-optic delay line in systems of information processing, in which fast regulation by hold time of signals is required.

In this context electronically controlled acousto-optic delay line (fig.1) with small time of installation of a required delay [3,4], has high potential abilities. Here the beam of the laser 1 is splitted on n bundles by the forming cascade 2. The spectrum of a treated signal is transferred in the area of working frequencies of acousto-optic modulator 3 by ampli-

tude modulator 7, modulating on amplitude made by a generator 6, high-frequency oscillations, which face values frequencies are selected by governing voltage U and can accept one of n discrete values thus remaining, in a band of acousto-optic modulator 3. The modulated high-frequency oscillations act on an input of acousto-optic modulator 3 and raise in it elastic waves of an appropriate frequency. Light bundles intersecting the aperture of acousto-optic modulator 3 deviate on elastic waves and form signal bundles hitting on a photosensitive surface of a photoreception device 5, on exit of which an entering signal with a constant multiplicand corresponds to delayed on time $\tau=h/\vartheta$, where h is a distance from electro-acoustic converter 8 of acousto-optic modulator 3 up to a signal bundle, which passes through an appropriate hole of a screen 4. The modification of controlling voltage given on a high-frequency generator 6 results in a modification of frequency of an elastic wave and angle of diffraction of deviating orders in a focal plane of acousto-optic modulator 3. As a results, through the hole other signal bundle will passes, i.e. the distance h and hold time τ vary.

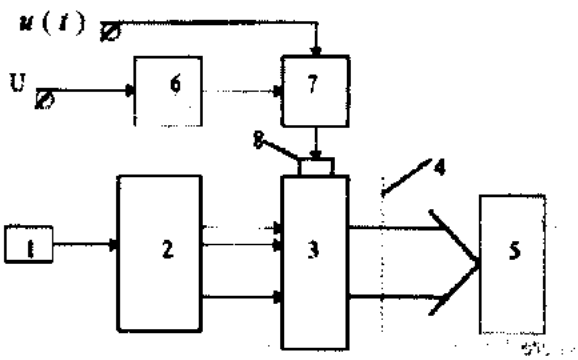

Fig.1.

In the offered device the improvement of parameters of formed time intervals is ensured by transition of acousto-optic modulator relative to a beam of the laser.

Experimentally the possibility of construction of discrete acousto-optic delay line with the possibility of choice of three values of hold time, 1; 1,7; and 2,5 μs., accordingly was checked. As a photoelastic medium the mesh from TF-7 was used, and the electro-acoustic converter was made from $LiNbO_3$. The central frequency of acousto-optic modulator was 80 MHz.

3. SEPARATION OF CHANNEL SIGNALS ON A TEMPORAL BASIC

The method of temporal division of channels consists of translational means (communication circuit, the instrument tract etc.) are represented by various sourses in turn; each elementary signal (signal possessing necessary and sufficient properties for its selection from the aggregate of all transferred signals of a multichannel system) exists during a strictly defined time interval. In general case it can be premises of a binary code, reference of a signal, sine wave oscillation of definite frequency etc.

For a separation of channel signals in modern selectors the presence of controlling impulses for each channel is necessary. These controlling impulses are broadcasted on appropriate communication circuits, resulting in complication of the system in whole.

The offered acousto-optic method allows to replace n controlling impulses for n of channels by one clock pulse for all channels. As a results the number of communication circuits is reduced by n-1.

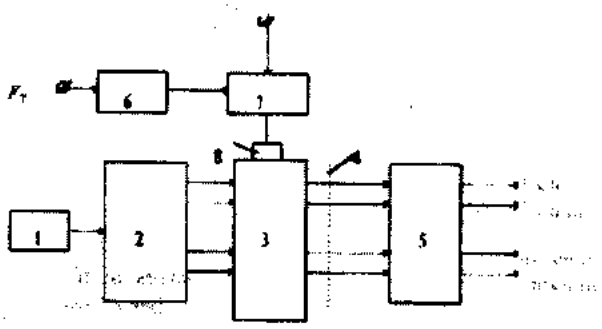

Fig.2.

The structural electrical scheme of acousto-optic selector of channel signals is represented on figure 2. A ray of the laser 1 is splitted into n bundles by the forming cascade 2, and any k- th light bundle falls in the aperture of acousto - optic modulator 3 under an angle Bragg θ_{Bk}, defined from the relation

$$sin\theta_{Bk}=0,5\lambda/\Lambda_k \quad , \qquad (4)$$

where Λ_k is the length of an elastic wave appropriate to any k-th channel n-th channel signal in photoelastic medium of acousto-optic modulator 3.

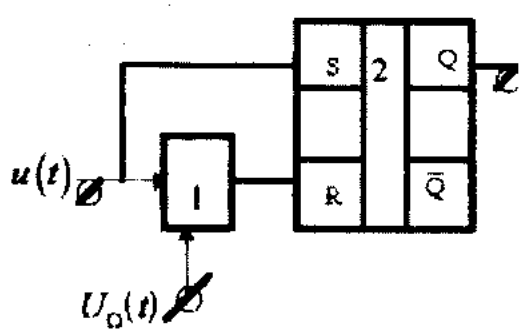

Fig.3.

The group signal modulates in the modulator 7 high-frequency line frequency-modulated oscillations of a generator 6, started by clock pulses with frequency F_T. The radioimpulses will be transformed by an electro-acoustic converter 8 into an elastic wave spreading in photoelastic medium of acousto-optic modulator 3.

The incident light bundles diffract on elastic wave packets. Diffracting orders, spreading at angles

$$\theta_{dk} = 0,5f_k \lambda/\vartheta \quad , \qquad (5)$$

where $f_k = \vartheta/\Lambda_k$ is the frequency of an elastic wave packet appropriate to any k-th channel of a n-th channel signal, are selected with the help of appropriate diaphragms with orifices 4 and fall on a photosensitive surface of a multichannel

photoreception device 5, on which exits the channel signals turn out. The diaphragms are placed in such a manner that any k diaphragm selects only bundle diffracted at the angle θ_{dk}.

The virtue of the offered device is, also, a possibility of operating regulation of time intervals of reception.

The possibility of construction of acousto-optic selector of channel signals was checked experimentally. As a photoelastic medium of acousto-optic modulator 3 the monocrystalline quartz was used, and the electro-acoustic converter 8 was made from ZnO, which was put on a surface of crystal by a method of vacuum dispersion. The central frequency of acousto-optic modulator 3 was 157 MHz. The device ensured a separation of channels of a 4 channel signal.

4. PULSE-WIDTH MODULATION OF A SEQUENCE OF RECTANQULAR IMPULSES

A basic unit of pulse-width modulators is the temporal modulator of a continuous operation, sensitive to amplitude of modulating low-frequency voltage. In this context smoothly controlled acousto-optic delay line has high [5] potential possibilities, which can ensure a large index of modulation in comparison with existing analogs, and these devices differ by high linearity of temporal modulation.

Because of explained above the acousto-optic method of pulse-width modulation is synthesized. The method [6] is explained by the block diagram given on fig. 3. Here modulated impulse sequence $u(t)$ acts on an input smoothly controlled acousto-optic delay line 1 and on an input «S» of the trigger 2. Under an operation of a modulating (primary) signal $U_\Omega(t)$ the hold time of an impulse sequence $u(t)$ in acousto-optic delay line varies. Thus, the delaying impulse sequence acts on an input «R» of the trigger 2. As a results on the exit of the trigger impulses are formed, which duration [6] is defined as:

$$\tau \approx \tau_0 \pm cU_\Omega, \qquad (6)$$

where τ_0 is the duration of an impulse on the exit of the trigger in a case $U_\Omega(t)=0$; c is a dimensionality factor, s/V.

From (6) it follows, that the increment of duration of an impulse on the exit of the trigger is directly proportional to the amplitude of modulating voltage $U_\Omega(t)$ on the input. In other words, the offered modulator is ensured with a linear pulse-width modulation.

The author checked experimentally the principle of a construction of acousto-optic breadth-impulse modulator ensuring linear modification of duration of impulse τ on the exit Q of the trigger 2 from 4 up to 5,8 μs., with modification of voltage on the input $U_\Omega(t)$ from 0 up to 3 V.

CONCLUSION

The proposed methods and devices of handling of signals in temporal area allow to expand the boundaries of application of peculiarities of photoelastic effect for transformation, transmission and reception of information. These devices are distinguished by simplicity and do not require special set-up. Besides, the visualization of basic processes in acousto-optic modulator (a laser radiates in visible range) considerably simplifies a specification of separate parameters of the device in whole. During last years acousto-optic modulator with satisfactory maintenance and engineering by indices (low power of an elastic wave excitations, high effectiveness of a diffraction etc.) and semiconductor lasers with a sufficient coherence of a radiation have been developed. Taking into account all this it is possible to state, that in the nearest future some compact acousto-optic device of handling of signals considerably exceeding their electronic analogs in characteristics will be created.

[1] *J.N. Lee, A. Vanderlugt.* Acoustooptic signal processing and computing. Proc. of the IEEE, 1989, vol. 77, №10, p.1528-1557

[2] *A.R. Hasanov.* Osnovi teory i texniki formirovaniya i obrabotki signala akustoopticheskimi metodami. "Elm", 1999, s. 55, (in Russian).

[3] *A.R. Hasanov i dr.* Pribori I sistemi upravleniya. 1997, №6, s. 46, (in Russian).

[4] A.R. Hasanov. Radioelectronica, 2000, t. 43, №5. s..73-76, (in Russian).

[5] A.R. Hasanov. Pribori i sistemi upravleniya, 1997, №6, s..45, (in Russian)..

[6] A.R. Hasanov. Fizika, 1998, t.4, №4, s. 12-13, (in Russian).

A.R. Həsənov

SİQNALLARIN ZAMAN OBLASTINDA İŞLƏNMƏSİ ÜÇÜN AKUSTOOPTİK ÜSULLAR VƏ QURĞULAR

Siqnalların electron-tənzimləməli ləngiməsi, kanal siqnallarının paylanması və düzbucaqlı impulslar ardıcıllığının eninə-impuls modulyasiyası üçün fotoelastik effektdən istifadə olunması istiqamətində müəllifin apardığı elmi-tədqiqat işlərinin nəticələri ümumiləşdirilir.

А.Р. Гасанов

АКУСТООПТИЧЕСКИЕ МЕТОДЫ И УСТРОЙСТВА ОБРАБОТКИ СИГНАЛОВ ВО ВРЕМЕННОЙ ОБЛАСТИ

Обобщаются результаты научных исследований автора, направленных на использование особенностей фотоупругого эффекта для электронно-управляемой задержки сигналов, для разделения канальных сигналов по временному признаку и для широтно-импульсной модуляции последовательности прямоугольных импульсов.

Received: 14.05.01

SEMICONDUCTOR VIBRATIONAL FREQUENCY-RESPONSE SENSOR FOR PRESSURE MEASUREMENT

Sh.M. ABBASOV

Radiation Research Department of Azerbaijan National Academy of Sciences
H. Javid av.,31[a], Baku, 370143

The representing electromechanical resonator on elastic vibrations of monocrystals strings from semiconductor materials rather simple in manufacturing of string in tenzoconverter on the basis of monocrystals is described. The examples of such class of converters using in concrete designs of devices for measurement of various physical parameters are reported.

The aim of our efforts is to design a sensor combining the advantages of two types of sensors and opportunities of the microelectronic technology as well as the properties of the oscillating string and stress diaphragm. The principles of the oscillating string stress sensors [1] are further developed to overcome all the difficulties arose when one tries to design these transducers. The development of microelectronics makes it possible to realize a pressure sensor based on a semiconductor string.

The choice of a semiconductor string as an active element of this sensor is determined by the following properties of monocrystal fibres:

- extremely high mechanical strength due to structure perfection of the grown fibres;
- the fibres due to their size, geometry and crystallographic orientation can be used for the manufacturing of several sensors. In this case it is necessary to make ohmic contacts and to connect the fibre with the leads;
- the doping possibility during the fibre growth allows us to obtain the crystals with required electrodynamic parameters;
- fibre sensor manufacturing technology is simple and the waste of semiconductor material is minimal.

The basic advantages of the string pressure sensors are: high sensitivity, operating stability, linear characteristics and frequency output signal.

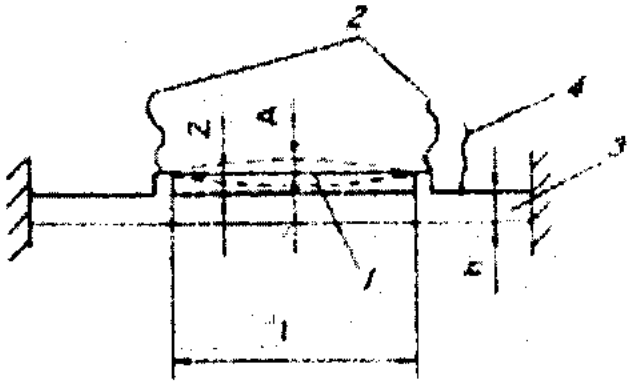

Fig.1. Schematic diagram of the electromechanical string resonator: 1 – fibre monocrystal, 2 – current terminal, 3 – diaphragm, 4 – electric connection

In comparison with all other types of electromechanical resonators used for the mechanical measurements the string sensors have the highest sensitivity. The best results were obtained with the diaphragm made of the same material. Concerning the piezoresistive properties, silicon is the best material for this purpose. Using the advantages of the microelectronic technology a new type of electromechanical resonator with electrostatic excitation was developed. Its structure is shown in fig.1. The resonator is prepared from a monocrystal fibre (string) 1 with current terminals 2. It is firmly fixed over the elastic element 3 (a silicon diaphragm in this case). The diaphragm surface is used as an exiting electrode as well. For this reason an electric contact 4 is attached to the diaphragm. The operation of this sensor can be described as follows.

When an alternating signal between the monocrystal fibre and the exciting electrode is applied, an induced electrostatic force F appears:

$$F = 1/2 \frac{dC}{dz} u_0^2 \sin^2 \omega t \qquad (1)$$

where: C is a string-diaphragm capacity; z is a distance between the string and the diaphragm equal to the height at which the string is fixed above the diaphragm.

The harmonic exciting force generates the harmonic oscillations of the string with magnitude. These oscillations cause the strain of the string monocrystal

$$\varepsilon = \frac{\pi^2 A^2}{8l^2} (1 - \cos 2\omega t) \qquad (2)$$

where: l is an oscillating length of the crystal.

As a result of the piezoresistive effect the variable component of the strain causes a generation of a variable component of the string resistance

$$\Delta R = k\varepsilon = \frac{\pi^2 k A^2}{8l^2} R_0 \cos 2\omega t \qquad (3)$$

where: k is a gauge factor, R_0 is a nominal string resistance.

If a direct current passes through the monocrystal fibre an alternative voltage is generated along the string. Its frequency is equal to the doubled mechanical oscillation frequency. The oscillation frequency is calculated by:

$$f = \frac{1}{2\pi l^2} \sqrt{\frac{BE_c(d_c/4)^2 + B' \sigma_c l^2}{\rho}} \qquad (4)$$

where: B and B' are numeric coefficients depending on the strain; d_c – string diameter; E_c is an elasticity modulus along

the string length; ρ is a crystal density; σ_c is stress, acting over the string. For a round shape diaphragm sensor the expression for stress is

$$\sigma_c = \frac{3P(1-\mu)^2 Ec(z+h/2)}{16E_m h^3}\left(D^2-1\right)^2 \qquad (5)$$

where: P is a pressure acting over the diaphragm; μ is a Poisson coefficient; D is a diaphragm diameter; h is a diaphragm thickness; E_m is a diaphragm elasticity module.

Equation (5) is valid when the diaphragm bending is less than the diaphragm thickness.

The elastic properties of the string are hundred times better than these of the bulk silicon [2]. The oscillations may be maintained with relatively low excitation energy as a result of the low density of silicon. Breaking strenght of a string crystal is relatively high. This ensures a maximum value of intrinsic mechanical oscillation frequency for a single crystal lenght. Crystal deformation sensitivity is relatively high.

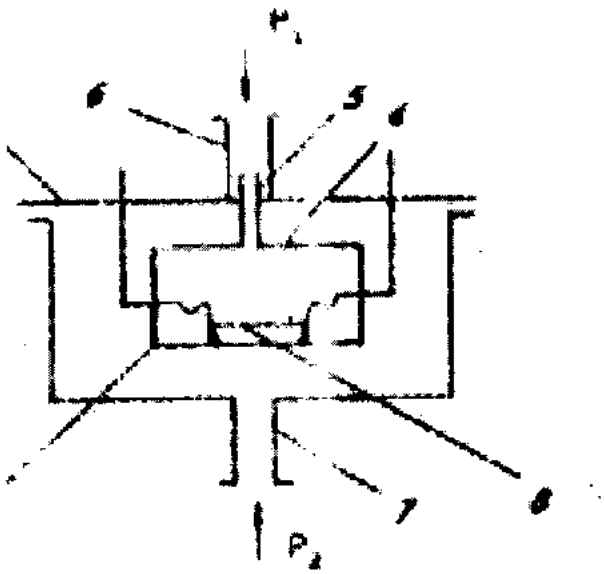

Fig.2. Design of a string transducer: 1,2,4 – package parts, 3 – silicon diaphragm, 5,6,7 – tubes, 8 – string monocrystal

The structure of the pressure sensor on the base of a semiconductor [3] is shown in fig.2. The sensitive element is mounted in the hermetical sealed package. The internal volume of the package is connected to the environment with pressure P_1 by a capillary tube. The second capillary tube connects the other side of the sensor to the measured pressure P_2. If the first tube is closed the hermetically sealed diaphragm modules may be used for absolute pressure measurements. The relative pressure changes can be measured when the diaphragm is not hermetically sealed.

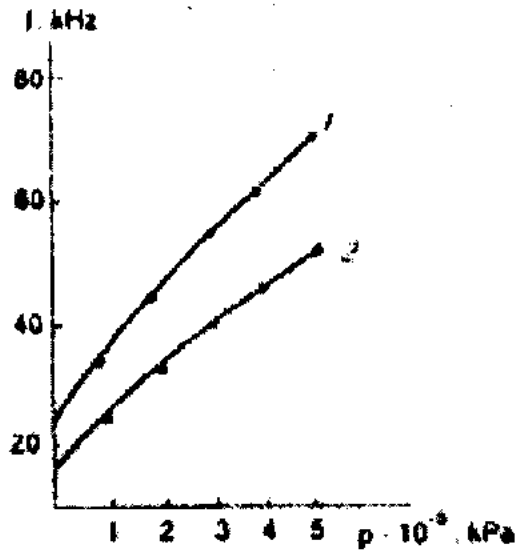

Fig.3. Sensor sensivity as a function of the string length: 1 - l=2mm, 2 – l =2.5 mm

When the difference between P_1 and P_2 changes a deformation of the diaphragm appears. This deformation is transformed into the variations of the output signal frequency. The sensor signal is transferred to interface circuit. It makes the sensor module operating in the permanent autoscillation mode. The sensor structure and dimensions depend on its practical application.

The theoretical investigations and the experiments show that the geometrical dimensions of the string and the diaphragm have a significant effect on the sensor operation characteristics. As it is discussed above the intrinsic oscillation frequency of the monocrystal resonator depends on the diaphragm dimensions. fig.3 shows the results for the square shape diaphragm. The obtained sensitivity (output frequency as a function of the applied pressure) is in a good agreement with the discussed theory and depends on the string length. The investigations show that the transducer is thermostable.

[1] *N. Milohin.* Frequency Sensors for Control Systems, Energia, Moskow, 1968.

[2] *N. Bogdanova, R. Baizar, V. Voronin, E. Krasnogenov.* Single-crystal Silicon Resistors as Sensitive Elements for Sensor. – Proc.Annual School on Semiconductor and Hybrid Technology, Sozopol, 1990.

[3] Auth.Cert.of USSR, №1458737 – Bull.Inventions, 1989, №6.

Ş.M. Abbasov

YARIMKEÇİRİCİLƏR ƏSASINDA SIMLİ TƏZYİQ ÇEVİRİCİLƏRİ

Konstruksiyasına və hazırlanmasına görə sadə olan simli yarımkeçirici monokristallardan hazırlanmış, elastik rəqslər əsasında işləyən elektromexaniki rezonatordan ibarət olan təzyiq tenzo çevirici təsvir edilmişdir. Müxtəlif fiziki parametrlərin ölçülməsi üçün konkret konstruksiyada bu cür təzyiq çevirilmələrindən istifadə edilməsinə dair misal gətirilir.

Sh.M. ABBASOV

Ш.М. Аббасов

ПОЛУПРОВОДНИКОВЫЙ ВИБРАЧАСТОТНЫЙ ТЕНЗОПРЕОБРАЗОВАТЕЛЬ ДАТЧИК ДАВЛЕНИЯ

Описан сравнительно простой по конструкции и в изготовлении струнный тензопреоброзователь, представляющий собой электромеханический резонатор на упругих колебаниях монокристаллических струн из полупроводниковых материалов. Приводятся примеры использования тонкого класса преобразователей в конкретных конструкциях устройств для измерения давления.

Received: 30.09.01

THE INFLUENCE OF THE MAGNETIC FIELD ON THERMALCONDUCTIVITY AND THERMAL POWER IN Bi-BASED SUPERCONDUCTING CERAMICS NEAR PHASE TRANSITION POINT

S.A. ALIEV, S.S. RAGIMOV, V.M. ALIEV, R.I. SELIM-ZADEH
Institute of Physics of Azerbaijan National Academy of Sciences
H. Javid, av., 33, Baku, 370143

The influence of the magnetic field to thermal conductivity (K) and thermal power (S) in phase transition (PT) region is investigated. The electron part of the thermal conductivity (K_e) is calculated. It is shown, that the ratio $K(B)/K_0$ increases with the increase of B, that is stipulated by the thermal conductivity of despaired electrons. The decrease in $S(T)$ in the normal phase is associated with the simultaneous participation of electrons and holes in conductivity.

INTRODUCTION

One of the peculiarities of $HTSC$ is that, the pushing force of magnetic fields is significantly weaker, and the second critical field (B_{c2}) is much higher, than in SC-1 $B_{c2}^{II} >> B_{c2}^{I}$. The magnetic force lines inside SC create around themselves SC -vortex fluxes. Starting from a certain value of B (from B_{c1} up to B_{c2}) a lattice by shrinking begins to destruct. The destruction of SC is accompanied by formation of normal electrons, partial restoration of conductivity and as a consequence by the electronic part of thermal conductivity. Depending on defect concentrations and investigated temperature interval the vortices may exhibit themselves as the scattering centers of electrons and phonons. Such conditions are fulfilled at low temperatures when, the electrons and phonons mean free paths reach the size of vortices section. The destruction process of SC under magnetic field is well studied by magnetoconductivity $\sigma(B)$ investigations and thermal power $S(B)$ and some peculiarities of $HTSC$ have been derived. In this connection it is interesting to investigate the magnetothermal conductivity and magnetothermal power $S(B)$ of $HTSC$. However, the experimental observation of the change of $K_{el}(B)$ becomes complicated by the fact that, in $HTSC$ in spite of high concentration of charge carriers, the lattice thermal conductivity is significantly larger than electronic part. Therefore for similar investigations it is necessary either to increase the concentration of charge carriers, or select an object with small K_l. Among known $HTSC$ the Bi-based ceramics have the smallest value of K_l.

Last years a number of theoretical and experimental work devoted to electron and phonon scattering on vortices as well as to restoration of electronic thermal conductivity in magnetic fields have been published [1-5]. In the present work, the influence of magnetic field on thermal conductivity and thermal power in bismuth ceramics of 2212 phase in phase transition region (PT) has been analyzed.

EXPERIMENTAL RESULTS AND DISCUSSIONS.

The details on ceramics preparations experimental method are reported in [5]. The measurements have been carried out in the magnetic field $B=2.2T$ in direction perpendicular to a heat flux. The temperature has been controlled within an accuracy of ± 0.05K and with a precision of 0.1K by carring out the measurement in the dynamical regime. Each measurement has been carried out twice by cooling down and heating up the sample. Any thermal hysteresis on dependencies of $K(T,B)$ and $S(T,B)$ have not been observed. The magnetic field dependencies of $K(B)$ and $S(B)$ have been measured at different temperatures. The temperature stabilization was achieved within 60-77 K with accuracy to 0,05 K and at $T>77K$ to 0,1 K accuracy. A temperature interval of 60-77 K has been obtained with a special pressure regulator of liquid nitrogen vapor.

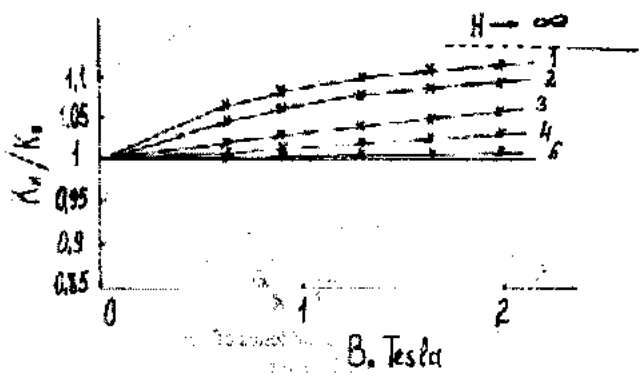

Fig.1. The magnetic field dependence of thermal conductivity 1-76K, 2-70K, 3-80K, 4-65K, 5-90 K.

In fig.1 the magnetic field dependence of thermal conductivity as $K(B)/K_0$ (K_0 - total thermal conductivity at a given temperature) ratio is shown. As it is seen the ratio $K(B)/K_0$ increases with increase of B. However, $\Delta K(B)$ increases only on the limit region of T (65-95K). The vanishing of this effect above 90 K is stipulated by the low mobility of holes in normal phase state while the absence of this effect at $T<65$ K can be explained by sufficiently increase of $Bc2$. At such temperatures the magnetic fields up to 2,2T are failed to break a sufficient number of pairs. It is clearly seen from the temperature dependence of $K(B)$ at $B=2,2T$ (fig.2).

As it is seen the maximal effect corresponds to 75 K. Therefore, it can be concluded that the thermal conductivity increasing effect in magnetic field is stipulated by despaired electrons in a heat transport.

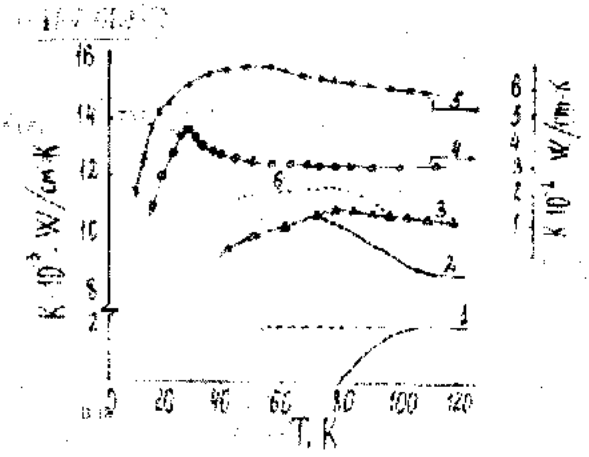

Fig.2. The temperature dependence of thermal conductivity 1- K_{e1}, 2-K_{lat}, 3-K_o, 4- bismuth, 5-yttrium.

The temperature dependence of experimental and calculational data of total $K_o(B)$ (3), lattice $K_l(T)$ (2) and electron part $K_e(T)$ (1) of thermal conductivities is presented in fig.2. In the same figure also the temperature dependence of total thermal conductivity of crystalline Bi-type SC (4) and yttrium ceramics (5) is presented.

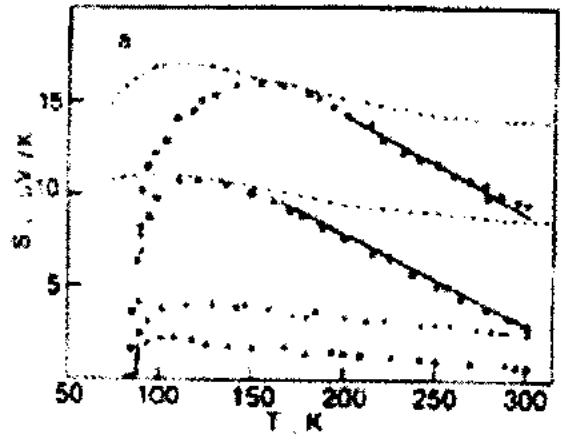

Fig.3. The temperature dependences of experimental and calculated thermal power.

The calculation of electron part $K_e(T)$ was carried out by Widemann-France law ($K_e=L\sigma T$) in the electron elastic scattering approach. The dotted curve (1) corresponds to the calculation in the absence of SC (taking into account $\rho n(T)$). Lattice part of thermal conductivity at T>80K is determined as $K_l=K_o-K_e$ and at temperatures lower than PT, $K_o(T)$ (at B=0) was taken as lattice K_l since the electrons do not take part in thermal conductivity. In this fig.3 the curve (6) corresponding to total thermal conductivity $K(T)$ is presented in the case if the superconductivity is absent in the sample. As it is seen from temperature dependences of $K(T)$(1) for the sample with high value of the K_e the at SC transition condition its decreasing is observed while in crystalline sample (4) of Bi-type SC and in yttrium ceramics the tendency to decrease of K_o(5) is absent. In crystalline sample it is related to the high value of ρo and K_o, and in Y-ceramics to relatively high value of K_l one. The gap between curves (4) and (6) is stipulated by superconductivity phenomenon. Between these curves in small temperature interval data of $K(B,T)$ at 2,2 T are presented. It is seen that, as B increase the $K(T)$ curve rises to $K_o(T)$ curve (6).

What the temperature dependence of thermal conductivity of HTSC ceramics is concerned one can notice that it strongly differs from $K(T)$ of metals, semiconductors and dielectrics. In particular, they have very weak temperature dependence up to low T_c as well as high value T_{max} and in several ceramics the maximum on $K(T)$ is not arised, in particular for bismut ceramics also. These pecularities of $K(T)$ are inherent to amorphous and glasslike semiconductors. This is related to the absence of strict crystallic lattice. Probably, this may be addressed to ceramic condition too. The temperature $S(T)$ and field $S(B,T)$ dependences are presented in fig.3 and fig.4. It is seen that $S(T)$ and $S(B,T)$ curves are of similar character. Approximately 10 K below the phase transition, the value of S passes through a peak and then decreases with temperature.

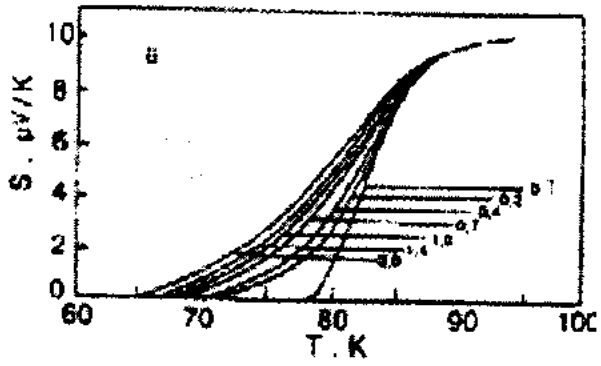

Fig.4. The temperature dependences of thermal power at various magnetic fields..

The value of S in Bi-based SC decreases sharper, than in Y-based SC. It can be seen that the transition width $\Delta T(B)$ increases with B. The arising of S under magnetic field is related to dispairing of Cooper's pairs. It can be seen that this effect significantly decreases with T disappears (T<70K). The change of $S(B)$ disappears at T>90K also. The data of S(B) are confirmed by data of $K(T)$.The results of $S(T)$ in normal phase have been interpretated according to the theory [6]. According to [6] the Fermi level for these materials lies near the narrow peak ΔE at the density of states $g(e)$ due to overlapping p-and d-band of oxygen and copper. Taking this circumstance into account, the authors of ref. [7] obtained the expressions for S in the cases when $\Delta E>kT$ in analogy with electron prosesses in noncrystalline materials. In ref. [8], this model was developed for an arbitrary ΔE, which made it possible to describe the results for S and ρ quantitatively and to determine the allowed band width ΔE in each individual case. The dashed curves in fig.3 show the results of calculations of $S(T)$. It can be seen that $S(T)$ of Bi-based ceramics strongly differs from the calculation. We believe that this is due to electrons which simultaneously take part in conductivity In this case the two-band model was applited. The parameters of electrons were obtained from Hall and specific electroresistivity data. The results of calculations of S are represented by solid curves in fig.3a. Thus, the participation of electrons in conduction of Bi-based $HTSC$

materials is beyond doubt , although the question on the nature of electrons and holes is disputable. This problem is analized in [9] where it was proposed that holes were the main charge carriers in negatively charged CuO_2 planes, whole electrons play the major role in positively charged $(BiO)_2$ planes. Holes dominate in the conduction of single crystals in the direction of the c-axis, while charge transfer in a direction perpendicular to the c- axis can be executed both by holes in the CuO_2 plane and by electrons in the $(BiO)_2$ layers.

[1] *V.B. Efimov, L.P. Mejov-Deglin, Low.Tem.* Phys., 1997, 23, №3, p.278-289.

[2] *V. Pogorelov, M.A. Arranz, R. Villar, S. Vieria.* Phys.Rev. B, 1995, v.51 № 21, p.15474-15477.

[3] *M. Houssa and M. Ausloss.* J.Phys. Conden.Matter, 1997, 9, p.201-210.

[4] *S.A. Aliev, S.S. Ragimov, V.M. Aliev.* Low Temp. Phys, 1996, v.22, № 6, p.522-524.

[5] *S.A. Aliev, S.S. Ragimov, D.A. Bagirov.* Turkish J.of Phys, 1994, v.18 №10, p.1051-1057.

[6] *L.F. Matties.* Phys.Rev.Letters, 1987, v.58, №10, p.1028.

[7] *V.I. Tsidilkovsky and J.M. Tsidilkovsky.* Phys. Metal , Metalloved (Sov), 1988, v.65, p.83.

[8] *S.A. Kazmin, Y.J. Kaydanov, G. Leysing.* Fiz.Tverd. Tela, 1988, v.30, № 10, p.2655-2958.

[9] *I. Tot, G.H. Panova, V.D. Corobchenko.* Superconductivity, (USSR), 1990, v.3.№8, p.1821-1830.

S.A. Əliyev, S.S. Rəhimov, V.M. Əliyev, R.İ. Səlim-zada

FAZA KEÇİDİ YAXINLIĞINDA BİSMUT İFRATKEÇİRİCİ KERAMİKALARDA MAQNİT SAHƏSİNİN İSTİLİKKEÇİRMƏ VƏ TERMOEHQ TƏSİRİ

Faza keçidi *(FK)* oblastında maqnit sahəsinin istilikkeçirmə *(K)* və termoehq *(S)* təsiri tədqiq edilmişdir. İstilikkeçirmənin electron hissəsi *(Ke)* hesablanmışdır. Maqnit sahəsinin artması ilə qırılmış electron cütlərinin istilikkeçirməsi nəticəsində $K(B)/K_o$ nisbətinin artması göstərilmişdir. *S(T)* normal fazada azalması keçiricilikdə eyni zamanda həm elektron, həm də deşiklərin iştirakı ilə əlaqədardır.

С.А. Алиев, С.С. Рагимов, В.М. Алиев, Р.И. Селимзаде

ВЛИЯНИЕ МАГНИТНОГО ПОЛЯ НА ТЕПЛОПРОВОДНОСТЬ И ТЕРМОЭДС В ВИСМУТОВЫХ СВЕРХПРОВОДЯЩИХ КЕРАМИКАХ ВБЛИЗИ ФАЗОВОГО ПЕРЕХОДА

Исследовано влияние магнитного поля на теплопроводность *(K)* и термоэдс *(S)* в области фазового перехода *(ФП)*. Вычислена электронная доля теплопроводности *(Ke)* . Показано, что отношение $K(B)/K_o$ растет с увеличением магнитного поля, что обусловлено теплопроводностью распаренных электронов. Уменьшение *S(T)* в нормальной фазе обусловлено одновременным участием в проводимости электронов и дырок.

Received: 23.05.01

DETERMINATION OF DEFECTFORMATION PARAMETERS IN Ag_2Te

F.F.ALIYEV, B.A.TAIROV, T.F. YUSIFOVA
Institute of Physics Academy of Sciences of Azerbaijan
H.Javid, av., 33, Baku, 370143

M.A. KERIMOV, FIRUZA M. HASHIMZADEH
Azerbaijan Technical University
H.Javid, av., 25, Baku, 370143

On the basis of electrical, thermoelectrical and thermodynamic parameters the concentration of defects N and energy of defectformation in Ag_2Te up to and at phase transitions are calculated. It is shown that the transitions $\alpha \rightarrow \alpha'$ and $\beta' \rightarrow \beta$ occur in the sublattice of Ag_2Te structure, and the transition $\alpha' \rightarrow \beta'$ is accompanied simultaneously by a change of vacancy concentration of Te atoms in a lattice site and interstitial atoms of Ag in the sublattice. It is established that the probability of spontaneous formation of nuclei in the transitions $\alpha \rightarrow \alpha'$ and $\beta' \rightarrow \beta$ is less than in the $\alpha' \rightarrow \beta'$ transition.

Tellurid of silver belongs to compounds such as $Ag^{I}_{2}B^{VI}$, having native defects owing to an arrangement of silver atoms in interstitials and presence of vacancy at sites of a crystal lattice. The concentration of defects (N) in them increases with temperature and at certain temperature due to defects there is a structural phase transition (PT) accompanied by a drastic change of electrical, thermal and other physical parameters.

In the work [1] it is shown that in Ag_2Te PT from monoclinic α-phase into face-centered cubic β-phase is accompanied by additional transitions $\alpha \rightarrow \alpha'$ and $\beta' \rightarrow \beta$ approximately according to the scheme $\alpha_{385} \rightarrow \alpha'_{405} \rightarrow \beta'_{420} \rightarrow \beta_{440K}$.

A number of works [2-3] is devoted to study of defects in Ag_2Te. However, there is no information on the domain of PT in them, which is actual and important for an explanation of PT process, therefore a present work is devoted to determination of defectformation parameters in Ag_2Te up to and in the domain of PT.

METHOD OF CALCULATION

At present with reference to compounds $A^{I}_{2-x}B^{VI}$ there are two models of possible defects formation: models of Rau [4] and Weiss [5], in each of which there is a dominant type of defects causing a deviation from stoichiometry. In the first model it is necessary, that the formation of defect goes in two stages: the jump forms neutral vacancy of metal V_A, then there is an ionization of vacancy, therefore a hole is formed. Hence, the complete concentration of defects is determined as $N=V_A+V'_A$ and the holes concentration is $p=V'_A$.

In the second model the introduction of metal atoms in interstitials is possible: $A_i=A_i^+ + n$, where A_i, A_i^+ and n concentrations of neutral, ionized donors and electrons, respectively

A complete concentration of defects is

$$N = V_A + V'_A - A_i - A_i^+$$

or

$$N = V_A + p - A_i - n \qquad (1)$$

where $p - n = V'_A - A_i^+$

The concentrations V_A and A_i are determined by the method described in [3], p and n are determined according to [6],

$$p = \frac{(2m_p^* k_0 T)^{3/2}}{4\pi^{3/2}h^3} F_{r+1}(\mu_p^*)$$

$$n = \frac{(2m_n k_0 T)^{3/2}}{3\pi^2 h^3} I^0_{3/2,0}(\mu_n^*, \beta) \qquad (2)$$

Here m_n and m_p are effective masses of electrons and holes, $\beta=\varepsilon_g/k_0T$ is a parameter of nonparabolocity of a band, ε_g is a width of the forbidden band (7), $\mu_p^* = \mu_p/k_0T$ and $\mu_n^* = \mu_n/k_0T$, μ_p and μ_n are chemical potentials, $I^0_{3/2,0}(\mu_n^*, \beta)$ is two-parametric integral of Fermi. The chemical potentials, determined from the following expressions [6], are

$$\alpha_p = -\frac{k_0}{e}\left[\frac{F_{r+2}(\mu_p^*)}{F_{r+1}(\mu_p^*)} - \mu_p^*\right] \qquad (3),$$

$$\alpha_\infty = -\frac{k_0}{e}\left[\frac{I'_{3/2,0}(\mu_n^*, \beta)}{I_{3/2,0}(\mu_n^*, \beta)} - \mu_n^*\right] \qquad (4)$$

where α_p is a thermo-emf of holes at absence of magnetic field, α_∞ is a thermo-emf of electrons in strong magnetic fields, $F_r(\mu_p^*)$ and $I^m_{n,k}(\mu_n^*, \beta)$ are one and two-parametric integrals of Fermi, respectively.

In work [3] it was reported that Ag_2Te is characterized by the defects of Frenkel, vacancies of Ag in interstitials, appearing for the account of statistically arranged atoms of Ag in sublattice. Then on distribution of Frenkel [8],

$$N/N_0 = Ae^{-\varepsilon_\phi/k_0T} \quad (5)$$

where N_0 is a general concentration of atoms, A is an integer (close to 1), describing the quantity of identical interstitials in account on one atom of a lattice and ε_ϕ is an energy of defectformation, measured in electronvolts. Using values of N/N_0 it is possible to find ε_ϕ (see a table).

At PT the general concentration of defects is equal to $\left(N + N_i \frac{\Delta N}{N_0}\right)$, where N_i is a concentration of silver atoms in interstitials, which is determined by the method [3], ΔN is a change of concentration of defects at PT. The relation $\Delta N/N_0$ is calculated as follows. Frenkel [8] has put forward an idea about a dynamic balance of nuclei, which essence consists of a fact that at given temperature the nuclei, which sizes are less critical, fluctuationally arising and disappearing, are in some statistic balance. It Is equivalent to the existence of some set of constant nuclei with the sizes less critical.

In Ag_2Te factor, promoting stabilization phase of fluctuations, is presence of defects in a crystal lattice, which is caused by deformation of structure. From [8] it is possible to conclude that at critical temperatures (T_0) fluctuation volumes (V_ϕ) are more than elementary subsystems (V_0). It is possible to expect that the following in this case is fulfilled

$$(V_\phi - V_0)/V_0 = \Delta N/N_0 \quad (6)$$

where $V_\phi = ak_0T_0^2/Q_0$, $V_0 = ak_0T_HT_0/Q_0'd$ here α is a temperature constant of the transition [9], Q_0 and Q_0' are a heat of PT for unit of volume and mass accordingly and d is a density of a crystal. Using the data of α, T_0 and Q_0 [9] and d [10] it is possible to calculate $\Delta N/N_0$ (see the table).

The calculated data for three samples are given in the table.

Table

Defectformation parameters in Ag_2Te

parameters / zamples	Transition	$N\cdot10^{18}$ cm^{-3}	T_0, K	$V_\phi\cdot10^{20}$ cm^{-3}	$V_0\cdot10^{20}$ cm^{-3}	$\frac{\Delta N}{N_0}$ %	ε_ϕ eV	E_{act}, cal/mol	B, eV	ε'_ϕ eV	$\frac{dL}{dT}$	ΔH^* cal/mol	ΔS^* cal/mol K	Q_0^* cal/g
Ag_2Te		1,2	300				0,13							
	$\alpha\rightarrow\alpha'$	2,1	400	2,28	2,09	8,3	0,10	24,02	1,00	0,12	0,13	309	0,77	0,9
	$\alpha'\rightarrow\beta'$	6,0	416	0,82	0,42	48,0	0,07	20,01	0,08	0,05	0,17	1304	3,13	3,9
	$\beta'\rightarrow\beta$	2,8	432	2,90	2,66	8,3	0,12	23,51	1,30	0,11	0,14	285	0,69	0,83
Ag_2Te+ 0,75at% Te		22,0	300				0,13							
	$\alpha\rightarrow\alpha'$	41,0	394	1,70	1,57	7,6	0,12	23,80	0,99	0,20	0,14	412	0,52	1,2
	$\alpha'\rightarrow\beta'$	78,0	416	0,89	0,51	43,0	0,08	1961	0,06	0,05	0,18	1340	3,32	3,9
	$\beta'\rightarrow\beta$	39,0	430	2,38	2,21	11,7	0,11	23,1	1,04	0,13	0,15	343	0,80	1,0
Ag_2Te+ 0,25at% Ag		0,4	300				0,13							
	$\alpha\rightarrow\alpha'$	0,6	393	1,30	1,20	7,7	0,10	25,10	0,97	0,12	0,14	549	1,40	1,6
	$\alpha'\rightarrow\beta'$	1,2	414	0,73	0,42	42,0	0,06	2100	0,06	0,06	0,18	1407	3,41	4,1
	$\beta'\rightarrow\beta$	0,7	430	2,38	2,10	11,8	0,13	24,80	1,23	0,14	0,15	378	0,88	1,1

THE ANALYSIS OF THE RESULTS

As it is seen from the table, the value ε_ϕ for $\alpha\rightarrow\alpha'$ and $\beta'\rightarrow\beta$ transitions is more than for $\alpha'\rightarrow\beta'$. Apparently, it is connected to the following facts.

The temperature speed of transition dL/dT on the data [9] looks as follows:

$$(dL/dT)_{\alpha\rightarrow\alpha} < (dL/dT)_{\alpha\rightarrow\beta} > (dL/dT)_{\beta\rightarrow\beta}.$$

At the same time dL/dT depends on energy of activation E_a ($E_a = RT_H^2/V\tau$ [11], R is a gas constant, τ is time of transition and V is a speed of heating), necessary for the transition to become allowed. With increase of temperature the internal energy of a crystal changes due to PT. If thus the crystal should pass through an intermediate state with energy exceeding energy of a final state, this intermediate state creates an energy barrier of height B, and the speed of transition is proportional to number of atoms having energy, sufficient for overcoming of this barrier, namely $\sim exp(-B/kT)$. If the portion of such atoms is less than unit, the speed of a transition is small. If the intermediate state of high energy does not prevent a transition, such transition occurs rapidly [12]. B can be determined, as the energy of activation of one defect (or energy of ionization of vacancy), i.e. $B = E_0/N'$, where $N' = N_i\frac{\Delta N}{N_0}$ Accordingly [12] it is possible to mention that the large value of B, ε_ϕ and small $\Delta N/N$ and dL/dT for $\alpha\rightarrow\alpha'$ and $\beta'\rightarrow\beta$ transitions testify that these transitions are limited by a speed of duffusion or carry of Ag from α- phase into α'- phase and from β'- phase into β - phase. It means that the atoms of Ag are hardly displaced from initial positions, that does not cause changes of symmetry of Ag_2Te structure and the transitions $\alpha\rightarrow\alpha'$ and $\beta'\rightarrow\beta$ are of displacement type [9].

The high values of dL/dT and small B and ε_ϕ at the $\alpha'\rightarrow\beta'$ transition testify that the atoms Ag and Te easily overcome possible energy barriers (B) and the transition occurs rapidly.

For understanding of the received results about the $\alpha\rightarrow\alpha'$ and $\beta'\rightarrow\beta$ transitions it is necessary to note the following. As it is known [13], in Ag2Te structure in sites of monoclinic (α) and face-centered (β) cubic lattice the atoms of Te

(anions) and cations of Ag in interstitials in several positions forming sublattice are located. For displacement of Te atoms high ΔH (change of enthalpy at PT) is required, what is not energetically favourable. Therefore low ΔH at $\alpha \rightarrow \alpha'$ and $\beta' \rightarrow \beta$ transitions are provided only with displacement of Ag atoms. Due to their displacement relatively to Te atoms in a direction of one of a lattice edges to a new position there is a rearrengement in sublattice. Thus the changes of interatoms distances because of displacement of Ag atoms do not exceed the sizes of elementary cells, and for displacement of Ag high heat Q_0 is not required [9].

The authors [14] consider that the transition in a state of superionic conductivity (SIC) in $Cu_{2-x}Se$ is complex transformation of evtectic type. The occurrence of SIC in β-phase of Cu_2Se is caused by disorder of cation sublattice. In [15] it is also noted that PT in superionic state, when cation lattice is completely disordered, can preceed PT with partial ordering. The authors [16] on curve temperature dependence of ionic conductivity at room temperature have found PT, which has been attributed to the second order PT.

It is known that all compounds such as $A_2^{I}B^{VI}$ belong to SIC group, in particular in Ag_2Te interstitial ions of Ag^+ have high mobility and can be ordered before and after the $\alpha' \rightarrow \beta$ transition in sublattice, as a result the $\alpha \rightarrow \alpha'$ and $\beta' \rightarrow \beta$ transitions occur.

ABOUT THE MECHANIZM OF TEMPERATURE SMEARING OF TRANSITIONS

Using as a base the assumption [17], it is possible to accept that unit of volume of a crystal is divided into N areas, where $N^{-1}=V_0$ is the volume of one area accordingly. At temperatures close to T_0, i.e. "macroscopic" PT, state in microareas more and more intensively fluctuates, thus the ratio of number of areas not "transformed" (n') to number of spontaneously formed nuclei ($N-n'$), determined in each moment of time, varies depending on a temperature change. The probability of phase fluctuation in volume $exp(-V_\phi \Delta\Phi/kT)$, where change of thermodynamic potential ($\Delta\Phi$) under state of $\Delta T=T_0-T<<T_0$ is determined by expression $\Delta\Phi=Q_0\Delta T/T$ [18]. It is possible to assume that there is a connection between the ratio $\Delta N/N$ and $exp(-V_\phi \Delta\Phi/kT)$, i.e. for definition of $\Delta N/N$ there is

$$\Delta N/N=exp(-V_\phi \Delta\Phi/kT) \qquad (7)$$

Further more the question is reduced to a low value of $\Delta N/N$ and a large value of "smearing" $T_0/\Delta S$ (ΔS is a change of enthropy at PT) at the $\alpha \rightarrow \alpha'$ and $\beta' \rightarrow \beta$ transitions. It can occur by two reasons: 1) the probability of spontaneous formation of nuclei is small; 2) the structure of Ag_2Te does not allow an occurrence of distinct PT in the sublattice.

In case of Ag_2Te in the $\alpha \rightarrow \alpha'$ and $\beta' \rightarrow \beta$ transitions the probability of phase fluctuation (~7-10 %) is small, i.e. because of a high value of B the spontaneous formation of nuclei is weak. Thus transition of Ag atoms from one sublattice to another, on account of large ionic radius of Te, needs the large energy of activation E_α (see the table). Here the multiplicity of ratio of the periods of sublattice of different phases and closeness of parameters "c"and "a" low- and high- temperature phases correspondingly are possible, that does not cause a delay of the transition in time and on temperature, not observable experimentally [9]. The heat of transition Q_0 can result in weak change of interatom interaction at a variation of lengths and number of bonds. Therefore insignificant change of Ag_2Te structure can entail to evolutionary passage of PT in time and on temperature.

So, the offered versions are in complete agreement with experimental and calculated data.

A small value of $T_0/\Delta S$ and large values of Q_0 and $\Delta N/N$ at the $\alpha' \rightarrow \beta'$ transition cause preservation of distinct PT at T_0~415K. The high probability of fluctuation phase (~45 %) allows to assert that the essential spontaneous formation of nuclei takes place at the $\alpha' \rightarrow \beta'$ transition.

In Ag_2Te the $\alpha' \rightarrow \beta'$ transition is related to "order - disorder" category, for which the drastic change of the ratio of a number of disordered atoms of Ag to a number of interstitials is characteristic. It results in a growth of a number of defects: numbers of vacancies of Te atoms in sites and Ag atoms in interstitials, causing rearrangement in both lattices.

Thus, in Ag_2Te the $\alpha' \rightarrow \beta'$ transition is accompanied simultaneously by a change of a number of vacancies of Te atoms in the lattice and Ag atoms in interstitials of the sublattice.

[1] *J. Bartkowicz, S. Mrowec.* J.Phys. Stat. Sol., 1972, 42, 1, 101. *Andre and C. Simon.* J.Phys. Chem. Sol., 1983, 42, 295.

[2] *H. Rau.* J. Phys. Chem. Sol., 1974, v.35, №11, pp. 1553-1559.

[3] Sol. Stat. Comm., 1975, v.16, №8, pp.1041-1042.

[4] *K. Weiss.* Phys. Chem., 1969, v.75, pp.338-344.

[5] *B.M. Askerov.* Kinetik effects in semiconductors. L., "Nauka", 1970, s. 303 (in Russian)

[6] *Ya.I. Frenkel.* Statisticheskaya fizika M-L. Izd-vo AS USSR, 1958, s. 264. 8 (in Russian)

[7] *S.A. Aliev, F.F. Aliev, I.S. Qasanov.* FTP, 1998, t.40, №9, s.1693-1697 (in Russian).

[8] *V.M. Qlazov, N.M. Maxmudova.* Neorgan. materiali, 1970, t1, .№8, s. 1409-1415 (in Russian).

[9] *Q.O. Piloyan.* Vvedenie v teoriyu termicheskoqo analiza. Nauka, 1962, s. 264 (in Russian)

[10] *M.D. Berger.* Kristallog. 1971, t.16, №3, s.1084-1092 (in Russian).

[11] Kristallokhimicheskie, fiziko-khimicheskie i fizicheskie svoystva poluprovodnikovikh veshestv. M. Izd-vo standartov. 1973, s. 101(in Russian).

[12] *N.X. Abrikosova, V.F. Baukina, M.A. Korjiev i dr.* FTP, 1983, t. 25, №10, s. 2911 (in Russian).

[13] *Y.Ya. Gurevich, Q.V. Reznik, Y.I. Kharkach.* FTP, 1978, t. 20, №6, s. 1661 in Russian).

[14] *E.S. Krupnikov, F.Y. Aliev, A.Q. Abdullaev.* FTP, 1983, t.25, №10, s. 2911(in Russian).

[15] *V.A. Ginzburq.* FTP, 1960, t.2, №9, s. 2031-2035(in Russian).

[16] *V.Ya. Frichberq, B.I. Rolov.* Izv. AN SSSR, S. Fizika. 1964, XXVIII, №4, s. 649-652 (in Russian)

F.F.Əliyev, B.A.Tahirov, T.F. Yusifova, M.A. Kərimov, Firuza M. Haşımzadə

Ag_2Te KRİSTALINDA DEFEKTƏMƏLƏGƏLMƏ PARAMETRLƏRİNİN TƏYİNİ

Ag_2Te kristalında elektrikkeçirmə, termoeds və termodinamik parametrlərin əsasında defektəmələgəlmə parametrləri, konsentrasiya, defektərin əmələgəlmə enerjisi və faza fluktuasiya ehtimalı faza keçidlərində təyin olunmuşdur. Alınan hesablama nəticələri göstərmişdir ki, $\alpha \rightarrow \alpha'$ və $\beta' \rightarrow \beta$ keçidi alt qəfəsdə, $\alpha' \rightarrow \beta'$ keçidi isə əsas qəfəsdə baş verir. Müəyyən olunmuşdur ki, özəklərin spontan əmələ gəlməsi $\alpha \rightarrow \alpha'$ və $\beta' \rightarrow \beta$ keçidində azdır, nəinki $\alpha' \rightarrow \beta'$ kecidində.

Ф.Ф. Алиева, В.А. Таиров, Т.Ф. Юсифова, М.А. Керимова, Фируза М. Гашимзаде

ОПРЕДЕЛЕНИЕ ПАРАМЕТРОВ ДЕФЕКТООБРАЗОВАНИЯ В Ag_2Te

На основании электрических, термоэлектрических и термодинамических параметров рассчитаны концентрации дефектов и энергия дефектообразования, а также вероятность фазовой флуктуации в Ag_2Te при фазовых переходах. Анализ расчетных результатов показал, что переходы $\alpha \rightarrow \alpha'$ и $\beta' \rightarrow \beta$ происходят в подрешетке структуры, а переход $\alpha' \rightarrow \beta'$ сопровождается одновременно изменением числа вакансии атомов Te в решетке и Ag в междоузлиях подрешетки. Установлено, что вероятность спонтанного образования зародышей в переходах $\alpha \rightarrow \alpha'$ и $\beta' \rightarrow \beta$ меньше, чем в $\alpha' \rightarrow \beta'$ переходе.

Received:30.04.01

THE SEMICONDUCTING NANOCRYSTALS

A.S. ABBASOV, S.I. MEKHTIYEVA
Institute of Physics of Azerbaijan National Academy of Sciences
H. Javid, av., 33, Baku, 370143

The paper reviews a recent state of physico-chemical studying of semiconducting nanocrystals. There have been highlighted the major factors to condition special physico-chemical properties of semiconducting nanocrystals. It has been revealed a difference in chemical conversions on their surface and in the volume dealt with a dimensional factor. Most of nanoparticle surface atoms determine melting temperature and pressure as the conditions under which semiconductor lattice rearrangement occurs depending on the size of nanoparticle.

Non-linear optical effects and dependence of optical characteristics and physico-chemical properties versus the size are brought about by comparability of the size of nanoparticles and the radius of delocalization of charge carrier.

INTRODUCTION

As known the properties of semiconductors containing a macroscopic number of atoms do not depend their size. During the past few years it has been shown that at a characteristic size of semiconducting particles <10 nm many of their physico-chemical properties vary. It is stipulated by the fact that in the semiconductors the energy of intermolecular interaction is high and the crystal might be considered as a whole big molecule in the description of electronic properties.

Crystal excitation leads to the formation of light-bound electron-hole pair whose delocalization area might significantly outsize a constant of crystal lattice. The given decrease in the size of crystal has an effect on its electronic properties.

Supersmall crystals are known in the literature as nanoparticles, nanocristals or the quantum-sized particles.

Investigations of nanocrystals have brought to light a line of their peculiar properties to be of a great interest.

Dependence of electronic excitation radiation life time versus size, melting temperature, pressure necessary for rearrangement of crystal structure characteristic physico-chemical properties are conditioned by three major reasons: firstly,the size of nanoparticles is comparable with a Bohr radius of excitons in the semiconductors. This determines optical, luminescent and another properties of nanoparticales.

Secondly, for nanoparticles a number of atoms to be on the surface accounts for a quite significant part of the total. So, for 6 nm-sized CdSe about 20% of atoms is situated on the surface. Surface atoms contribute to the thermodynamic properties, and determine a structural transition and melting temperature; thirdly, own size of nanoparticles is comparable with the size of molecules which determines the thermodynamics and kinetics of chemical conversions on the surface. To date the following nanoparticles have been synthesized and studied: CdSe, CdC, MoC, HgC, ZnO, SiO_2, etc. For some nanoparticles there have been studied structure of electronic zones, electrochemical and thermal properties. The present paper overviews the methods of synthesis, quantum dimensional effects characteristic for semiconducting nanoparticles.

METHODS OF SYNTHESIS

Nanocrystals are produced by the method of chemical synthesis in colloidal solutions, polymers, glasses, zeolites, micelles [1-4]. The simplest method is the synthesis from initial reagents in solution by means of interrupting a reaction at a certain moment of time. Nanoparticles of metal sulfides are synthesized by the reaction between water-soluble salt of metal and H_2S or Na_2S in the presence of stabilizer-sodium metaphosphate:

$$Cd(ClO_4)_2+Na_2S=CdS\downarrow+2NaClO_4$$

In the course of reaction the growth of nanoparticle CdS is interrupted as pH of solution is increased. Nanoparticles TiO_2 are formed in the hydrolysis of titanium tetrachloride:

$$T: Cl_4+2H_2O = T:O_2+4HCl$$

Large-sized nanoparticles are synthesized by adding extra molecules to an initial cluster stabilized in a solution with organic ligands. It is normally assumed that nanoparticles, containing some hundreds of atoms have spherical or ellipsoid shape and sometimes have distinct faces similar to macroscopic crystals.

Shape and size control is hold by the methods of electronic microscopy.

A gas-phase synthesis of nanoparticles $T:O_2$ and Si is submitted in [5] with a yield ~70%

In [6,7] there has been suggested the method of synthesis of semiconducting nanoparticles by of metal pulsed laser evaporation in the chamber containing a necessary amount of gas-reagent by means of controlled nanoparticles condensation on the carrier.

The given method is a modification of the method of synthesis in a diffusion chamber and enables the synthesis of nanoparticles with mixed molecular composition-oxides, nitrides carbides and their mixtures. By changing the composition of gases in a chamber and by varying a temperature gradient and the power of laser pulse, it is possible to control both composition and size of nanoparticles. Nanoparticles might also be synthesized by ultrasonic treatment of colloidal solutions of large particles of semiconductors. Nanoparticles of layered semiconductors are formed as a result of large particles dissolution in an appropriate solvent. MoS_2-type layered semiconductors are distinguished for Van der Waals force between separate layers S-Mo-S [8]. During the process of dissolution the molecules of solvent penetrate into the space between the layers of semiconductor and destroy large particles therein. With respect to MoS_2 the process proceeds until a bilayered particle is formed. The further destruction of layers is not observed because the formation of monolayered particle is accompanied by an increase of free energy.

The ultrasonic treatment of dispersed system with large particles also leads to the formation of nanoparticles MoS_2,

WS_2, PbJ_2, Fe_2O_3 [10]. In respect to PbJ_2-type layered semiconductors there have been observed discoid-nanocrystals featuring discrete magic "disc size" [11]. It is assumed that, in this case, a stable particle-crystallite holding a hexagonal symmetry of macroscopic crystal consists of two layers of iodine of seven atoms and of two layers of lead MoS_2 nanoparticles are an analogous structure.

There is a great interest shown to thin films of semiconducting nanoparticles, which are synthesized by means of the precipitation of previously synthesized nanoparticles from colloidal solutions onto the carriers, by means of direct precipitation of semiconductor molecules onto the carrier and by means of oxidative hydrolysis of metal salts at the anode. Normally, a film thickness is $0,1-1\mu m$.

Films of SnO_2, ZnO_3, Wo_3, Fe_2O_3 have been synthesized

Oxidative hydrolysis of $TiCl_3$ at $pH=2,3$ and potential of platinum anode leads to the formation of nanoparticles of 1-2nm in diameter on the surface of anode [12].

By the method of precipitation it is possible to form nanostructured films to contain nanoparticles of different semiconductors.

Another method of film synthesis consists of wetting of the plate with a deposited film of certain type of nanoparticles in a solution containing ions of metal followed by wetting in a solution with sulphide ions. The films containing ZnO and CdS have been synthesized by this way [13,14].

OPTICAL PROPERTIES VERSUS THE SIZE OF NANOPARTICLES

Change of excitation energy of semiconducting crystals when their small are sizes is seen obvious. The electron excitation energy of an isolated molecule normally highly exceeds interband transition energy in the macroscopic semiconductor. It means that in the transition from crystal to molecule there should be a certain size range within which a smooth change in crystal electron excitation energy from a smaller magnitude to a greater one to characterize a given molecule is observed. For the semiconducting crystals such the transition occurs over a nanometric range. For a variety of semiconductors, there has been shown the influence of the size of nanoparticles on the optical spectra.

In [7] the spectra for different-size nanoparticles CdSe have been represented and it has become clear that nanoparticles absorption spectrum shifts to a short-wave region with an increase in their size. Dependence of nanoparticle electron excitation minimum energy on the size could approximately be calculated if the correlation between the uncertainty (Δx) in position and the uncertainty (Δp) in momentum of an exciton in the macroscopic crystal and in nanoparticle

$$\Delta p \cdot \Delta x \geq \frac{\hbar}{2} \tag{1}$$

is taken into account.

The position of delocalized exciton in a periodic potential of the macroscopic crystal is not fixed, but the energy (E) and momentum ($p = \hbar K$) are strictly determined and at small (K)

$$E = \frac{\hbar^2 K^2}{2\mu}, \tag{2}$$

where μ is an exciton effective mass.

For nanoparticle the uncertainty in an exciton position depends on a nanoparticle characteristic size $\Delta x=d$. If one assumes that the ratio between the energy and momentum does not depend on the size of a particle, the energy of exciton will vary inversely with the square of nanoparticle characteristic size.

More rigorous analysis of the effect of the size of spherical nanoparticles upon an exciton excitation energy E_n leads to the following equation:

$$E_n = E_m + E_1 \tag{3}$$

where E_m is an interband transition energy in the macroscopic semiconductor; E_1 is the energy of an exciton localization on the nanoparticle

$$E_1 = \frac{h^2 n^2}{8R^2\mu} - \frac{1.78e^2}{\varepsilon R} - 0.248E_R^X \tag{4}$$

n is integer number, R is the nanoparticle radius,

$$\mu = \left(m_e^{-1} + m_n^{-1}\right) \tag{5}$$

m_e and m_n are effective masses of electron and hole respectively; ε is a semiconductor dielectric permittirity semiconductor dielectric permeability; E_R^X is Ridberg effective energy. First term in the right hand side of the equation is a dominating one, the second one allows for a Coulomb interaction between an electron and hole inside the nanoparticle, third is responsible for a spatial correlation. The values $n>1$ in the equation are consistent with the transition of an exciton to the higher excited states. In the case of anisotropic semiconductors effective masses of electron and holes are direction-dependent: in view of anisotropy the equation takes more complicated form:

$$E_{n_x,n_y,n_z} = \frac{h^2}{8}\left(\frac{n_x^2}{\mu_x\alpha_x^2} + \frac{n_y^2}{\mu_y\alpha_{yx}^2} + \frac{n_z^2}{\mu_{zx}\alpha_{zx}^2}\right) - \frac{1.78e^2}{\varepsilon R} - 0.243E_R^X, \tag{6}$$

where n_x, n_y, n_z are integer numbers; μ_x, μ_y, μ_z are exciton effective masses along the corresponding directions; α_x, α_y, α_z are nanoparticle geometrical sizes. The nanoparticle exciton excitation energy is well described by function $1/R^2$. The given equation is frequently used to calculate the nanoparticle size:

$$KR = \frac{n}{\sqrt{8\mu E}} \tag{7}$$

Another manifestation of size effect in the optical characteristics of nanoparticles is found to be a short-wave shift of the optical spectrum of nanoparticles under "the placing" an excess electron on them. There may be three reasons to explain the given shift: firstly, an increase in the energy of an exciton as a result of the effect of the excess electron electric field; secondly, the effect of low vacant state occupation by the excess electron, much energy is needed to excite the electron to a higher state; thirdly, a decrease in the power of exciton transition oscillator because due to the effect of electrons and holes trapped. The recombination of light-generated charges leads to nanoparticles luminescence. With an increase in their size, a short-wave shift is observed under these conditions. The luminescence of ZnO, ZnS, CdS, CdSe has been comprehensively studied. One more manifestation of quantum size effect is the growth of oscillator strength fixed on volume of an excitonic absorption. This growth occurs with the size decrease with an increase in integral of electron and hole wave functions overlapping in parallel with a decrease in the size of nanoparticles [16-17].

DEPENDENCE OF THERMODYNAMIC PROPERTIES ON NANOPARTICLES SIZES

A big number of atoms in nanoparticles find themselves on the surface and increase with a decrease of the nanoparticles size. Their contribution to the energy of nanocrystal is high enough. Because of that there is a regular dependence of melting temperature of nanoparticles on their sizes.

In the case of CdS nanoparticles:

1.5 nm-600 K; 2 nm-100 K; 3.7 nm-1200 K [18-20]. As known, liquid surface energy is lower than that of crystal.

A decrease in the size of nanoparticles leads to an increase in surface energy, and consequently, to a decrease in melting temperature.

The pressure may change the geometry of the crystal lattice of macroscopic crystal to come to a tighter packing (the same is observed in the case of nanocrystals). The pressure brought to bear on CdS nanocrystal CdS with a structure of vurtzite (tetrahedron coordination) results in the change of structure to face-centered cubic one. As a result, less ordered surface with high energy is formed. In the case of JnP, CdS, CdSe and Si an increase in the pressure necessary to change the geometry of crystal lattice with a decrease in the size has been observed. This phenomenon is characteristic of nanocrystals, which account for a great portion of the surface centres.

The colloidal solutions of nanocrystals are found to be useful in the demonstration of their application in photocatalysts. It should be noted that their practical usage is complicated due to the necessity of separating nanoparticles from solution after the completion of a photocatalytic process. In this aspect thin layers of nanoparticles adsorbed on the film to consist of heteronanoparticles are seen more promising. This expands the range of spectral sensitivity referred to wide-band semiconductors and increases a quantum effect of photoseparation with respect to the charges. Porous films of nanoparticles display a high adsorbability.

The application of the above-mentioned features allows to increase their photocatalytic effects at the cost of films sensibilization to the visible region of spectrum [21,22].

CONCLUSIONS

From the present review of papers dedicated to the investigation of semiconducting nanocrystals, it follows that their extraordinary physicochemical characteristics are caused by the following factors:

The size of nanoparticles is comparable with that of molecules and this defines the difference between chemical conversions on their surfaces and in the bulk.

The number of atoms on the surface of nanoparticles accounts for a great amount of the total what has an effect on the thermodynamic properties of the particles. This condition defines dependence of melting temperature and pressure, at which the rearrangement of semiconductor crystal lattice occurs, on its size.

Non-linear optical effect and dependence of execution transition energy, oscillator strength and other characteristics on the size of nanoparticles are brought about by comparability of the size of nanoparticles and the radius of delocalizition of charge carriers.

At present the development of the methods of nanoparticles synthesis, integrated study of their physicochemical properties, introduction of results obtained in electronics, ecology, etc. are of a great interest.

[1] *L.E. Drus.* J.Chet., 1984, 80, 4403.
[2] *Y. Wang.* Opt. Commun., 1987, 61,233.
[3] *N.F. Borreli.* J.Appl.Phys., 1987, 61, 53999.
[4] *M. Visca, E. Matijevic.* J.Cilloid Interface Sci., 1979, 68, 308.
[5] *M.W. Peterson.* J.Phys. Chem., 1988, 92, 1400.
[6] *J. Kavan, T. Stot.* . J.Phys. Chem., 1993, 97, 9493.
[7] *S. Hotchadani, P.V. Kamat.* J.Phys. Chem., 1992, 96, 6834.
[8] *A.L. Efros.* The Physics and technics of semiconductors. 1982, 16, 1209.
[9] *C.R. Berry.* Phys. Rev., 1967, 161, 948.
[10] *Y. Kayanuma.* Phys. Rev., 1988, 38, 9797.
[11] *T.S. Moss.* Proc. Phys. Soc. B., 1954, 76, 775.
[12] *W.J. Albery, G.T. Brown.* J.Chem.Soc., 1985, 1, 81, 1999.
[13] *A. Henglun, A. Kumar.* Chem. Phys.Left., 1986, 132, 133.
[14] *E. Hilinski.* Phys.Rev., 1954, 93, 632.
[15] *W.G. Becker, A.J. Bard.* J.Phys. Chem., 1983, 87, 4888.
[16] *R.F. Khairutdinov.* Chem., 1993, v.24, №2.
[17] *N.M. Dimitrievic.* J.Chem., 1987, 83, 1193.
[18] *J. Crysochoos.* J.Phys. Chem., 1992, 96, 2868.
[19] *M. Haase, A.P. Alivisatos.* J.Phys. Chem., 1971, 96, 6756.
[20] *A.P. Alivisatos.* J.Phys. Chem., 1996, 100, 13226.
[21] *R.F. Khairutdinov, N. Serphone.* Prog. React. Kinet., 1996, 21, 1.

THE SEMICONDUCTING NANOCRYSTALS

A.S. Abbasov, S.İ. Mehdiyeva

YARIMKEÇİRİCİ MONOKRİSTALLAR

Nanozərrəciklərin fiziki-kimyəvi tədqiqatlarının perspektivləri nəzərdən keçirilib. Yarımkeçiricilərdə nanozərrəciklərin qeyri-adi xassələrinin əsas faktorları təyin edilib. Nanozərrəciklərin termodinamik xassələri, (təzyiq, ərimə temperaturu) onların ölçüsündən asılılığı aydınlaşdırılıb. Qeyri-xətti effektlərin əmələ gəlməsi və onların nanozərrəciklərin ölçüsündən asılılığının səbəbkarı nanozərrəciklərin ölçülərinin uyğunluğudur.

А.С. Аббасов, С.И. Мехтиева

ПОЛУПРОВОДНИКОВЫЕ КРИСТАЛЛЫ

Рассмотрено состояние исследования физико-химических характеристик нанокристаллов. Определны основные факторы, обуславливающие необычные их свойства.

Выяснена зависимость термодинамических свойств (давление, температура плавления) от размеров нанокристаллов.

Обсуждены возникновение нелинейных эффектов и их зависимость от размеров нанокристаллов.

Received:21.09.01

THE KANE OSCILLATOR

A.M. BABAEV
Institute of Physics of Azerbaijan National Academy of Sciences
H.Javid, av., 33, Baku, 370143

The energy spectrum and wave functions for Kane oscillator describing the spectra of electrons, light hole and spin-orbit-splitting bands in a quantum dot with harmonic lateral confinement is found.

1. INTRODUCTION

As shown in [1], for description of an energy spectrum of quantum dots either "infinite potential barries", or a model of parabolic potential confinement can be used. It has been established, that the model of parabolic potential is realistic enough for describtion of not too large quantum dots. Within the framework of this model a number of problems of quantum dots physics were considered for the standard dispersion of electrons, including quantum crystallizations in an external magnetic field [2].

The semiconductor compounds (InAs, GaAs, InSb etc.) on which quantum dots are created now, have a complex energy spectrum described by multiband Hamiltonian. In particular, nonparabolicity of a spectrum is possible to take into account within the framework of eight-bands Kane model [3].However due to complexity of the obtained equation in [3], the analysis of its solution was carried out in the framework of rather special approximation.

The complexity of the equation mentioned above arises in a standard way of introduction of parabolic confinement potential through scalar potential. If the external potential is introduced by minimal substituting [4]:

$$\vec{p} \to \vec{p} - i\beta\lambda\vec{r} \tag{1}$$

then for Dirac Hamiltonian the oscillator equation would be obtained with additional constant term originated from spin-orbital coupling as shown [4-7].

In the present paper we have shown that if one introduces the external potential into the equations invariant under the rotational group [8,9] by way like (1) it would be transformed to the oscillator equation. Note that method [8] directly gives a system of equations for radial functions for any number of considered bands.

We have called the obtained equation Kane oscillator, by an analogy to Dirac oscillator . To obtain the Kane spectrum from the system of equations (18) in [8] we consider the values (j=1/2, τ=0) for the conduction, heavy and light hole (j=3/2, τ=1), and spin-orbit-splitting (j=1/2, τ=1) bands. The first index characterizes the weight of an irreducible representation and a second one indicates the subspace with the same weight. We have chosen indices for the states which clearly show that they are created from corresponding s, p states. In order to give a physical meaning to the equations we consider the coupling coefficients s, and p, correspondingly, τ=0, τ=1 to be nonzero, where τ is a label of the subspace.

Substituting

$$\frac{d}{dr} \to \frac{d}{dr} + \beta\lambda r \tag{2}$$

(where λ is a parameter characterizes a steepness of a well, β is a diagonal matrix with elements $(-1)^{\left(\tau+\frac{1}{2}-j_z\right)}$, j_z is a magnetic quantum number) the system of the equations , including also the dispersionless band of heavy hole take a form [8,9]:

$$\frac{-ia}{2(E-E_g)}\left[\frac{d}{dr}+\lambda r+\frac{1\mp(l_0+\frac{1}{2})}{r}\right]f_3^{\mp}-\frac{i\sqrt{2}b}{E-E_g}\left\{\left[\frac{d}{dr}+\lambda r+\frac{5\pm(l_0+\frac{1}{2})}{r}\right]f_2^{\pm}+\frac{\alpha}{r}f_2^{\pm}\right\}+f_1^{\pm}=0 \tag{3}$$

$$\frac{i\sqrt{2}b\alpha}{r}f_0^{\pm}-f_1^{\pm}=0 \tag{4}$$

$$\lambda-\frac{i\sqrt{2}b}{E}\left[\frac{d}{dr}-\lambda r-\frac{1\pm(l_0+\frac{1}{2})}{2r}\right]f_0^{\pm}+f_2^{\pm}=0 \tag{5}$$

$$\frac{-ia}{2(E-E_g)}\left[\frac{d}{dr}-\lambda r+\frac{1\mp\left(l_0+\frac{1}{2}\right)}{r}\right]\cdot f_0^{\mp}+f_3^{\pm}=0 \qquad (6)$$

$$\alpha=\frac{\sqrt{3}}{2}\sqrt{\left(l_0-\frac{1}{2}\right)\cdot\left(l_0+\frac{3}{2}\right)}$$

Here the following notations:

$$\begin{aligned} f_0^{\pm} &= f^{l_0}_{\frac{1}{2},\frac{1}{2},0} \pm f^{l_0}_{\frac{1}{2},-\frac{1}{2},0}\\ f_1^{\pm} &= f^{l_0}_{\frac{3}{2},\frac{3}{2},1} \pm f^{l_0}_{\frac{3}{2},-\frac{3}{2},1}\\ f_0^{\pm} &= f^{l_0}_{\frac{3}{2},\frac{1}{2},1} \pm f^{l_0}_{\frac{3}{2},-\frac{1}{2},1}\\ f_0^{\pm} &= f^{l_0}_{\frac{1}{2},\frac{1}{2},1} \pm f^{l_0}_{\frac{1}{2},+\frac{3}{2},1} \end{aligned} \qquad (7)$$

are used.
As well as:

$$\frac{C^{0,1}_{1/2,1/2}}{i\chi}=\frac{ia}{E-E_g},\quad \frac{C^{1,0}_{1/2,1/2}}{i\chi}=\frac{ia}{E+\Delta},$$
$$\frac{C^{0,1}_{1/2,3/2}}{i\chi}=\frac{ib}{E-E_g},\quad \frac{C^{1,0}_{3/2,1/2}}{i\chi}=\frac{ib}{E} \qquad (8)$$

where Eg is the energy of the bottom of conduction band, Δ is the spin-orbit-splitting energy. The parameters a,b are matrix elements of coupling between the conduction and valence bands. The quantities like $C^{0,1}_{1/2,1/2}$, $f^{l_0}_{\frac{1}{2},\frac{1}{2},0}$ etc. and χ are determined in Gelfand et al [8]. The system of equations (1)-(6) are rewritten so in order to separate the independent solutions ("even" and "odd").

2. THE ENERGY SPECTRUM

Substituting (4)-(6) in (3) we have obtained:

$$\left\{\left[\frac{d^2}{dr^2}+\frac{2}{r}\frac{d}{dr}-\frac{(l_0+\frac{1}{2})(l_0+\frac{1}{2}\pm 1)}{r^2}-\lambda^2r^2-3\lambda\left[\frac{a^2}{4(E-E_g)(E+\Delta)}+\frac{2b^2}{E(E-E_g)}\right]+1\right.\right.$$
$$\left.\left.\pm\left[\frac{a^2}{2(E-E_g)(E+\Delta)}-\frac{2b^2}{E(E-E_g)}\right]\lambda\left(l_0+\frac{1}{2}\pm 1\right)\right\}f_0^{\pm}=0 \qquad (9)$$

Energy spectrum is given by:

$$\varphi(E)=2\lambda\left(N+\frac{3}{2}\right) \qquad (10)$$

where

$$\varphi(E)=\frac{4E(E-E_g)(E+\Delta)}{a^2E+8b^2(E+\Delta)}\pm\lambda\left(l_0+\frac{1}{2}\pm 1\right)\frac{2a^2E-8b^2(E+\Delta)}{a^2E+8b^2(E+\Delta)}-3\lambda \qquad (11)$$

and the corresponding eigenfunctions read:

$$f^{\pm}_{0,n}=A_{nl_0\pm\frac{1}{2}}r^{l_0\pm\frac{1}{2}}\exp\left(-\frac{\lambda r^2}{2}\right)L_n^{l_0\pm\frac{1}{2}+\frac{1}{2}}(\lambda r^2) \qquad (12)$$

where $L_n^{l_0\pm\frac{1}{2}+\frac{1}{2}}(\lambda r^2)$ is an associated Laguerre polynomial, $N=2n+l_0\pm1/2$,n=0,1,2,..is a principal quantum number. The normalization constants are:

$$A_{nl_0\pm\frac{1}{2}}=\left[\frac{2\lambda^{l_0\pm\frac{1}{2}+\frac{1}{2}}n!}{\Gamma\left(n+l_0\pm\frac{1}{2}+\frac{3}{2}\right)}\right]^{\frac{1}{2}},\ \lambda=\frac{m_n\omega}{\hbar} \qquad (13)$$

The parameters a and b are related to the effective mass as follows [11]:

$$\frac{\hbar^2}{2m_n}=\frac{2b^2}{E_g}+\frac{1}{4}\frac{a^2}{E_g+\Delta}\ ;\ \frac{\hbar^2}{2m_{sh}}=\frac{1}{4}\frac{a^2}{E_g+\Delta};$$

$$\frac{\hbar^2}{2m_{1h}}=\frac{2b^2}{E_g} \qquad (14)$$

where m_n, m_{1h} and m_{sh} are the effective masses of electron, light hole and spin-orbit splitting hole, correspondingly.

A case $a=\frac{2}{\sqrt{3}}P$, $b=\frac{1}{\sqrt{3}}P$ corresponds to one parameters Kane model and using (14) we find:

$$\varphi(E)=\frac{2mn}{\hbar^2}\cdot\left(\frac{E(E-E_g)(E+\Delta)}{E_g(E_g+\Delta)}\frac{E_g+\frac{2}{3}\Delta}{E+\frac{2}{3}\Delta}\mp\frac{\frac{2}{3}\Delta}{E+\frac{2}{3}\Delta}\frac{\hbar\omega}{2}\left(l_0+\frac{1}{2}\pm1\right)-3\frac{\hbar\omega}{2}\right) \qquad (15)$$

Using (12) in (4), (5) and (6), we get $f_1^{\pm}$, $f_2^{\pm}$ and $f_3^{\pm}$:

$$f_{1,n}^{\pm}=\frac{i\sqrt{2}b}{E}\frac{\alpha}{r}f_{0,n}^{\pm} \qquad (16)$$

$$f_{2,n}^{\pm}=\frac{i\sqrt{2}b}{E}\left[\left(\frac{4n-1+2l_0\pm1\mp(l_0+1/2)}{4r}-\lambda r\right)f_{0,n}^{\pm}-\frac{\sqrt{n(n+1/2+l_0\pm1/2)}}{r}f_{0,n-1}^{\pm}\right] \qquad (17)$$

$$f_{3,n}^{\pm}=-\frac{i\alpha}{E+\Delta}\left[\left(\frac{2n\mp1+l_0(1\mp1)}{2r}-\lambda r\right)f_{0,n}^{\mp}-\frac{\sqrt{n(n+1/2+l_0\pm1/2)}}{r}f_{0,n-1}^{\mp}\right] \qquad (18)$$

The equations (15) describes the spectrum of electrons, light and spin-orbit splitting hole bands .

As well as in a case Dirac of oscillators in ground state energy appears twice more, than for isotropic oscillator of the standard Schrodinger equation .

The equations (15) might be useful in analysis of an influence of the nonparabolicity on a energy spectrum of electrons in a quantum dot.

CONCLUSION

The oscillator equation is obtained from a system of the equations for multiband Hamiltonian describing spectrum of electrons, light and spin-orbit-splitting hole bands in Kane semiconductors by the method of a minimal interaction.The solution of this equation allows to describe the influence of nonparabolicity on a spectrum of electrons in a quantum dot.

Recently this problem has been considered in [10,11] within the framework of the infinite potential barrier model. The advantage of our consideration consists of obtaining of the analytical expressions and the possibility of their analysis in comparision with numerical calculations [10,11].

The author thanks Prof. Gashimzade F.M.and Alekperov O.Z. for helpful discussions.

[1] *N.E.Kaputkina, Y.E.Lozovik.* Fiz. Tver. Tela, 1998, v.40, 11, p. 1753-1759.

[2] *N.E.Kaputkina, Y.E.Lozovik.* Fiz. Tver.tela v, 1998, 40,9,2134-2135.

[3] *O. Darnhofer, U.Rössler.* Phys. Rev., B47, 1993, 23, 16 020.

[4] Janes P Crawford J. Math. Phys., 1993, v. 34, 10, p. 4428-4435.

[5] *J.Benitez*, R. P. Martinez y Romero Phys. Rev Lett., 1990, v.64, 14.

[6] *M. Moshinsky and A .Szezepanik*, J. Phys., 1989, A 22, L817.

[7] *P. A. Cook* Lett. Nuovo Cimento, 1971, 1, 419.

[8] *I.M. Gelfand, R.A. Minlos, Z.Y.* Shapiro. Representation of group of rotations and group of Lorentz, Fizmatgiz, 1958.

[9] *G.Y. Lyubarskiy.* Group theory and its application to physics. Fizmatgiz, 1957.

[10] *Al. L.Efros and M. Rosen.* Phys. Rev B58, 1998, p. 7120-7135.

[11] *F.M. Gashimzade, A.M. Babaev, M.A. Bagirov* J.Phys.:Cond.Matter 2000, 12, p.7923-7932.

THE KANE OSCILLATOR

A.M. Babayev

KEYN OSSİLYATORU

Parabolik saxlayıcı potensiala malik kvant noqtələrində elektronların, yüngül və spin-orbital parçalanmis deşiklərin spektrlərini xarakterizə edən Keyn ossılyatorunun enerji spektləri və dalğa funksiyaları tapılmışdır.

A.M. Бабаев

КЕЙНОВСКИЙ ОСЦИЛЛЯТОР

Найден энергетический спектр и волновые функции кейновского осциллятора, описывающего спектр энергии электронов, легких дырок и спин-орбитально отщепленной зоны дырок в квантовой точке с параболическим удерживающим потенциалом.

Received:21.09.01

THE IMPROVEMENT OF THE SUPER CONDUCTING PROPERTIES OF THE $YBa_2Cu_3O_{7-\delta}$ COMPOUNDS BY NEUTRONS IRRADIATION

G. KARCHAVA, N. KEKELIDZE, G. TSINTSADZE
Tbilisi State University, Department of Physics,
Chavchavadze Ave.,1, Tbilisi, 380028, Georgia

N. GUSKOS, P. EUTHYMIOU
University of Athens, Department of Physics, Section of Solid State Physics,
Panepistimiopolis, GR 157 84 Zografos, Athens, Greece

V. ALIYEV
[3]Institute of Physics of National Academy of Sciences
H.Javid Ave., 33, Baku, 370143, Azerbaijan

The effect of the increase of the critical temperature T_c by the irradiation of the Y123 samples with small doses of fast neutrons has been investigated by the temperature dependence of resistance and by EPR studies. The results indicated that T_c and EPR signals of all specimens increased with growth of irradiation doses. Meanwhile all three-lattice parameters decreased. These results are explained in terms of redistribution of the oxygen. which promotes the intensification of the interaction between Cu^{2+} ions and the improvement of super conducting properties of the specimens.

1. INTRODUCTION

The irradiation of some materials with small doses of radiation stimulated some processes, which result in the improvement of the crystal structure. This phenomenon is attributed to the decrease of defects by the recombination of the interstitial atoms with the vacancies [1,2]. In such case neutrons act like billiards. This is known as the effect of small doses in semiconductor physics and later was applied to high temperature superconductors.

In reference [3] it was found that the irradiation of the $Yba_2Cu_3O_{7-\delta}$ and $Pb_xBi_{1-x}Ca_2Sr_2Cu_3O_{10}$ samples with small doses of fast neutrons resulted in the increase of the critical temperature by ΔT_c =3.9K for the former system and by ΔT_c=5.8K for the latter system. It was attributed to reduction of the number of defects in the Cu-O chains.

It was reported [4] that the magnetism associated with the Cu-O units plays an important role in the super conducting properties of HTSC. Observation of the EPR signal in the cuprite superconductors was expected because the majority of copper ions are in the divalent state, as nuclear magnetic resonance, neutron scattering, photoemission and muon resonance studies have indicated it. HTSC cuprites and their insulating AFM parent compounds have been subjects of numerous EPR investigations in view of the possibility of direct access to the static and dynamic properties of the intrinsic Cu^{2+} ions. EPR signals of the superconductor compounds were attributed to the interaction between these ions [4].

Authors [5] investigated the effect of the fast neutron irradiation on the critical current density (J_c) and microstructure characteristics of highly textured YBCO bulks prepared by the powder melting process (PMP). Five similar samples were irradiated by fast neutrons with different fluents, from $5,1\times10^{16}$ to 6×10^{17}n/cm^2. The results indicated that the critical temperature (T_c) of (PMP) specimens decreased insignificantly after irradiation with fluents up to 6.1×10^{17}n/cm^2, and the J_c values increased monotonically with radiation doses.

It was reported [6], that the critical temperature enhancement was detected in the same compound by the gamma irradiation at the nitrogen boiling temperature. This experiment was held in our laboratory.

In this report we investigate the effect of small doses in the HTSC cuprites by the temperature dependence on the resistance and by the EPR measurements for several samples before and after irradiation with small doses of fast neutron irradiation.

2. EXPERIMENT

$YBa_2Cu_3O_{7-\delta}$ (Y123) ceramic samples were prepared using the solid-state reaction method. The powders were mixed and sintered in air three times and afterwards the materials were annealed in the flowing oxygen. Samples were identified by XRD measurements and Rietveld refinement, which showed that they were single phase with a high degree of orthorombicity.

We have taken four Y123 samples with different T_c. We have measured their critical temperatures from the dependence of the resistivity versus the temperature by the ordinary four contacts method (which were made of silver paste), and also the EPR signals before and after the irradiation. We have detected the super conducting transition temperature (T_c) by the middle point of the transition.

We have measured the EPR signals from the powders of the samples at the room temperature. We have taken the exactly same masses for the corresponding powders of the samples before and after irradiation.

The fast neutrons held the irradiation of the samples in the horizontal tunnel of the reactor at the temperature about 340K. The slow neutrons were cutted by a filter of the cadmium. Each specimen was irradiated once. The first N1 specimen was irradiated with three fluents of 10^{11}n/cm^2, 10^{12}n/cm^2 and 10^{13}n/cm^2. The second specimen N2 was irradiated with two fluents of 10^{11}n/cm^2 and 10^{12}n/cm^2. The third N3 and fourth N4 specimens were irradiated with one fluent

fluent of 10^{12}n/cm^2. For the fourth N4 specimen we have performed the Rietveld refinement before and after the irradiation.

3. RESULTS AND DISCUSSIONS

The dependence of the resistance versus temperature for the specimen N1 is shown on fig.1. We observed the increase of the T_c with growth of irradiation fluents, which is accompanied by a decrease of the resistance transition width.

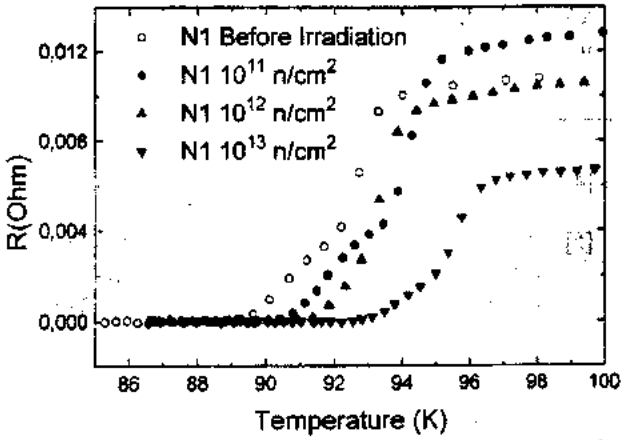

Fig.1. The temperature dependence of the resistance for the sample N1 before and after the irradiation for different fluent.

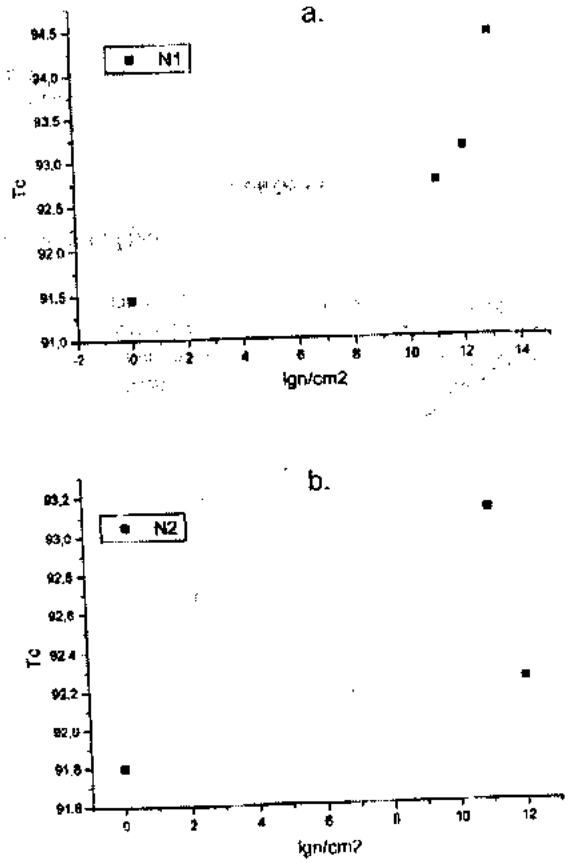

Fig2. The critical temperature versus the fluent: 2(a) sample N1, 2(b) sample N2.

Fig.2 (a) shows that for specimen N1 before the irradiation T_c was 91.44K and after the irradiation with fluents 10^{11}n/cm^2, 10^{12}n/cm^2 and 10^{13}n/cm^2 was 92.19K, 93.19K and 94.43K respectively. Fig.2 (b) shows that for the sample N2 the T_c was 91.79K before the irradiation and after the irradiation with the fluent 10^{11}n/cm^2 it increased to 93.12K but with the fluent 10^{12}n/cm^2 it decreased to 92.24K. From comparison of T_c's for specimens N1 and N2, we can see that the T_c of the specimen N1 increases up to 10^{13}n/cm^2, whereas for the specimen N2, the T_c decreases between the fluents of 10^{11}n/cm^2 and 10^{12}n/cm^2. We have also found that for the specimen N3 before the irradiation T_c was 90.02K and after the irradiation with the fluent 10^{12}n/cm^2 T_c became 91.34K. Regarding the sample N4 before the irradiation its T_c had been 90.04K and after the irradiation with the fluent 10^{12}n/cm^2 T_c became 91.34K. Fig.3 shows the EPR spectra for the N1 and N3 specimens. For both of them the EPR signal increased after the irradiation with the fluent 10^{12}n/cm^2 with respect to the EPR signal before irradiation.

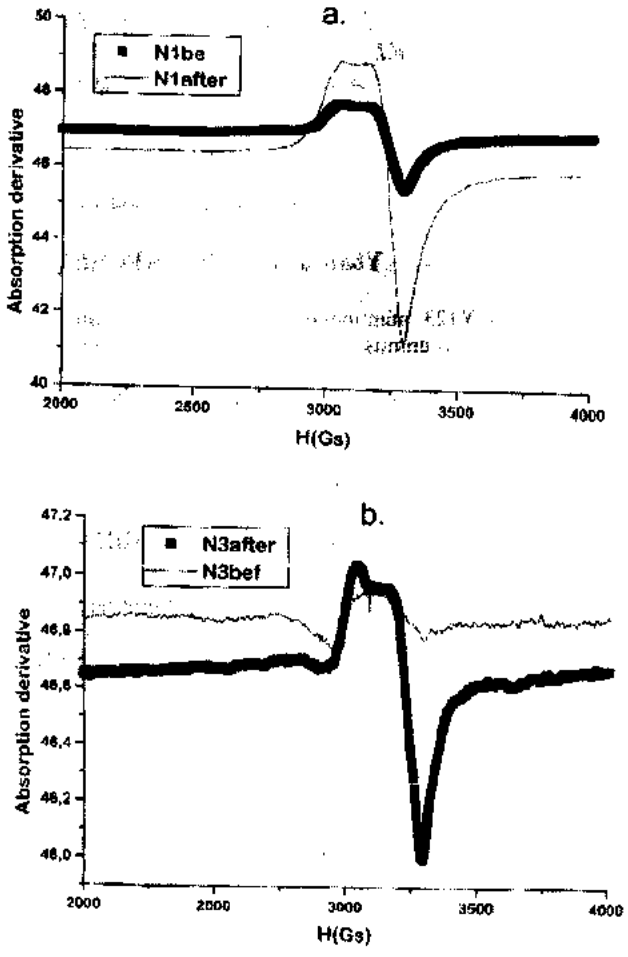

Fig.3. EPR spectra before and after the irradiation: 3(a) sample N1, 3(b) sample N3.

We have also calculated the lattice parameters for the specimen N4 before and after the irradiation with the fluent 10^{12}n/cm^2. The lattice parameters that we have obtained are as follows:

(a=3.82506⇒b=3.88615⇒c=11.67384⇒) before the irradiation and

(a=3.82486⇒b=3.88459⇒c=11.67069⇒) after the irradiation.

So, the reduction of the lattice parameters confirms that the superconducting properties are improved after the irradiation.

These results suggest a correlation between the increase of T_c and the EPR intensity and decrease of the lattice parameters after fast neutron irradiation. We suppose, that small doses of fast neutrons cause the recombination effect of the interstitial atoms with the vacancies. This effect mainly concerns the oxygen atoms, because of their lightness. We think that this process improves the crystal lattice, orders of the conducting planes and Cu-O chains, reduces the lattice parameters and increases T_c.

We suppose that the reduction of the lattice parameters (or in the other words the compression of the elementary cell) provokes the reduction of the distance between Cu^{2+} ions and therefore the reinforcement of the interaction between them. We assume that this reinforcement is the reason of the rise of the EPR signal and the critical temperature and generally the improvement of the super conducting properties of the compound by small doses of the neutrons irradiation.

AKNOWLEDGEMENT

We thank the members of the Institute of Materials Science NCSR 'DEMOKRITOS': Dr. K. Papastaikoudis, Dr. D. Andonopoulos, Dr. K. Papasgeogiou, Mr. N. Salamouras and Ms. M. Giannouri for their help at the experimental measurements.

[1] *G.P. Peka, O.A. Tokalin.* Optoelectronic and Semiconductor technics. 1988, 14, 1.

[2] *A.P. Galushka N.S Bogdaniuk, G.E. Davidiuk.* Izv. Vuzov. Ser. "Physica", 1982, 3, 126.

[3] *A.A. Alekseenko, A.V. Bukalov, A.P. Galushka, P.P. Gorbik, B.M. Gorelov, V.I. Marchenko, V.M. Ogenko, A.P. Pogoreli.* Superconductivity: physics, chemistry, techniques. 1992, 1, 100.

[4] A.Punnose and R.J.Singh, Int. J. Mod. Phys. B 35, 1994, 1123.

[5] P.X. Zhang, L. Zhou, W.M. Bian, P.Ji, K.J. Wang, X.Z.Wu, R.Puzniak, A.Wisnievski, M. Baran, and H. Szymczak. Physica C, 1, 282-287 (1997)

Q. Karçava, N. Quskov, V. Əliyev, N. Kekelidze, Q. Tsintsadze, P. Eufemiu

$YBa_2Cu_3O_{7-\delta}$ İFRATKEÇİRİCİSİNİN XASSƏLƏRİNİN YAXŞILAŞDIRILMASI

Məqalə Y123 nümunələrini kiçik dozalı sürətli neytronlarla şüalandırdıqdan sonra T_c kritik temperaturunun artmasının tədqiqinə həsr olunmuşdur. Nümunələrin EPR spektri və müqavimətin temperatur asılılığı öyrənilmişdir. Tədqiqatlar göstərir ki, şüalanma dozası artdıqda nümunələrdə T_c və EPR siqnalı artır. Bu zaman həm də qəfəs parametrlərinin kiçilməsi müşahidə olunur. Alınmış nəticələr oksigen atomlarının yenidən paylanması və bununla da Cu^{2+} ionları arasında qarşılıqlı təsirin güclənməsi ilə izah olunmuşdur.

Г. Карчава, Н. Гуськов, В.Алиев, Н. Кекелидзе, Г. Цинцадзе, Р. Эуфемиу

УЛУЧШЕНИЕ СВЕРХПРОВОДЯЩИХ СВОЙСТВ $YBa_2Cu_3O_{7-\delta}$ ПОСЛЕ ОБЛУЧЕНИЯ НЕЙТРОНАМИ

В работе изложены результаты исследования эффекта увеличения критической температуры T_c Y123 образцов после облучения малыми дозами быстрых нейтронов. Изучены ЭПР-спектры и зависимости сопротивления от критической температуры. Результаты показали, что T_c и ЭПР сигналы всех изучаемых образцов растут с увеличением дозы облучения. Наблюдается также уменьшение параметров кристаллической решётки. Полученные результаты объясняются перераспределением атомов кислорода, что в свою очередь вызывает усиление взаимодействия между ионами Cu^{2+} и улучшение сверхпроводящих свойств образцов.

Received: 12.07.01

APPLICATIONS OF MID-IR LASERS

O.I. DAVARASHVILI, M.I. ENUKASHVILI, N.P. KEKELIDZE, L.P. BYCHKOVA, M.T. EBRALIDZE

Tbilisi State University

1, ave. Chavchavadze, 380028, Tbilisi, Georgia

V.A. ALIYEV

Institute of Physics of Azerbaijan National Academy of Sciences

H.Javid, av., 33, Baku, 370143

The new stage is creation of the multicomponent laser gas-analyzator for early diagnostics and measure of pollutants in atmosphere with the high sensitivity on the level $\sim 10^{-8} \div 10^{-9}$. Thus in this work was established that mid-IR lasers are very promising for creation of: a) Devices for early diagnostics and control of therapy; b) Devices for the atmosphere monitoring of SO_2, CO, NH_3, N_2O and other components content in the air on of the level of 10^{-7}-10^{-9} of main components; c) New type spectrometers with 10^{-4}cm^{-1} resolution; d) Technological control devices for chemistry, metallurgy, electronics.

Three types of compound semiconductor materials are used to make mid-IR lasers: IV-VI materials (lead salts), III-V materials containing antimony, III-V quantum cascade (QC) structures. Mid-IR lasers made from IV-VI compound semiconductors are in the best position to reach pulse and CW operational temperature above 200-220 K, when thermoelectric cooling modules operate. However today the operating temperature for the most of laser devices in practical experiments is 77 K (liquid nitrogen temperature).

Mid-IR lasers were fabricated on the basis of IV-VI multicomponent semiconductor materials, which allow to reduce the generation threshold, and increase radiation power [1]. The lasers are easily tunable under external influence – temperature, magnetic field, pressure and operate in the spectral range 5-25 μm which involves "atmospheric windows" and oscillatory-rotatory absorption bands of the most molecular gases. Therefore they are mainly used in the following fields:

1. High – resolution molecular spectroscopy.
2. Analysis of gas mixture samples at a low pressure.
3. Measurements in the open atmosphere.

In table 1. basic parameters of pulsed lasers are presented.

Table 1

Parameters measured	Parameter variation range
1. Operating temperature range T, K	77-180
2.Total range of radiation frequency tuning with current and temperature, cm^{-1}	200-300
3.Range of a single mode tuning cm^{-1}	0,5-4
4.Power in all modes, mW	1-5
5.Power in a single mode, mW	0,1-1,5
6.Rate of radiation frequency tuning of a single mode, cm^{-1}/s	10^2-10^6
7.Generation linewidth, cm^{-1}	$\leq 10^{-4}$

Requirements imposed upon semiconductor lasers depend essentially on the problem being decided. The most stringent of them are determined by molecular spectroscopy problems and in particular, by spectroscopy of collisional broadening and shift with the spectral resolution $\delta\nu \leq 10^{-3}$cm^{-1} and S/N ratio$\approx 10^3$ which is important for the required precision level of measurements.

For the spectral absorption gas analysis performed at a reduced pressure (e. g. sampling into a multipass optical cell) the spectral resolution $\approx 10^{-3}$-10^{-2}cm^{-1} should be provided, which is necessary for a spectral contrast increase and selective isolation of separate slightly broadened lines at the expense of a buffer gas pressure – air, as a rule. At the output of the recording system the S/N ratio should be $\geq 10^3$. In this case detection of molecular impurities with minimal relative concentration $C_{min} \approx \frac{1}{\sigma l N_0} \cdot \frac{\Delta P}{P} = 10^{-7}$ is possible (Here the absorption cross-section $\sigma = 10^{-17}$cm^{-2}, the absorbing layer thickness l=100m, the total molecular number per unit volume $N_0 = 10^{17}\,cm^{-3}$, $\frac{\Delta P}{P} = \frac{N}{S}$). The important feature of this problem is the need for such high parameters at field measurements, i. e. at laser operating temperatures not less than 80-100 K (liquid nitrogen temperature).

During measurements in the open atmosphere, at so-called route measurements, the resolution may be below $\approx 10^{-2}$ cm^{-1}. However, high output power of semiconductor lasers is also required in order that after passing the route up to 500 m long the S/N ratio at the output of the recording system (without accumulation) should be not less than 10^3.

Let us define laser's power satisfying the above mentioned requirements. Laser power can be estimated as $P = P_n S/N$, here $P_n = NEP\sqrt{\Delta\beta}$ - noise power, $NEP \approx 10^{-10} W\ Hz^{-1/2}$ – power equivalent to noise for Ge or Si and CdHgTe photodetectors. Then at ΔB=1 MHz mode radiation power $P_n \approx 100 \mu W$ is required to obtain $S/N \approx 10^3$.

Together with the Institute of General Physics and Institute of Spectroscopy Russian Academy of Sciences out investigations were realized in high-resolution spectroscopy, applied spectroscopy and gas analysis; using heterolasers with PbSnSeTe isoperiodic layers and homolasers with controlled carrier concentration.

High – resolution spectroscopy. Absorption spectra of a whole numbers of molecular gases: H_2O, NH_3, O_3, SF_6, GeH_4, CF_4, CO_2 and etc. have been recorded with high – resolution and investigated. In particular, by application of lasers with controlled carrier concentration profile n^+-n-p^+

PbSe, extended and completely resulted areas of SO_2 absorption spectra in the ν_1 and ν_3 fundamental band region have been investigated [2]. Frequencies and intensities of 497 absorption lines have been determinated. The accuracy of line frequencies measured experimentally is $3 \cdot 10^{-4}$ cm^{-1}, which is significantly above the error $\approx 10^{-3}$ cm^{-1} of theoretical description based on the available theoretical models. In this case the generation pulse was up to 700 μs, which allowed to use comparatively low tuning rates and to obtain the mentioned accuracy of spectral parameter measurement.

CF_4 molecule spectrum was also recorded at a temperature T=77 K [3], which allowed to decrease the Doppler linewidth and observe in more detail the thin multiplet structure in the region of "overturn". The perfectly resulted spectrum obtained experimentally in this work is necessary for a quantitative evolution describing ν_3 CF_4 band R branches for high values $J \geq 20$.

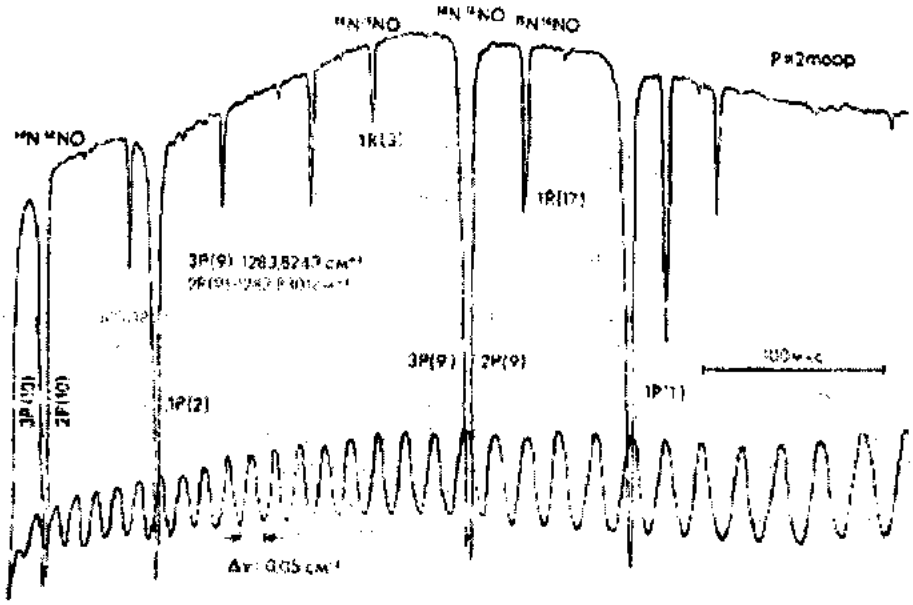

Fig.1. N_2O molecular spectrum in the range 1282.9-1284.4 cm^{-1}

In fig. 1 N_2O molecular spectrum portion within 1282,9 – 1284,4 cm^{-1} is shown [1]. The spectrum is recorded at a single diode laser frequency scan. On the spectrum the lines of three isotopic modifications of N_2O $^{14}N^{14}N^{16}O$ (1283, 669 cm^{-1}), $^{15}N^{14}N^{16}O$ (1283, 824cm^{-1}), $^{14}N\,^{15}N\,^{16}O$ (1283, 919 cm^{-1}) are clearly seen. In P(9) band $5 \cdot 10^{-3}$ cm^{-1} resolution is obtained. Below a Fabry – Perot etalon spectrum with 0,05 cm^{-1} free dispersion region is given.

Applied spectroscopy. In [4] a new method of TEA CO_2 – laser generation linewidth determination is proposed and used. Knowledge of TEA CO_2 – laser generation linewidth is important for evolution of molecule oscillatory excitation under non – collisional conditions from separate rotatory levels. The method of "burning out" of the downfall in the SF_6 absorption spectrum in a pulse supersound stream (fig. 2) and further measurement of the downfall with heterolaser enabled one to establish a CO_2 laser generation spectrum width 0,013±0,002 cm^{-1}.

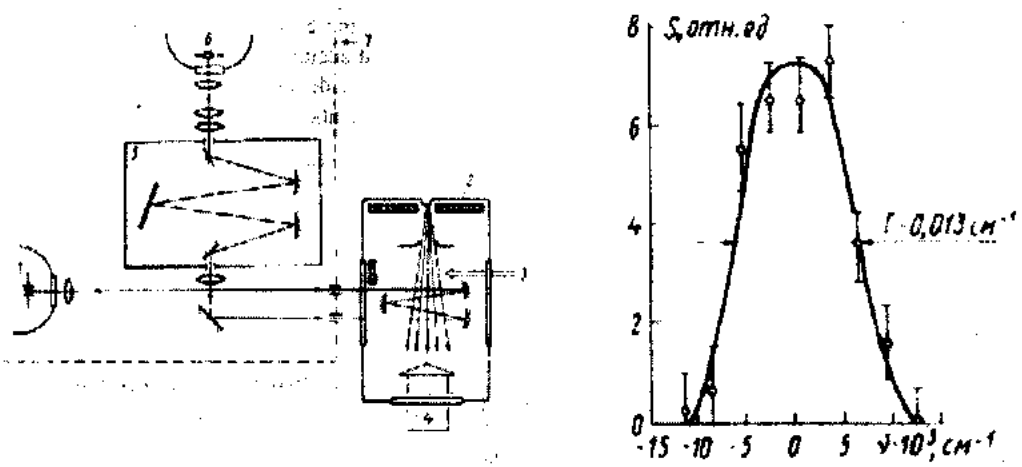

Fig.2. Experimental plant scheme: a) 1- Dl, 2– vacuum chamber with a nozzle. 4 – CO2 lazer measurement, 5– diffusion monochromator, 6– photoresistor, 7 – screen
b) induced clarification S in the SF6 molecula absorption spectrum

Gas analysis possible. On the basis of developed NH_3 microconcentration analysis operating within ≈ 10μm wave length range, where ammonia has the most intensive absorption lines up to 10^{-2} cm^{-2}. atm^{-1} [5]. Application of Ag Cl – Ag Br fiber optics, multipass cells and heterolasers for the 10μm range allows to achieve a minimally detectable ammonia concentration in the mixture – 10^{-7} and the sensitivity can be brought to 10^{-9} with a signal accumulation time increase. This sensitivity is sufficient for a measurement of NH_3 background content in the atmosphere (which is 10^{-8}).

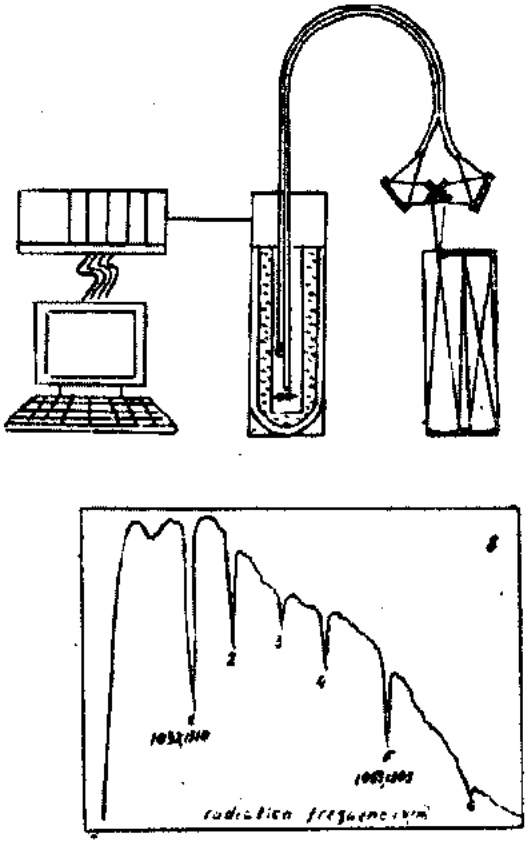

Fig.3. a) Fiber-optics gas analyzer scheme
b) NH_3 transmission spectrum in the range 1030-1055cm-1

Compact fiber optical devices also enable one to carry out classical spectral investigations. As an example a number of ν_2 fundamental ammonia absorption band lines were recorded whose parameters are given in table 2.

Table 2

N	Line colentification	Line frequency cm^{-1}	Line intensity $cm^{-2}atm^{-1}$
1	aR (4.3)	1032, 1310	5,2
2	aR (4.2)	1033, 1358	3,1
3	aR (5.5)	1049, 3464	1,2
4	aR (5.4)	1051, 5120	1,9
5	aR (5.3)	1053, 1305	4,6
6	aR (5.2)	1054, 2527	2,5

The application of fiber optics elements (fig. 3) simplifies essentially the optical scheme and device tuning.

In [6] lasers were used for SO_2 detection in the spectral ranges 1280 and 1065 cm^{-1}.

SO_2 spectrum portion evolution with a change in the buffer gas (nitrogen) pressure has been investigated. SO_2 line collisional broadening coefficients are determined and the dependence of spectrum contrast on partial pressures in the mixture is studied, which is necessary for the choice of optimal conditions for SO_2 recording in the atmosphere.

Multifunctional spectrometer on the basis of tunable mid-IR lasers was developed and created: with high resolution on the 10^{-4} cm^{-1} level, multicomponent gas analysis with 10^{-7} – 10^{-8} sensitivity, bench for investigation of new types of photoreceivers and lasers [7].

The new stage is creation multicomponent laser gas-analyzator for early diagnostics and measure pollutants in atmosphere with high sensitivity on the level $-10^{-8} \div 10^{-9}$ [8-9]. Thus in this work was established that mid-IR lasers are very promising for creation of:

1. Devices for early diagnostics and control of therapy.
2. Devices for atmosphere monitoring SO_2, CO, NH_3, N_2O and other components content in the air on the level of 10^{-7}-10^{-9} of main components.
3. New type spectrometers with 10^{-4} cm^{-1} resolution.
4. Technological control devices for chemistry, metallurgy, electronics.

[1] *L.P. Bychkova, G.G. Gegiadze, O.I. Davarashvili, M.I. Enukashvili, N.P. Kekelidze, V.G. Koloshnikov, V.M. Krivtsun, A.P. Shotov.* Bulletin of the Academy of Sciences of GSSR., 1989, v.136, № 2, 305.

[2] *O.I. Davarashvili, F. Klunemann, N.V. Lemekhov, O.V. Naumenko, E.V. Stepanov, C.N. Ulenikov.* In Coll.: Diode laser spectroscopy M, 1990, p. 65-91.

[3] *O.I. Davarashvili, B.I. Zhilinski, V.M. Krivtsun, D.A. Sadovski, E.P. Snegirev.* Pisma u IhETF. 1990, v. 5.1, № 1, p.17.

[4] *O.I. Davarashvili, A.V. Kunets, I.A. Kuritsin, G.N. Makarov, V.B. Mironenko, E. Pak, A.P. Shotov.* Quantum electronics, 1990, v. 17, № 8, p.1077.

[5] *O.I. Davarashvili, A.I. Kuznetsov, A.I. Nadezhdinski, S.V. Stepanov, I.I. Zasavitski, V.G. Plotnichenko, V.G. Artyushenko.* Proc-SPIE "Tunable diode laser application", 1992, v. 1724, p.1704.

[6] *L.P. Bychkova, O.I. Davarashvili, M.I. Enukashvili, N.P. Kekelidze, N.V. Lemekhov, A.I. Nadezhdinski, E.V. Stepanov, A.P. Shotov.* Bulletin of the Academy of Sciences of GSSR., 1989, 136, № 3, p.577.

[7] *L.P. Bychkova, O.I. Davarashvili, M.I. Enukashvili, N.P. Kekelidze, E.V. Stepanov, A.P. Shotov.* Bulletin of the Academy of Sciences of GSSR., 1998, 157, № 1, p.46.

[8] *O.I. Davarashvili, M.I. Enukashvili, N.P. Kekelidze, E.V. Stepanov, A.P. Shotov, V.A. Aliyev.* Fizika, 1999, № 2, p.78.

[9] *O.I. Davarashvili, E.V. Stepanov, I.V.Ponurovski and etc.* Procedings of the II International Conference on Molecular Spectroscopy. Moscow, 1998.

[10] *O.I. Davarashvili, M.I. Enukashvili, N.P. Kekelidze, E.V. Stepanov, A.P. Shotov.* Bulletin of the Academy of Sciences of Georgia 2000, v.161, № 2, 427.

O.I. DAVARASHVILI, M.I. ENUKASHVILI, N.P. KEKELIDZE, L.P. BYCHKOVA, M.T. EBRALIDZE, V.A. ALIYEV

O.İ. Davaraşvili, M.İ. Enukaşvili, N.P. Kekelidze, L.P. Bıçkova, M.T. Ebralidze, V.Ə. Əliyev

ORTA DİAPAZONLU İQ-LAZERLƏRİN TƏTBİQLƏRİ

$A^{IV}B^{VI}$ birləşmələrinin çoxkomponentli bərk məhlulları əsasında orta diapazonlu IQ lazerlər sürmə tərkibli $A^{III}B^{V}$ birləşmələri əsasında olan kaskad tipli lazerlərə nisbətən 200-220 K temperaturlarda impuls və kəsilməz rejimlərdə işləmək üçün daha perspektivlidir.

Bu lazerlərin yuksək ayırdetməli lazer spektroskopiyasında, tətbiqi spektroskopiyada və qaz analizində işlənmə nümunələri göstərilmişdir.

О.И.Даварашвили, М.И.Енукашвили, Н.П.Кекелидзе, Л.П.Бычкова, М.Т.Эбралидзе, В.А.Алиев

ПРИМЕНЕНИЯ ИК-ЛАЗЕРОВ СРЕДНЕГО ДИАПАЗОНА

Для среднего ИК диапазона лазеры на основе многокомпонентных твердых растворов соединений $A^{IV}B^{VI}$ перспективнее каскадных лазеров и содержащих сурьму на основе соединений $A^{III}B^{V}$ для работы в импульсном и непрерывном режимах при температурах 200 – 220 К лазеры в среднем ИК диапазоне.

Рассмотрены применения этих лазеров в спектроскопии высокого разрешения, прикладной спектроскопии и газоанализе.

Received: 11.06.01

VUV-REFLECTION SPECTRA OF PLUMBUM MOLYBDATE SINGLE CRYSTALS

N.G. DARVISHOV
Baku State University
Z. Khalilov str.23, Baku, 370148

The reflection spectra of $PbMoO_4$ single crystals have been studied in the energy range of 2÷41eV with the use of synchrotron radiation at T=300 K. The spectral dependences of optical functions, characterizing the electron structure of the given compound, have been calculated. It has been shown that the observed structure in the reflection spectra in the range of $h\nu$<20eV is attributed to interband optical transitions, and at $h\nu$>20eV is connected with intracentral transitions in Pb^{2+}. The bulk plasma vibration energy ($\hbar\omega$=26.5eV) of the valence electrons has been determined. The determining role of MoO_4^{2-} - tetrahedron in the formation of $PbMoO_4$ band structure is shown. It is assumed that the O 2p electron levels form the valence band, while the conduction band is formed by Mo 4d orbitals.

The $XMeO_4$ single crystals with the scheelite structure (where X=Pb,Ca,Sr, Me=Mo,W) are widely used in different acoustooptical devices as the fast deflectors of laser radiation [1], the active elements in solid-state lasers and ionizing radiation detectors in radiative-aggressive media [2]. For successful and effective usage of the given crystals in different optoelectron devices, the knowledge of their electron energy spectrum in the fundamental absorption region is necessary. The certain information about their peculiarities can be obtained from absorption and reflection investigations. In literature only several papers, dealing with the study of reflection spectra of scheelite series in the near-ultraviolet (UV) spectrum region, are known [3-7].

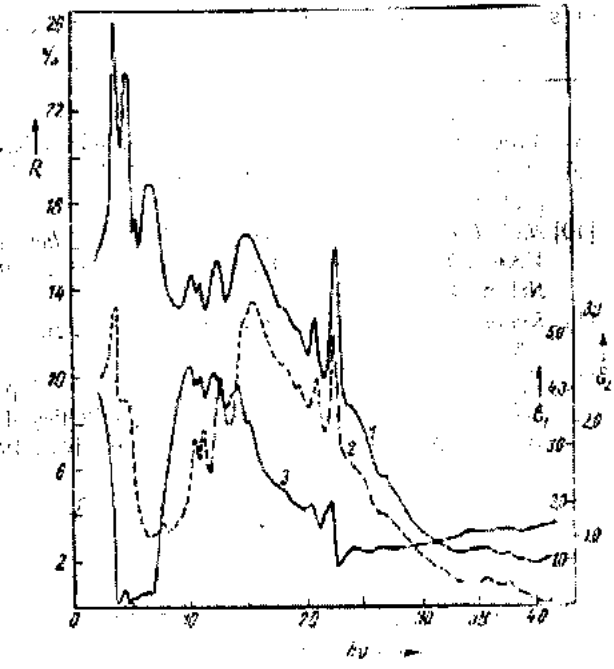

Fig.1 The spectral dependences of the reflection coefficient R(1), real ε_1 (2) and imaginary ε_2 (3) parts of the dielectric constant in $PbMoO_4$.

In the present paper the reflection spectra of $PbMoO_4$ crystals in vacuum UV region are first investigated with the use of the storage ring of synchrotronous center IYaF CO AN RF as the radiation source [8]. The energy region under study was 2÷41eV. The $PbMoO_4$ single crystals grown by the Czochralski method were investigated. The samples with the sizes of 10x8x6 mm cut off along the principal axes of the crystal were mechanically treated, their surfaces were treated according to the 14 class of accuracy. The measurements were carried out in the plane perpendicular to the c-axes of the crystal.

The spectral dependences of real ε_1 and imaginary ε_2 parts of the dielectric constant ε, the refractive and absorption indices, n and k, respectively, the characteristic loss functions $-Im(\varepsilon^{-1})$, the reduced density of states $\rho\sim\varepsilon(h\nu)^2$, the effective number of the valence electrons in the unit cell n_{eff}, and the effective value of the dielectric constant $\varepsilon_{0,eff}$. were calculated from the reflection spectra of $PbMoO_4$ by means of the Kramers-Kroning relationship according to the method described in [9].

The results of $PbMoO_4$ reflection spectra measurements are shown in fig.1. The spectral dependences of ε_1 and ε_2 are also presented in figure. As seen in fig.1, more than 10 reflection maxima, i.e. 3.65eV, 4.64eV, 5.08eV, 5.56eV, 6.8eV, 10.16eV, 10.97eV, 11.5eV, 12.27eV, 15.2eV, 18.1eV, are observed in the reflection spectrum in the energy range measured. The maximum reflection value at 3.65 eV is 45%. In the range of low energy values shown in fig.1 the reflection spectrum of $PbMoO_4$ has the similar form as other crystals with scheelite structure [3-5].

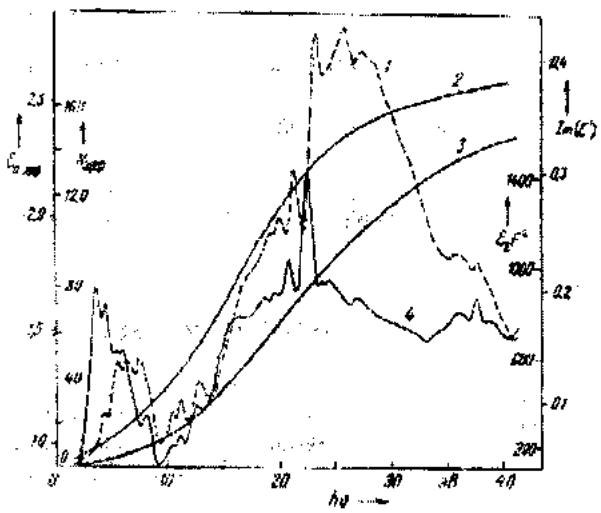

Fig.2 The spectra of the effective value of the dielectric constant $\varepsilon_{0,eff}$ (1), the reduced density of states $\rho\sim\varepsilon(h\nu)^2$ (2), the effective number of the valence electrons in the unitcell n_{eff} (3), the characteristic loss functions – $Im(\varepsilon^{-1})$ (4) in $PbMoO_4$.

The spectra of ε_1 and ε_2 well correlate with the reflection spectrum and reach the maximum values in the region

$h\nu$=3÷16eV. The low values of ε_1 and ε_2 indicate on a high degree of ionization of the given crystals. At $h\nu$>18eV the decay of optical functions of ε_1 and ε_2 is observed. The $\varepsilon_2(h\nu)^2$, $-Im(\varepsilon^{-1})$, n_{eff} and $\varepsilon_{0,eff}$ spectra are shown in fig.2. As seen from the $\varepsilon_2(h\nu)^2$ spectra, the density of states at the optical transitions at 18.1 and 22.2eV is rather high. The analysis of the- $Im(\varepsilon^{-1})$ spectrum allows to determine the energy of plasma vibrations of free electrons, $\hbar\omega$ =26.5eV. The dependence of $\varepsilon_{0,eff}$ on the energy $h\nu$ for $PbMoO_4$ has also a distinct saturation region at energies of $h\nu$>21eV. It means that the transitions corresponding to the two absorption bands with the maxima at 3.65 and 15.2eV make the most contribution to $\varepsilon_{0,eff}$. The low value of $\varepsilon_{0,eff}$ in saturation region also points on the essential role of the optical transitions from the deep d bands to $\varepsilon_{0,eff}$. The spectral dependence of n_{eff} indicates its continuous increase with distinct steps of growth at 3.65, 15.2 and 30eV, respectively. As n_{eff} is determined only by the behaviour of ε_2 and presents a total oscillator strength, then given steps of growth on the curve of n_{eff} point on the appearance of the new types of optical transitions in the investigated photon energy region.

The band structure calculations [10] and the similarity of reflection spectra of the crystals with scheelite structure in the low-energy spectrum region [3-7] points on the essential role of the MoO_4^{-2} tetrahedral groups in the formation of their band structure [3, 5-7, 10-12].

It is known that the chemical bond in tetraoxyanions is realized by the valence s, p and d - electrons of metal and $2p$-electrons of oxygen [3, 5, 10]. In the indicated complex tetraoxyanions the d- electron density of the central atom transforms through the irreducible representations of t and e symmetries, and the $2p$ - electrons of oxygen transform through the t, e, t_1 and a_1 symmetries [10-12]. Theoretical calculations and experimental investigations of mutual position of the X-ray spectra of oxygen and the central atom [11] allow to conclude that for the MoO_4^{-2} tetrahedron, the molecular orbitals, involving the $2p$-electron density of oxygen, are the upper occupied levels, and the d-states of molybdenum characterize the vacant molecular orbitals of the given complex. In this case, the conduction band in $PbMoO_4$ is splitted into two subbands separated by Δ=10.5eV. Such splitting is typical for electron states of the d-transition elements in the crystal field [12, 13]. A high value of Δ in $PbMoO_4$ is connected probably with the role of the heavy Pb atom involved in the scheelite lattice. Due to its large ionic radius and mass, it can considerably effects on the d - state of MoO_4.

The analysis of the reflection spectra in PbMoO and other compounds containing Pb and Bi, at $h\nu$>20eV, and also the X-ray photoelectron spectra of tetraoxyanions of transition metals [7,11,12] allow to assert that the observed triplet in the reflection spectrum (20.82; 22.53; 23.83 eV) is caused by intracentral transitions $5d_{5/2} \rightarrow 6p_{3/2}$, $5d_{3/2} \rightarrow 6p_{1/2}$, $5d_{3/2} \rightarrow 6p_{3/2}$ in the Pb ion. But the spectrum peculiarities at $h\nu$>30eV (35.4 and 37.55 eV) can be attributed to $O2s \rightarrow Pb6p$ transitions. Undoubtedly, some peculiarities take

[1] *L.G. Van Uiter*. In: Luminescence of inorganic solids. Academic Press, New York, 1966, p.465-540.

[2] *A.M. Gurvich, E.R. Ilmas, T.I. Savikhina, M.I. Tombak*. Zh. Prikl Spectrskopii, 1971, v.XIV, №6, p.1027.

[3] *R. Grasser, E. Pitt, A. Scharman, and G. Zimmerer*. Phys. Stat. Sol.(b), 1975, v..60, №1, p.359.

[4] *W. Walter and K.H. Bulter*. J.Electrochem.Soc., 1969, v.116, p.1245.

[5] *E.G. Reut*. Izv. AN SSSR, ser. Phys., 1985, v. 49, №10, p.2032.

[6] *Y. Zhang, N.A.M. Holzwarth, R.T. Williams*. Physical Rev. B, 1998, v.57, Iss.20, p.12738-12750.

[7] *X.L. Ye, C.S. Shi, C.X. Guo, X.Y. Yang, L.Q.Guo*. J.of Electron Spectroscopy and Related Phenomena, 1999, v.103, Iss. NSI., p.637-640.

[8] *Mamedov Amirulla M.* JETP, 1982, v.83, №11, p.1804.

[9] *D. Roesslor, M. Brit*. J.Appl. Phys., 1965, v.16, №18, p.1119.

[10] *N.G. Darvishov, B.M. Kasimov, Sh.M. Efendiev, and V.Kh. Sharbatov*. Vestnik of Baku University, 1983, №1, p.146-148.

[11] *Kebabchioglu and A. Muller*. Chem. Phys. Lett., 1971, v.8, p.59.

[12] *E.A. Kravtsova*. Zh. Struct. Khim., 1982, v.23, №5, p.55.

[13] *I.B. Bersuker*. Electron structure and the propeties of the coolrdination compounds. Leningrad, "Khimiya", 1986, p. 287.

N.H. Dərvişov

MOLİBDAT-QURĞUSUN MONOKRİSTALLARINDA VUB QAYTARMA SPEKTRİ

Sinxrotron şüalanma ilə T=300 K da 2-dən 41 eV qədər enerji intervalında $PbMoO_4$ monokristallarında qaytarma spektri öyrənilmişdir. Bu birləşmələrin elektron quruşunu xarakterizə edən optik funksiyaların spektral asılılıqları hesablanmışdır. Qeyd edilmişdir ki, qaytarma spektrində $h\nu$<20 eV oblastında müşahidə olunan struktura zonalararası keçidlərlə, $h\nu$>20 eV isə Pb^{2+} daxili keçidlər ilə əlaqədardır. Valent elektronların plazma rəqslərinə uyğun enerjisi təyin edilmişdir ($\hbar\omega$ =26,5 eV). Göstərilmişdir ki, MoO_4^{2-} tetraedri $PbMoO_4$ sona strukturunun formalaşmaşında əsas rol oynayır. O $2p$ elektron səviyyəsinin valent zonanı, Mo$4d$ orbitalın isə keçirici zonanı təşkil etdiyi söylənilmişdir.

Н.Г. Дарвишов

ВУФ-СПЕКТРЫ ОТРАЖЕНИЯ МОНОКРИСТАЛЛОВ МОЛИБДАТА СВИНЦА

Изучены спектры отражения монокристаллов $PbMoO_4$ в интервале энергий от 2÷41 эВ с использованием синхротронного излучения при T=300K. Рассчитаны спектральные зависимости оптических функций, характеризующих электронное строение данного

соединения. Показано, что наблюдаемая структура в спектрах отражения в области $h\nu$<20эВ связана с межзонными оптическими переходами, а при $h\nu$>20 эВ внутрицентровыми переходами в Pb^{2+}. Определена энергия объемных плазменных колебаний ($h\omega$ =26,5 эВ) валентных электронов. Показана основополагающая роль MoO_4^{-2} тетраэдра в формировании зонной структуры $PbMoO_4$. Сделано предположение о том, что электронные уровни O2p образуют валентную зону, а зона проводимости образована Mo4*d* орбиталями.

Received: 10.09.01

LUX-AMPERE CHARACTERISTICS AND PHOTOCURRENT KINETICS IN $Au_3In_5Se_9$ CRYSTALS

N.F. GAHRAMANOV, S.S. SADULOVA
Sumgait Technical University
373208, Sumgait, 43 quarter

Lux-ampere characteristics, kinetics and temperature dependence of the photocurrent for $Au_3In_5Se_9$ compound have been investigated under the light impact and Π-pulse excitation. The lifetime for non-equilibrium charge carriers has been determined.

INTRODUCTION

Photoconductivity spectra of $Au_3In_5Se_9$ compound at different directions of the electric field have been studied elsewhere [1].

In this paper results of the studies of lux-ampere characteristics (LAC), measured at different energies of incident quanta as well as the kinetics and temperature dependence of photocurrent under the light impact and excitation by Π-pulses are presented.

We used the method of rectangular modulation of light illumination to determine the non-equilibrium charge carriers lifetime. It is well known [2] that in this case exciting pulses must be classified as on intensity, and their duration in comparison with characteristic relaxation times of the majority and minority charge carriers.

In the measuring installation we have used light pulses of incandescent lamp (Π-pulse) as exciting source with a few minutes duration and light flash of $3\cdot10^{-6}$s duration by ИСШ-100 lamp. Exciting pulses have been divided in [3,4] on the intensity as follows: short pulses have high intensity (light impact), and long Π-pulses have low intensity. The chosen pulses allowed to find charge carriers lifetimes determined through slow and quick levels.

RESULTS AND DISCUSSION

Fig.1 presents LAC at different energies of incident quanta, corresponding to different points of the photoconductivity (PC) spectrum. Such choice of excitation energies allows to compare recombination processes in the volume and surface, as quanta, whose energies are higher than the band gap, are absorbed on the surface. It is seen from fig.1, that recombination mechanism for all cases is identical and LAC are sublinear ($n\propto I^{-1/2}$), fulfilling the square, bimolecular recombination mechanism.

From the analysis of LAC one can find only qualitative information on non-equilibrium charge carriers recombination mechanism. In fig.2 (curve 3) PC spectrum is presented at 100 K with 82 Hz frequency of the light intensity modulation. Light pulses had rectangular shape. It is seen from comparison of curves 3 and 2 (without modulation) that in the impurity absorption region the photoconductivity under modulated light is absent, and in other regions spectra have identical run. Difference is only in the fact, that the photocurrent in the range 1.2-1.38 eV under modulated light is higher, and in the 1.5 eV region is lower, than under the permanent illumination. The first difference is characteristic for all high-resistance photosensitive semiconductors [2].

The second difference can be connected with the fact, that quanta with energies higher than ΔE_g are adsorbed near the surface, where a number of localized states is greater than in the volume, i.e. a lifetime for non-equilibrium charge carriers may be calculated, if the amplification coefficient is known [5]. Calculated value for the non-equilibrium charge carriers lifetime is equal to $\tau\approx10^{-5}$c.

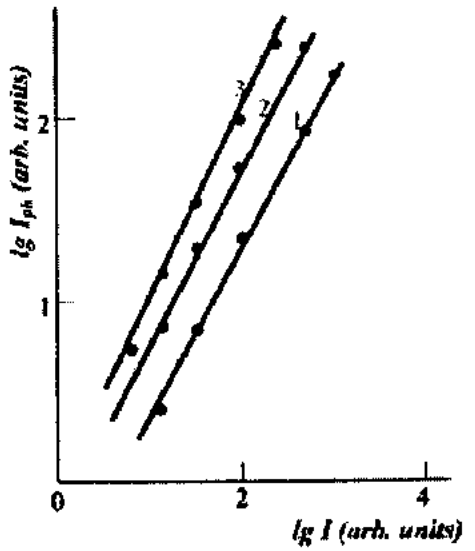

Fig.1 Lux-ampere characteristics of $Au_3In_5Se_9$ compound at different energies of incident quanta $h\nu$, eV: 1-1.1; 2-0.9 and 3-0.8 eV.

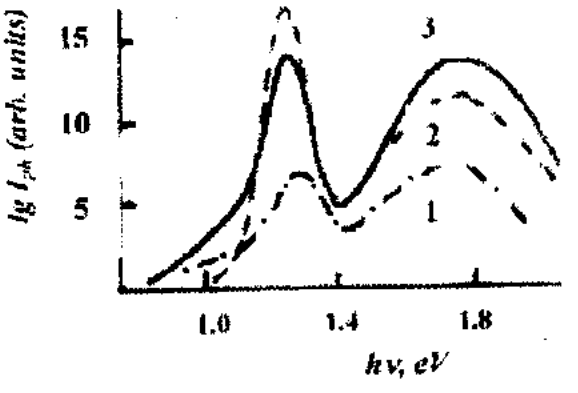

Fig.2 Photocurrent spectrum of $Au_3In_5Se_9$ single crystals under steady-state (1,2) and modulated illumination (3) at different temperatures, K: 1, 3 – 100, 2 – 300 K.

Non-equilibrium charge carriers lifetime can be determined more precisely from measurements of the photoconductivity kinetics [3]. Dependence of the photocurrent under

the fundamental excitaion of $Au_3In_5Se_9$ single crystals was studied. Energy of exciting quanta was equal to 1.3 eV and the light intensity of Π-pulse was $9 \cdot 10^2$ Lx. This value corresponds to the maximum of the photocurrent in the PC spectrum. Duration of the light pulse Δt many times exceeds the lifetime τ_n of majority charge carriers, i.e. we have the steady-state regime: $\Delta t \gg \tau_n$.

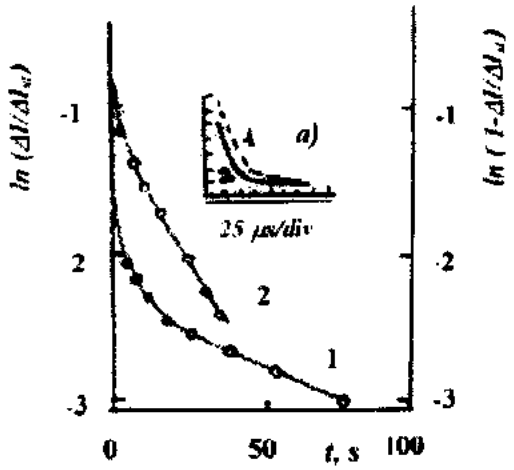

Fig.3 Kinetics of the current in $Au_3In_5Se_9$ compound under the light impact (a) and Π-pulse excitation: 1 – decay and 2 – rise curves.

As have been noted above, $Au_3In_5Se_9$ single crystals possess the high photosensitivity. In such semiconductors for considered levels of the steady-state excitation $\tau_s \ll \tau_r$ (where τ_s and τ_r are lifetimes for the non-equilibrium charge carriers, determined by s- and r- centers, respectively). Rise and decay curves are determined only by the time τ_r from the photocurrent kinetics, i.e. S-section is absent on the decay curve. It means, that owing to the high coefficient of electrons capture by r-centers, steady-state excitation will not lead to appreciable accumulation of holes in these centers.

One can calculate τ_r from dependences $\ln (\Delta I/\Delta I_{st})$ and $\ln [1-(\Delta I/\Delta I_{st})]$ versus time. fig.3 shows photocurrent decay (1) and rise (2) curves at 300 K. Relaxation time, determined from the slope of the linear section, is equal to 4.2 s.

As it follows from the photocurrent kinetics, a variation of the non-equilibrium charge carriers via slow levels is small in comparison with the total density. Relaxation of the photocurrent is determined mainly by recombination via fast centers.

Relaxation time, characterized by these centers, was determined from the photocurrent kinetics under the excitation by short-term pulses of light (light impact). Duration of light pulses for ИСШ-100 lamp is equal to 3 μs. Kinetics of relaxation of the "light impact" excitation is represented on fig.3a. Relaxation time, determined as time, in which an amplitude of the photocurrent decreases by e-times, is equal to $4 \cdot 10^{-6}$s. Lifetime for non-equilibrium charge carriers excitation by light, absorbed near surface, was estimated from the PC measurements. This value is ~10^{-5}s and does not correlate with the relaxation time of fast centers. However it confirms the assumption made at interpretation of results of PC spectrum measurements under steady-state and modulated illumination. We supposed there that the volume lifetime for non-equilibrium charge carriers appreciably lower than surface one. Calculated lifetime, determined from curves of non-equilibrium conductivity at different Π-pulses excitation levels for $Au_3In_5Se_9$ specimens, in practice does not depend on the light intensity (maximum intensity was not higher than 10^3 Lx at the experiment).

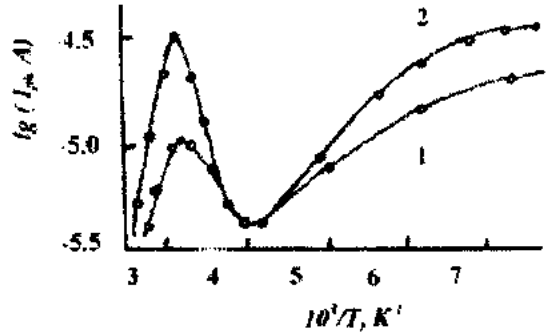

Fig.4 Temperature dependence of the current in $Au_3In_5Se_9$ compound for two light intensities: $I_2 > I_1$.

Temperature dependence of the photocurrent $I_{ph}(T)$ is shown on fig.4 at different excitation levels in photosensitive $Au_3In_5Se_9$ specimens for two intensities. It has the complicated shape and its interpretation requires taking into consideration temperature dependences of the concentration and mobility of non-equilibrium charge carriers. Photocurrent decreases in temperature ranges 130-250 K and 320-350 K. Drop of the photocurrent in the region 320-350 K apparently is caused by the thermal quenching of PC, observed in photosensitive semiconductors [4]. This assumption is based on the change of $I_{ph}(T)$ curves course under different optical excitation levels. The region of temperature quenching of PC (TQPC) shifts to higher temperatures with increase of excitation intensity. However, multiplicity of TQPC is so small, that in practice it is very hard to determine energetic positions of photosensitive centers. Comparison of the photocurrent decay in the range 130-250 K with the temperature dependence of the charge carriers mobility allows to assume, that decrease of I_{ph} in the specified range results from decrease of the mobility with the temperature growth.

[1] *N.F. Gakhramanov.* Scientific Reports of the Sumgayit State University, 2001, №1, pp. 20-24.

[2] *S.M. Ryvkin.* Photoelectrical Phenomena in Semiconductors. Moscow, Fizmatgiz, 1963, p.494.

[3] *E.I.Androvin, Ye.M.Kuznetsova.* Doklady AN SSSR, 1962, v. 1476, №4, pp.813-816

[4] *R.Bube.* In "Photoconductivity in Solids". 1962, Moscow, p.409.

[5] *N.M.Kolchanova, D.N.Nasledov.* 1966, FTT, v.8, №4, p.1907-1914.

N.F. GAHRAMANOV, S.S. SADULOVA

N.F. Qəhrəmanov, S.S. Sadulova

$Au_3In_5Se_9$ KRİSTALLARININ LÜKS-AMPER XARAKTERİSTİKALARI VƏ FOTOCƏRƏYANIN KİNETİKASI

İşdə $Au_3In_5Se_9$ birləşməsinin LAX, fotocərəyanın kinetikası və temperaturdan asılılığı işıq zərbəsi və Π –şəkilli işıq impulsunun təsiri şəraitində öyrənilmişdir. Tarazlıqda olmayan əsas yükdaşıyıcılarının yaşama müddəti təyin olunmuşdur.

Н.Ф. Кахраманов, С.С. Садулова

ЛЮКС-АМПЕРНЫЕ ХАРАКТЕРИСТИКИ И КИНЕТИКА ФОТОТОКА В КРИСТАЛЛАХ $Au_3In_5Se_9$

В работе исследованы ЛАХ, кинетика и температурная зависимость фототока соединения $Au_3In_5Se_9$ при световом ударе и возбуждении Π-импульсами. Определено время жизни неравновесных носителей заряда.

Received: 18.04.01

CHARGING OF POLYMER DIELECTRICS UNDER THE ELECTRICAL EXPOSURES

N.M.TABATABAEI
Tabriz Tarbiyat Moallem University
P.O.Box : 51745-406, Islamic Republic of Iran

A.M. HASHIMOV , R.N. MEHTIZADEH
Institute of Physics of Azerbaijan National Academy of Sciences
H. Javid av., 33, Baku, 370143

Results of research of the charged state formation are presented in some polymeric dielectrics under their treatment by strong electrical fields and electrical discharges. It is shown, that formation of electrical charge of high density takes place in investigated materials. This charge is revealed only at the material heating. The new composite material for the electrets making is offered which has the high charge density and stability.

INTRODUCTION

In polymeric materials subjected to various external effects such as a radiation, mechanical loads, high and low temperatures, strong electrical fields and electrical discharge etc., the essential change of their chemical and physical structure and, hence, their basic properties are observed [1]. Many investigators applying the direct research methods (electrical and optical microscopy, *X*-rays diffraction, infra-red spectroscopy, electron-paramagnetic resonance etc. [2]) have rather successfully solved a number of problems concerning with polymer dielectrics properties. However, despite of plenty spent researches in this field, the decision of many questions remains open.

The submited work is devoted to research of a charge formation in the film samples on base of Polyvinylidenfluoride (PVDF) subjected to electrical discharges effects. The basic purpose of given research is study of basic laws and physical mechanisms of a charging formation in polymers and composite systems under effects of the strong electrical fields and discharges.

EXPERIMENT

The samples of PVDF and composite material formed on PVDF as a base and porous adsorbent- KCM mark Silicagel (mainly consisting in silicon dyoxide–SiO_2) as a filler are used. The PVDF films of 180μ thickness were made by hot pressing from melting state at the temperature T= 170°C under the pressure P=10 MPa (100 athm). The size of initial powders was within the range of 63μ.

The filler-Silicagel was comminuted by special apparatus and in a powder state passed through a sieve for reception of the size no more than 63μ. The received powder was previously exposed to the heating treatment at T=200°C under the vacuum for 3 hours. Then the PVDF and Silicagel components in a powder state were mixed up in the vibrating mixer at a necessary volumetric proportion which accounted for 80 % PVDF and 20 % Silicagel.

Received homogeneous powder mixture of components was placed in special pressform, heated up to temperature T=170°C and pressed for 3-5 minutes. Received film samples have thickness 180 μ and size (50×50) mm^2.

The studies of charged state of the film samples subjected to effect of flame and corona types electrical discharges and thermal polarization in a constant electrical field are carried out. The charged state in samples was revealed by the thermal stimulated relaxation (TSR) method widely used at research of polymeric dielectrics [3]. At TSR method a material at first is charged (by means of polarization, corona discharge etc.) and then discharged on the current reading device at simultaneously heating with the constant speed of 1°C/min. According to TSR current function of time the value of storage charge into material may be determined.

Charging of samples by the flame discharge was carried out at AC voltage U=19κV and the current I=30μA at the distance between electrodes d=4cm. The typical TSR spectrum for a PVDF film, treated by flame discharge, is shown on fig.1, curve 1. The spectrum contains two peaks; the first of them is fixed at T=(95-100)°C, the second peak is observed at T=130°C. Obtained charge density is: σ_f=8.0x10^{-9} Coul/cm^2.

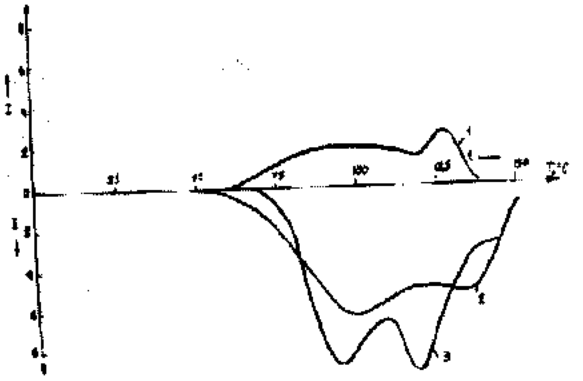

Fig.1

Charging of samples by the corona discharge at the negative polarity of coronal electrodes was carried out at U=6 κV and the current I=30μA during 30 minutes. The typical TSR spectrum for a PVDF film treated by corona discharge of the negative polarity is shown on fig. 1, curve 2. Spectrum also contains two peaks the first of them is fixed at T=(95-100)°C, the second peak is observed at T=135^{0}C. Obtained charge density is: σ_c =1.2x10^{-8}Coul/cm^2. Other kind of materials electrification used in experiments is the polarization in a constant electrical field. The investigated sample is displaced between electrodes of the heating TSR installation. There are

polarization temperature T_p=130°C, polarization voltage U_p=2 kV and polarization time is 1 hour.

After the exposure during 1 hour the heating of the sample is stoped and the sample begins to cool. At achievement of a sample of the room temperature, the applied voltage is stoped and TSR spectrum is picked off. The appropriate spectrum is shown on fig. 1, curve 3. The TSR spectrum also contains two peaks, first of which is observed at T=(95-100)°C, and the second-at T=125°C. Appropriate charge density is: σ_p=2.0x10^{-7} Coul/cm^2.

Comparison of obtained results showes that all TSR spectra irrespective of a kind of an electrical effect contain two peaks and the appropriate peaks are fixed approximately in the same temperature intervals. This fact unequivocally testifies on a determining role of chemical structure and structural peculiarities of investigated materials in charge storage process.

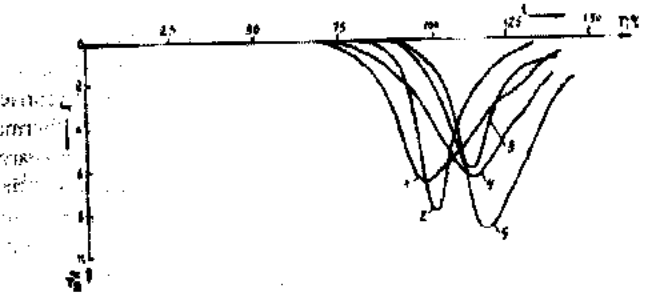

Fig.2. 1- 25°C; 2- 50°C; 3- 70°C; 4- 100°C; 5- 130°C.

Analysis of results have shown that the value of the total charge storaged in the materials treated by flame and corona discharges by an order of magnitude less than at polarization in a direct electrical field. In development of these research we spent the series of experiments on revealing of the effect of polarization temperature to the charge introduction into the material. The PVDF films were polarized in a constant electrical field at a number of temperatures (25, 50, 70, 100, 130)°C during 1 hour. The appropriate TSR spectra are shown on fig. 2.

As it is seen from fig.2, at increase of polarization temperature the TSR curves maximums shift to the higher temperatures area, however the total charge values obtained from TSR spectrum are equal in practice. The results obtained at higher electrification temperatures are apparently concerned with formation of more perfect and, hence, more stable structural units – grains.

Values of the stored charge density in PVDF and (80 % PVDF+20 % Silicagel) samples subjected to effect of the negative polarity corona discharge are equal to:

PVDF	80 % PVDF + 20 % Silicagel
σ_{PVDF}=3.9x10^{-8}Coul/cm^2 ;	σ_{COMP} = 1.8 x 10^{-7} Coul/cm^2 ;

These results showed that presence of Silicagel as a filler appreciable increases the stored charge in polymer composites. Research of the charged formation was carried out in the samples at various molding and crystallization temperatures of initial materials. It is obtained that at increase of initial materials molding and crystallization temperatures the maxima of peaks on TST spectra are shifted to the higher temperatures area and the values of total saved charge essentially decrease. However in case of (PVDF + Silicagel) composites these changes appear not so essential as in case of PVDF samples.

According to the linear model of amorphous-crystal polymers, we can consider that in samples subjected to electrical effect the electrical charges are trapped by both amorphous and crystal areas of a material. More less value of stored charge in moulded and crystallized samples at higher temperatures is connected with increase of a material crystalline degree, with defects reduction and formation of the more perfect crystal structural units in a material. The trapping of electrical that is charges in such materials carried by centres located in the amorphous areas which have insignificant sizes is the reason of stored charge reduction.

The stability of stored charge values in PVDF+Silicagel composites at increase of molding and crystallization temperatures is connected, obviously, with insignificancess of structural changes in a material.

The shifting of a current maximum to the higher temperatures area on TSR spectrum is caused by with a charge releasing from deeper trap levels and with more perfect structure.

CONCLUSIONS

1. Formation of electrical charge of high density takes place in dielectric film materials under the treatment by strong electrical fields and electrical discharges.
2. The value of stored charge in polymeric materials is in many respects determined by their above-molecular structures.
3. Charged state formation in materials is caused mainly by their amorphous areas.
4. The new composite material for the electrets making is offered. Material including the polymer PVDF and fine-pored Silicagel has the high charge density and stability.

[1] *L.M. Anishenko, S.B. Kusnetsov, V.A. Yakovlev.* Rhysics and Chemistry of materials treatment, 1984, №5, p.85-89 (in russian).

[2] *N.S. Ilchenko, V.M. Kirilenko.* Electriphysical apparatus and electrical insulation. M.: «Energy», 1970, p. 868 (in russian).

[3] By edition of *G. Sessler.* Electrets. M., «Mir», 1983, p.486 (in russian).

N.M.Tabatabaei, A.M. Həşimov, R.N. Mehdizadə

ELEKTRİK TƏSİRLƏRİ VASİTƏSİLƏ POLİMER DİELEKTRİKLƏRİN YÜKLƏNMƏSİ

Təqdim olunan məqalədə güclü elektrik sahələrinin və elektrik qazboşalmalarının təsirlərinə məruz qalan bəzi polimer dielektriklərdə yüklü vəziyyətlərin yaranmasının tədqiqindən alınmış nəticələr verilmişdir.

Müəyyən edilmişdir ki, tədqiq edilən materiallarda yüksək sıxlığa malik olan elektrik yükləri cəmlənir. Bu yüklər yalnız material qızdırıldıqda özünü büruzə verir.

Yüksək elektrik yüklərinin sıxlığına və bu yüklərin davamiyyətli zaman müddətində stabilliyinə malik olan, yeni kompozisiyalı elektret materialı təklif edilmişdir.

Н.М. Табатабаен, А.М. Гашимов, Р.Н. Мехтизаде

ЗАРЯДКА ПОЛИМЕРНЫХ ДИЭЛЕКТРИКОВ ПРИ ЭЛЕКТРИЧЕСКИХ ВОЗДЕЙСТВИЯХ

В работе представлены результаты исследования образования заряженного состояния в некоторых полимерных диэлектриках при их обработке электрическими полями и разрядами.

Показано, что в исследуемых материалах имеет место накопление электрического заряда высокой плотности. Этот заряд выявляется только при нагревании материала.

Предложен новый композиционный материал для изготовления электретов, обладающий высокой плотностью заряда и его стабильностью.

Received: 21.09.01

ON INFLUENCE OF STRUCTURE OF PIEZOELECTRIC PHASE ON PYROELECTRIC PROPERTIES OF POLYMER-PIEZOELECTRIC COMPOSITE

A.I. MAMEDOV, S.N. MUSAEVA, M.A. KURBANOV, A.Sh. GASANOV
Institute of Physics of Azerbaijan National Academy of Sciences
H. Javid, av., 33, Baku, 370143

It is shown, that the value of residual reorientation of polarization, in main, stipulated by domains which are distinct from 180°, their sizes and mobility determine pyroelectric properties of composites. The piezoelectric ceramics with high activation energy of domain walls and with a coefficient of uniform deformation of a crystal lattice are less effective as piezophase for pyroelectric composites.

By numerous researches of pyroelectric properties of composites on the basis of polar and non-polar polymers (matrix) and piezoelectric ceramics (disperser) of various structure it was shown earlier, that the pyroelectric effect in these heterogeneous systems is stipulated by residual domain-orientation polarization in the filler particles compensated by a charge stabilized on the polymer-piezoelectric ceramics phase boundary []1,2]. In this connection it is necessary to find out from what structural parameters of disperser particles the value of domain-orientation polarization for the pyroelectric effect, after their thermopolarization depends on.

As the structural parameters it is possible to accept a number of possible directions (N) of a vector of spontaneous polarization, a mobility of domain walls, a value of residual reorientation (P_r) and spontaneous (P_s) polarization, a degree of domain reorientations which are distinct from 180° (η, in %), a coefficient of a homogeneous deformation of a crystal lattice (δ) and sizes (μ) of grains (domains) in piezoparticles.

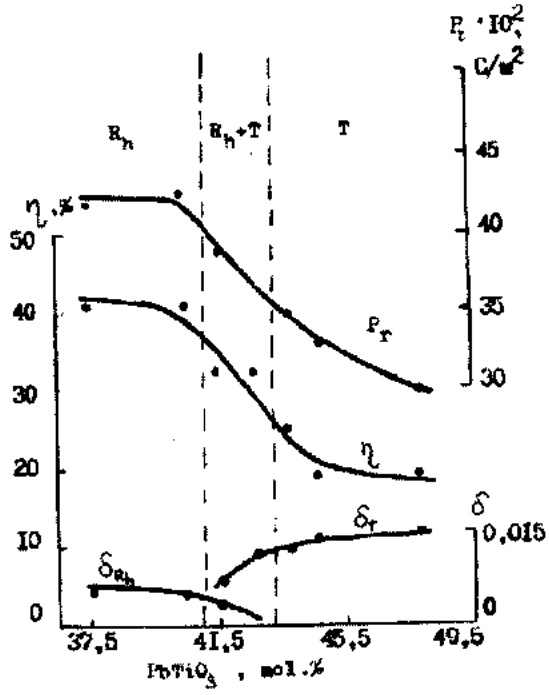

Fig.1. Dependences of η, δ and P_r on the content of $PbTiO_3$ in the $PbTiO_3$-$PbZrO_3$ - $PbNb_{2/3}Zn_{1/3}O_3$ - $PbN\ b_{2/3}Mg_{1/3}O_3$ system.

In fig.1 the change of some structural parameters of piezoelectric ceramics of the set PCR (piezoelectric ceramics Rostov) in dependence of their position with respect to a morphotrope region (MR) is represented. It is seen, that η, P_r and δ by approaching from the part of rhombohedral region (R_h) to MR and by going away from it into tetragonal (T) region vary by a complex law. However, values of η and P_r in a case of rhombohedral structure are larger, in comparison with one's of tetragonal structure ceramics .A value of the parameter δ in the case of rhombohedral structure is noticeably less , than in the case of ceramics of tetragonal structure. A number N=8 for ceramics of rhombohedral structure, N=6 for ceramics of tetragonal structure and N=14 for ceramics of morphotrope region.

It is known, that the reorientation polarization P_r is a part of spontaneous polarization P_s of domains of crystal grains and is determined by a collection of all domain rotational displacements accomplished during polarization of ceramics [3]. At realization of all possible rotational displacements the reorientation polarization is maximum, thus its value depends on N in different phases. So, for a piezoelectric ceramics of the set PZT in rhombohedral and tetragonal phases the ratio P_r/P_s is equal 0,866 and 0,831, accordingly. In the case of existence of two phases, i.e. for R_h+T P_r/P_s=0,922. However the indicated number N is not a defining one for the value P_r, since practically at strong polarizing fields not all possible domain rotational Displacements are implemented. The residual domain reorientations, accomplished during polarizations distinct from 180° bring the major contribution into the value of P_r and reaches the maximum value in a rhombohedral phase (fig.1).

Let us consider a connection of the structural characteristic of η piezoparticle with a pyroelectric coefficient γ and P_r of the composite. At realization of all possible domain orientations in piezoparticles during their polarization the value of the maximal P_r is in tetragonal ceramics $P_r = \left(\frac{1}{3} + \frac{2}{3}\eta\right) 0{,}831 P_S$ and in rhombohedral ceramics $P_r = \left(\frac{1}{4} + \frac{3}{4}\eta\right) 0{,}866 P_S$. Into the total value of P_r the domains, which direction coincides with strength of polarization E_p, 180°domains and domains, which are distinct from 180° contribute. As it is known, the domains distinct from 180°, which determine are more mobile. They, as it seems, determine, mainly, pyroelectric properties of composites as a whole. Really, in the pyroelectric composites with piezoparticles possessing high value of η, the value of

pyrocoefficient is larger, than in similar composites with the piezoparticle with smaller value of η.

Other important structural parameter is δ. This parameter characterizes the value of mechanical tensions originating at domain reorientations. The less, the closer a unit cell form to a cubic one and that is less energies are expended on mechanical deformations during the reorientation of domains. It is clear, that the decrease of δ means an increase of mobility of domain boundaries, and consequently, an increase of a value residual reorientation polarization (fig.1). From fig.1 it is visible, that by approaching a morphotrope region on the part of rhombohedral structure the value of P_r decreases.

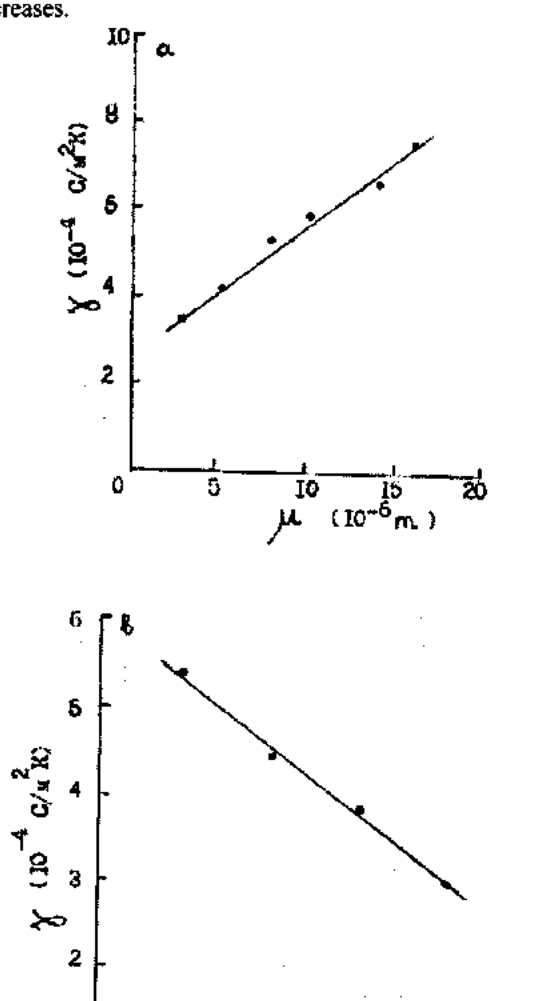

Fig.2. Dependences of pyrocoefficient γ on grain sizes μ of PVDF+PCR-8 (a) and PVDF+PCR-5 (b) composites.

In multicomponent ceramics such as PZT, utilised by us as fillers in compo-sites, the structural parameter η decreases at transition from a rhombohedral phase into tetragonal and δ increases. These both parameters have various influence on the pyrocoefficient: the increase η means decrease of a number of domain boundaries which are distinct from 180° and it leads to an increase of the pyrocoefficient: the increase of δ leads to the decrease of a mobility of domain walls and to the decrease of the pyrocoefficient. Therefore composites with the ceramics of rhombohedral structure having the low value of δ and the high value of η have more high pyrocoefficient than composites with the ceramics of morphotrope and tetragonal structures. In this case, in the tetragonal phase the main role is played by the decrease of the mobility of domain walls as a result of a growth of δ and in rhombohedral – the decrease of a number of domain boundaries as a result of a growth of η.

This proves to be true by the following experimental fact. It is known, that the ceramics of rhombohedral structure have more coarse domain structure with smaller number of domain boundaries in comparison with ceramics of tetragonal structure.

The grain sizes μ in the ceramics of rhombohedral structure can be changed over a wide range (from a several micron to a several tens of micron), while as in the ceramics of tetragonal structure μ varies in the range of several microns [3,4]. The increase of the grain size should result in increase of η and therefore, in increase of a pyrocoefficient, as it is observed experimentally for composites with the ceramics of rhombohedral structure. For example in fig.2 the dependence of pyrocoefficient of PVDF+PCR-5 composite on the grain size of the ceramics is presented.For the final solution of this problem the composites with the piezoelectric filler having tetragonal structure depending on grain size were investigated. For composites with ceramics of tetragonal structure the opposite pattern is observed – with an increase of grain size the pyrocoefficient decreases. As it is shown on fig 2,b the dependence of γ on μ for PVDF+PCR-8 composite can be explained by the fact to that in the case of tetragonal structure the change of the parameter η with change μ is practically unsignificant and weakly influences on η of composite, and the crucial factor here is the parameter δ, that increases with an increase of grain size [3].

Thus, composites with rhombohedral structure have maximum pyrocoefficient in which the values of δ and η are high. It is known, that in a rhonbohedral phase 180°, 109° and 71° domains exist, and in a tetragonal phase the same is true for 180° and 90° domains. Far from morphotrope region, both in rhombohedral and in tetragonal phases the behaviour of η and P_r of piezofiller is determined, in main, by the participation of 180° domains. By approaching morphotrope region from the part of tetragonal and rhombohedral phases in ferropiezoceramics on the basis of PZT the walls not only 180° domains, but also 90°, 109° and 71° domains accordingly vibrate. It leads to noticeable growth of values of P_r and η. It is possible to estimate the energy of domain wall, which it will have, for example, on boundaries of morphotrope region. In this connection we shall use the known formula

$$W = 0,88 P_r^2 d ,$$

where P_r is a polarization inside domains, d is a constant of elementary cell, d=4,08 and d=4,15 A for piezoceramics of rhombohedral and tetragonal structures, accordingly [3].

Therefore for the boundary of transition from a tetragonal phase in the smoothed (R_h+T) phase it is accepted, that P_r=0,831P_s , d=4,115 A and for transition from rhombohedral to tetragonal phase P_r=0,922P_s , d=4,08 A. The values of boundary their morphotrope region from the side of

R_h and T phases, are accordingly equal: 0,48 P_s^2 and 1,01 P_s^2 $\frac{J}{m^2}$. Such difference in values of energy of a domain wall of piezoceramics of the set PZT on boundaries of morphotrope region and on various distances from MR with the change of concentration of $PbTiO_3$, and also the difference of their crystallophysical and crystallochemical parameters contribute to the formation of residual reorientation polarization and pyroelectric characteristics in composites depending on the piezoparticle structure.

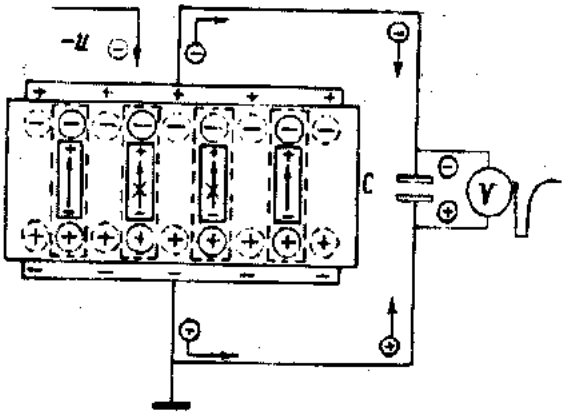

Fig.3. The model of the pyroelectric composite.

Thus, it is possible to consider, that the high pyroelectric state will be formed in polymer-piezoelectric composites in the case when the piezoelectric phase has a high values of P_r and η, and the mobility of domain walls is high too.

Taking into account the above-mentioned conclusion, on the basis of model offered in fig.3 it is possible to explain the origin of the pyroelectric effect in polymer-piezoelectric composites as follows: due to injection of charges in piezophase and its electric conduction the oriented domain of piezoparticle are neutralized by free charge of the oppozite sign and the effective charge defined as their difference, is equal to zero. Therefore, the presence of polarization outwardly does not appear. At heating the reprientation of domains occur,in main, the domains which are distinct from 180° and releasing part of the free charges supports a direct pyroelectric current as the function of temperature. Therefore, the origin of pyroelectric effect in polymer-piezoelectric composites can be connected with reorientation polarization of the composite under the change of its temperature. By cooling the orientation of domains in a field of the injected charges stabilized in various traps, in main, on the phase boundary of polymer matrix and piezoparticle and by that there is appear a pyroelectric current of a reverse polarity. These components of current arise at the expense of converted residual polarization. The increase of domain structure mobility and lowering of the Curie temperature should result in an increase of a pyrocoefficient. These conditions, naturally, are satisfied by piezoceramics of rhombohedral structure.

[1] *A.I. Mamedov, M.A. Kurbanov, M.G. Shakhtakhtinsky, A.Sh. Gasanov.* Preprint №8 of Institute of Physics, Azerbaijan Academy of Sciences, Baku, 1987, 68 p.

[2] *M.G. Shakhtakhtinsky, M.A. Kurbanov, F.I. Seidov, A.I. Mamedov, S.N. Musaeva.* Fizika, 1997, v.3, p.48-51.

[3] *E.G. Fesenko, A.Ya. Dantsiger, O.N. Razumovskaya.* New piezoceramic materials.-RGU, 1983, 154p.

[4] Polarization of piezoceramics.- edited of *E.G. Fesenko,* RGU, 1968, 133p.

A.İ. Məmmədov, S.N. Musayeva, M.Ə. Qurbanov, A.Ş. Həsənov

POLİMER PYEZOELEKTRİK KOMPOZİTİN PİROELEKTRİK XASSƏLƏRİNƏ PYEZELEKTRİK FAZANIN STRUKTURUNUN TƏSİRİ HAQQINDA

Göstərilmişdir ki, əsasən 180°dən fərqli domenlərin yaratdığı qalıq reoriyentasiya polyarizasiyasının qiyməti domenlərin yürüklüyü və ölçüləri kompozitlərin piroelektrik xassələrini təyin edir. Domen divarlarının aktivasiya enerjisinə və kristallik qəfəsin yüksək bircins deformasiya əmsalına malik olan pyezokeramikalar piroelektrik polimer kompozitlər üçün pyezofaza kimi az effektivdir.

А.И.Мамедов, С.Н.Мусаева, М.А.Курбанов, А.Ш.Гасанов

О ВЛИЯНИИ СТРУКТУРЫ ПЬЕЗОЭЛЕКТРИЧЕСКОЙ ФАЗЫ НА ПИРОЭЛЕКТРИЧЕСКИЕ СВОЙСТВА КОМПОЗИТА ПОЛИМЕР-ПЬЕЗОЭЛЕКТРИК

Показано, что величина остаточной реориентационной поляризации, в основном, обусловленной доменами, отличных от 180°-ных, подвижность и их размеры определяют пироэлектрические свойства композитов. Пьезокерамики с высокой энергией активацией доменных стенок и коэффициентом однородной деформации кристаллической решетки менее эффективны в качестве пьезофазы для пироэлектрических композитов.

Received: 20.06.01

CONFORMATIONAL POSSIBILITIES OF THE p21^{ras} PROTEIN FAMILY GTP-BONDING FRAGMENT

K.D. MZAREULOV, V.K. MZAREULOV
Baku State University,
Baku 370148, Z.Khalilov str. 23

Using a theoretical conformational of method analysis, a three-dimensional structure and conformational properties of Leu53-Ala59 fragment of p21 protein were investigated. The calculations were performed on the basis of the fragmental analysis, using nonvalence, electrostatic and torsional interactions and hydrogen bonds. The obtained data suggest, that this polypeptide can exist only in several low energy conformations. The results of this calculated experiment can be used for the study of structure-functional relationship.

The ras gene family is highly conserved from yeast to humans and ubiquitously expressed in eucaryotic cells. In mammals the gene family consists of three members: H-, K- and N-ras, which code for highly homologous proteins termed p21 according to their molecular weight – 21000 Daltons. The p21 proteins are membrane bound nucleotide binding proteins, which bind GDP and GTP with high affinity and have a low intrinsic GTP activity. They are members of the family of G-binding proteins, which includes the classical heterotrimeric G proteins, the elongation factors and the ras-superfamily. By analogy to the hormone receptor-coupled G proteins, the p21 proteins are believed function as signal switch molecules. In the active GTP conformation, they transmit a signal to an effector molecule that leads to cell proliferation. The p21 effector interaction is switched off by GTP hydrolysis, returning p21 to the inactive GDP bound state [1,2].

The efficiency of the GDP-binding essentially depends on amino acide substitutions in positions 59 and 61 [3,4]. Likeness of 57-63 segment and GDP-binding fragments of another proteins was determinated by Shih, Hattori et.al. [5]. Bolonick, Bollag and McCormick [6] established, that mutations at codone-61 influence on conformation state of Gly60, which determine the dissociation of GTP and GDP from the complex with p21. Therefore 57-63 fragment of ras family is responsible for the guanosine-phosphate binding.

In order to investigate the three-dimensional structure of the address fragment, the next peptide was taken: Leu53-Asp54-Ile55-Leu56-Asp57-Thr58-Ala59.

The search of the optimum conformations was performed by minimization of the energy during variations of the dihedral angles. For the calculations we used the program for semiempirical calculations of conformations of macromolecular components on the computer, developed in the Research Laboratory of Molecular Biophysics of the Baku State University [7]. The conformational energy was determined as the sum of the contributions of nonvalence and electrostatic interactions, hydrogen bonds and torsional barriers. The investigations was carried out on the basis of the step by step approach proposed by Popov [9,10].

At first stage of calculations the conformational possibilities of the 53-55, 55-57 and 57-59 tripeptides were investigated. A total 81 structural models were examined for every fragment.

Leu53-Asp54-Ile55 tripeptide shows high degree of the conformational lability. The representatives of all structural shapes, including the exotic forms BLR, RLR, LRR and LBR, belong to the relative energy interval from 0.0 to 2.2 kcal/mole. A global conformational state of this tripeptide is *ef*, and the most preferable conformations of *ff* and *fe* shapes have E_{rel}=0.3 and 0.6 kcal/mole accordingly.

We have the analogous picture in Ile55-Leu56-Asp57 fragment. The optimal form *ff* outstrips the *ef* shape to 0.1 kcal/mole, and E_{rel}=0.6 kcal/mole corresponds to unfolded *ee* and E_{rel}=1.4 kcal/mole – to *fe* shapes.

A considerable difference of the structural forms was found for Asp57-Thr58-Ala59 sequence. The folded *ff* form yields 1.3 kcal/mole to the global conformation (*ef* shape).

The minimized values of dihedral angles of 53-55 and 55-57 tripeptides were used at the compiling of initial data for the calculation of Leu53-Asp54-Ile55-Leu56-Asp57 pentapeptide. We calculated 339 conformations of this amino acide sequence.

The investigation of this fragment revealed a sharp preference of the folded forms of the main chain. A global form RRRRR corresponds to the helical structure of the polypeptide backborne. Next form BRRRR belong to *efff* shape and outstrip lider only on 0.4 kcal/mole.

Then the calculation of the 345 structural models of 53-59 heptapeptide was realized. The initial conformations were compiled on the basis of the dihedral angles of the most preferable structures of Leu53-Asp57 and Asp57-Ala59 fragments. The main energy and geometrical parameters of the preferable conformations are presented in Table 1.

The conformational analysis data confirms, that folded structures are preferable for this amino acide sequence. The compact packing forms of main and side chains lead to the optimal balance of interatomic contacts, correspond to minimal values of the full energy. The preference of related conformations $B_3R_1R_1R_2R_3R_3R_3$ (*ef*$_5$ shape) and $R_2R_1R_1R_2R_3R_3R_3$ (helical f_6 structure) is obvious. The information, summarized in the Table 1, shows, that the folded shape of the main chain ensures a high intensity of the nonvalence interactions.

Table 1.

Values of the Relative Energy, Nonvalence, Electrostatic and Torsional Contributions for the Most Preferable Molecular Structures of the p21ras 53-59 fragment.

Shapes	Forms	E_{rel}	E_{nonval}	E_{el}	E_{tors}
ef_5	BRRRRRR	0.0	-40.5	13.2	7.7
f_6	RRRRRRR	0.7	-39.8	13.0	7.9
f_3eef	RRRBBRR	3.8	-33.4	11.7	5.7
$Effeff$	BRRBBRR	3.7	-33.1	11.7	5.5
	BRBLBRR	6.7	-31.1	12.9	5.3
f_4ef	RRRRBRR	4.2	-35.3	13.7	6.2
$Effeff$	BRBLRRR	4.3	-34.4	14.6	4.5
	BRRBRRR	5.3	-32.3	12.4	5.6
$Efefef$	BRBRBRR	4.5	-30.9	11.7	4.1
	BBLRBRR	7.2	-28.0	12.2	3.5
ef_3ef	BRRRBRR	4.7	-34.5	14.0	5.6
$ffefef$	RRBRBRR	5.0	-29.7	11.7	3.3
	RBLRBRR	7.2	-28.0	12.2	3.4
$efeffe$	BRBRRBR	5.6	-29.7	12.4	3.4
	BBLRRBR	7.1	-28.9	13.1	3.2
f_3eff	RRRBRRR	5.7	-33.3	12.3	7.1
$ffeffe$	RRBRRBR	5.8	-28.9	12.6	2.6
	RBLRRBR	6.9	-29.0	12.8	5.5
$efeeff$	BRBBRRR	6.3	-30.7	12.2	5.2

[1] *Y.C. Lacal, S.A. Aaronson.* Mol. and Cell. Biol., 1986, v.6, №.12, p.4214-4220.

[2] *Y.L. Dos, M. Verlaan, et.al.* Nucl. Acids Res., 1986, v.14, №.3, p.1209-1217.

[3] *P.A. Wright, N.R. Lemoine, et.al.* Brit. Y. Biophys., 1989, v.60, №.4, p.576-577.

[4] *Y.C. Lacal, S.A. Aaronson.* Proc. Nat. Acad. Sci. USA, 1986, v.83, №15, p.5400.

[5] *T.Y. Shih, S. Hattori, et.al.* Gene Amplificat. and Anal., v.4, №.Y.e.a., 1986, p.53-74.

[6] *Y. Bolonick, G.Bollag, F. McCormick.* Y.Cell. Biochem., 1992, Suppl.16B, P.205.

[7] *Н.М. Годжаев, И.С.Максумов.* Науч. Труды Минвуза Аз. ССР, 1979, №5, с.157-162.

[8] *E.M. Popov.* Molek. Biol., 1975, v.9, №4, p.578-593. (in Russian)

[9] *E.M. Popov.* Fizika molekul, Kyev. Naukova Dumka. 1980, v.8, p.69-113.

K.D. Mzareulov, V.K. Mzareulov

p21^{ras} ZÜLALLARIN GTP-BAĞLAYICI FRAQMENTİNİN KONFORMASİYA İMKANLARI

Nəzəri konformasiya analizi metodunun köməyi ilə p21ras zülalların Leu53-Ala59 fraqmentinin fəza quruluşu və konformasiya imkanları tədqiq olunmuşdur. Hesablamalar fraqmentar yaxınlaşma əsasında, qeyri-valent, elektrostatik, torsion qarşılıqlı təsiri və hidrogen rabitələri nəzərə almaqla yerinə yetirilmişdir. Tədqiqat nəticələri göstərir ki, bu polipeptid yalnız bir neçə alçaq enerjili konformasiya hallarında ola bilər. Bu hesablama eksperimentin nəticələri struktur-funksional əlaqənin öyrənilməsində istifadə oluna bilər.

К.Д. Мзареулов, В.К. Мзареулов

КОНФОРМОЦИОННЫЕ ВОЗМОЖНОСТИ GTP-СВЯЗЫВАЮЩЕГО ФРАГМЕНТА БЕЛКОВ СЕМЕЙСТВА p21^{ras}

С использованием методики теоретического конформационного анализа исследованы трехмерная структура и конформационные свойства фрагмента Leu53-Ala59 белка p21. Рассчеты проводились на основе пофрагментного подхода с учетом невалентных, электростатических и торсионных взаимодействий и водородных связей. Результаты исследований показывают, что данный полипептид может существовать лишь в нескольких низкоэнергетических конформоционных состояниях. Результаты этого вычислительного эксперимента могут быть использованы для изучения структурно функциональной зависимости.

Received: 21.09.01

PYRYLIUM FERROCHLORIDE AS A DYE LASER

S. MORADIAN
Polymer and colour engineering
Department of Amirkabir University of Technology

M. RABIE, A. SABBAGH ALVANI
Colour reproduction and colour control
Department of the Iranian Colour Research Center

In the present study the preparation of 2,6 –di (4-methil-phenyl) – 4- (3- chlor – phenyl) pyrylium ferrochloride and its application as a dye laser were investigated. The pyrylium ferrochloride salt was prepared, purified by recrystallisation and characterized by FTIR, DSC and elemental analysis techniques. The purified product was dissolved in a suitable solvent in order to give it rigidity (i. e decreased rotational mobility) and hence increased lasing efficiency. The measured fluorescence and lasing efficiency carried out at the laser division of the Iranian Atomic energy organization showed suitable fluorescence and good laser efficiency.

Keywords: pyrylium ferrochloride, dye laser, fluorescence, lasing efficiency, characterization.

INTRODUCTION

Pyrylium salts belong to a very important class of cationic compounds with a trivalent oxygen atom and 6 π electrons in a six membered ring system.

The pyrylium cation as a moiety having the deficiency of one electron will have an electron accepting character [1].

Molecules in this group of compounds i. e the group of doner-acceptor chromogenic dyes manifest strong fluorescence which can be increased in suitable solvents giving them increased rigidity and decreased mobility.

Observation of the laser emission from some pyrylium dyes were first reported by the Schafer's group [2].

From 1991 on wards the Tomasz Kotowsky group, reported the laser effects of a large group of pyrylium dyes. It is worth to mention that many of the pyrylium dyes in suitable solvents or in combinations with polymers will manifest excellent lasing properties in the visible spectral range [1,2].

EXPERIMENTAL

Pyrylium ferrochloride salt was prepared by the modification of the standard method described by Dilthey [3] as follows. In a 200 ml round bottomed flask 17 cc of acetic anhydride was placed. 0,08 moles of 4-methyl acetophenone and 0,03 moles of 3-chloro benzaldenyde were added and the mixture was slowly stirred for 5 minutes. Then a total of 5 grams of ferric chloride were added slowly to the mixture the temperature of the reaction being kept between 0-5 degrees centigrades. The reaction was continued for one and a half hours at the same temperature. The temperature was then raised to 80°C and kept at this temperature for a further two hours.

The product was filtered, washed ten times with acetic acid and was then recrystallised from acetone [4].

The mechanism of the reaction is as follows [5]:

1: Condensation of 3 chloro benzaldenyde with 4-methyl acetophenone.

2: Condensation with 4-methylacetophenone.

3: Ring formation.

1)

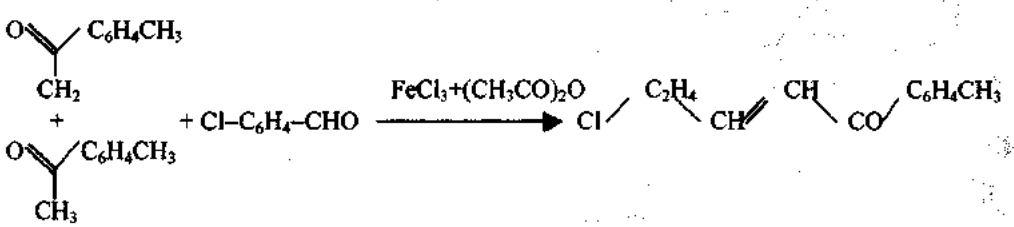

2)

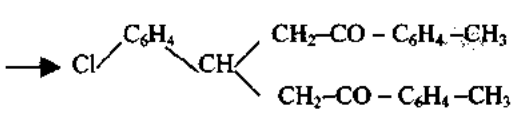

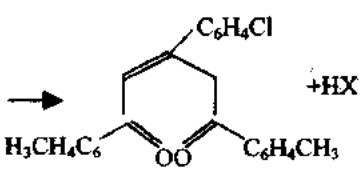

3)

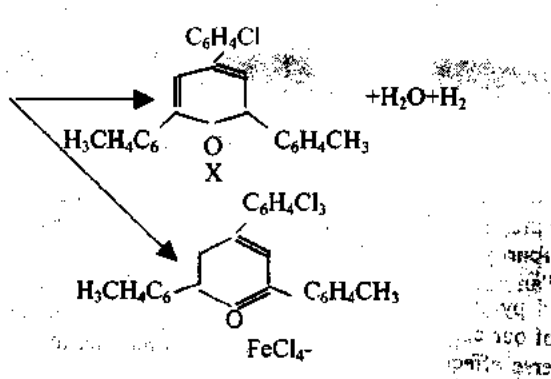

The dye was then characterized using FTIR, DSC and elemental analysis techniques and its fluorescence and lasing action was investigated by the use of a fluorimeter and a nitrogen laser respectively.

RESULTS AND DISCUSSION

The FTIR and DSC of the prepared dye laser are shown in figure 1 and 2 respectively. The results from the elemental analysis is tabulated in table 1.

Table 1.

Element analysis of the prepared pyrylium ferrochloride

Molecular Formula	Element analysis					
	calculated			Found		
	C	H	N	C	H	N
$C_{25}H_{20}OFeCl_5$	52.77	3.55	<0.1	52.1	3.8	<0.1

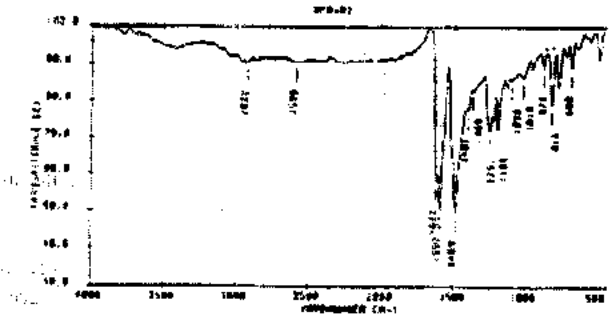

Fig.1. FTIR spectrum of the prepared pyrylium ferrochloride.

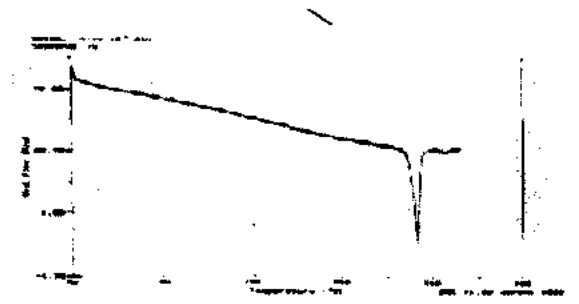

Fig.2. DSC of the prepared pyrylium ferrochloride.

The absorbtion and fluorescence properties and the corresponding lasing of the prepared dye are shown in figures 3 and 4 respectively.

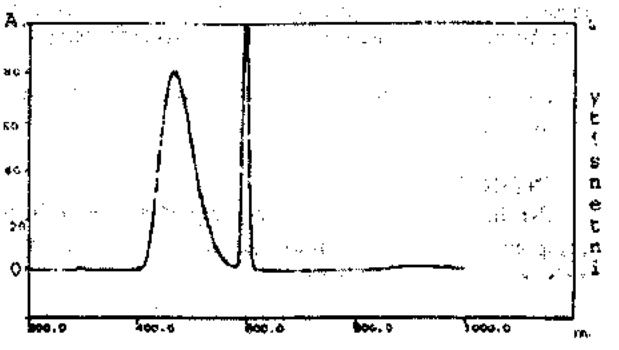

Fig.3. Absorption spectrum (484 nm) and Fluorescence spectrum (596 nm) for a 0.01 mol concentration of pyrylium dye in acetone.

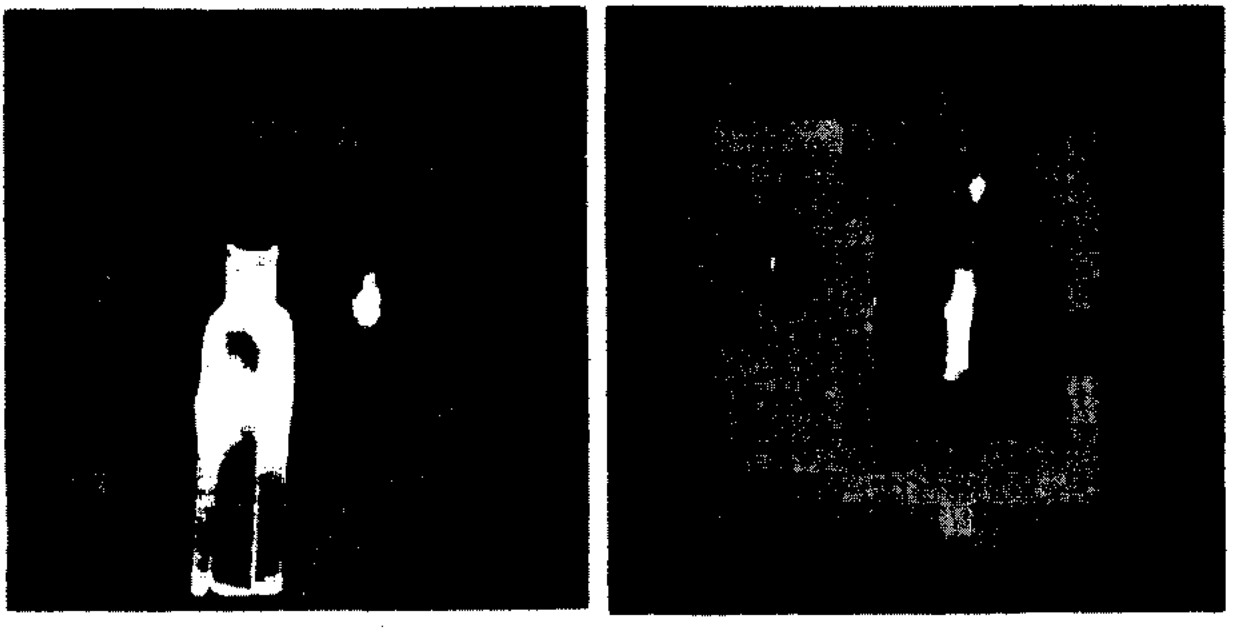

Fig.4. Lasing action of the prepared dye by nitrogen laser.

Dilthey observed a rather poor fluorescence for the three phenyl pyrylium dye under his investigation [3]. Contrary to his results results, we achived the laser emission for the prepared pyrylium dye. This can be attributed to the higher purity of our compound (it is known that impurities can have an adverse effect of quenching) and also to the fact that the choice of a suitable solvent causes the rigidification of the molecule increasing its fluorescence and laser efficiency [6,7].

CONCLUSION

The following conclusions can be summerised:

1 – Three phenyl pyrylium percholorate was prepared with hogh purity which was confirned by instrumental characterization techniques.

2 – The lasing properties of the product increased by the use of acetone as solvent.

[1] *Tomaz Kotovski.* Journal of luminescence, 1991, 50, p.39-45.

[2] J.opt. Soc. Am. B, 1985, vol. 2, № 7.

[3] *Dilthy.* J. pr. Chem., 1916, 94, 53.

[4] *Balaban and Nenitzescu* Annalen, 1961, 696, 97

[5] *Rene Lombard, Paul Stephan.* Societe chimique france Bulletin, 1958, p.1458.

[6] Encyclopedia of chemical technology. 1978, v. 14, p.42, p.554.

[7] *Hecht.* J., "versatility keeps dye lasers alive" laser focus world, 1992, 28 (7), p. 59-74.

S. Moradian, M. Rabie, A. Sabbagh Alvani

PERİLİUM FERROXLORİD BOYA ƏSASINDA LAZER KİMİ

Işdə 2,6 di-(4-metil-fenil) – 4 – (3xlor-fenil) perilium ferroxlorid duzunun alınması metodu və onun boya əssında lazer kimi işlədilməsi araşdırılmışdır.

С. Морадян, М. Рабие, А. Саббах Алвани

ПЕРИЛИУМ ФЕРРОХЛОРИД КАК ЛАЗЕР НА КРАСИТЕЛЯХ

В данной статье исследован метод получения соли 2,6 – ди-(4-метил-фенил) – 4-(3-хлор-фенил) перилиум феррохлорид и ее использование в качестве основы лазера на красителях.

Received:24.07.01

THERMODYNAMICAL AND STRUCTURAL ASPECTS OF STRUCTURAL TRANSFORMATIONS IN THE MONOCRYSTAL Cu_2Te.

F.Yu. ASADOV, A.I. MOVLAMVERDIYEVA, Sh.K. KAZIMOV, A.G. BABAYEV
Institute of Physics of National Academy of Sciences of Azerbaijan.
Nakhchivan State University

Structural transformations are investigated in the monocrystal Cu3Te by the high-temperature roentgendiffractometric method in the interval 290-1100K. Five structural transformations take place in the crystal in this temperature interval. The mechanism of given transformations is elucidated on the basis of lineary data on the heat capacity, heat of formation and entrophy, connected with structural transitions and taking into account structural parameters.

On the diagram of a condition of Cu - Te system, the compound Cu_2Te corresponds to the structure 33.33 at. % Te and fuses at the temperature 1393K [1] .It was shown in [2], that Cu_2Te crystallizes into the hexagonal structure with lattice parameters: a_0=4.237A, c_0=7.274A, sp.gr. P6mmm. elementary cell contains z=2, Density p_x=7.474g.см$^{-3}$. According to [3] for Cu_2Te at the room temperature the orthorhombic structure is determined with following lattice parameters: a=a_0=7,319A, b=3c_0=22,236A, which is the over structure hexagonal phase.

In the literature there are data on temperatures of phase transformations in Cu_2Te received by different authors and accordingly by different methods, which are shown as result in the table 1.

Table 1.

Temperatures of structural transformations in Cu_2Te.

Temperature of transformation .T.K					Methods of research	The literature
468	538	593	-	713	Roentgenography	3
463	-	583	633	823	DTA	4
433	531	590	633	835	Dilatometry	5
-	533	589	635	833	DTA	6
445	-	578-593	633	698-833	DTA	7
445	537	578	633	813	Electroconductivity	8
448	548	593	638	848	DTA	9

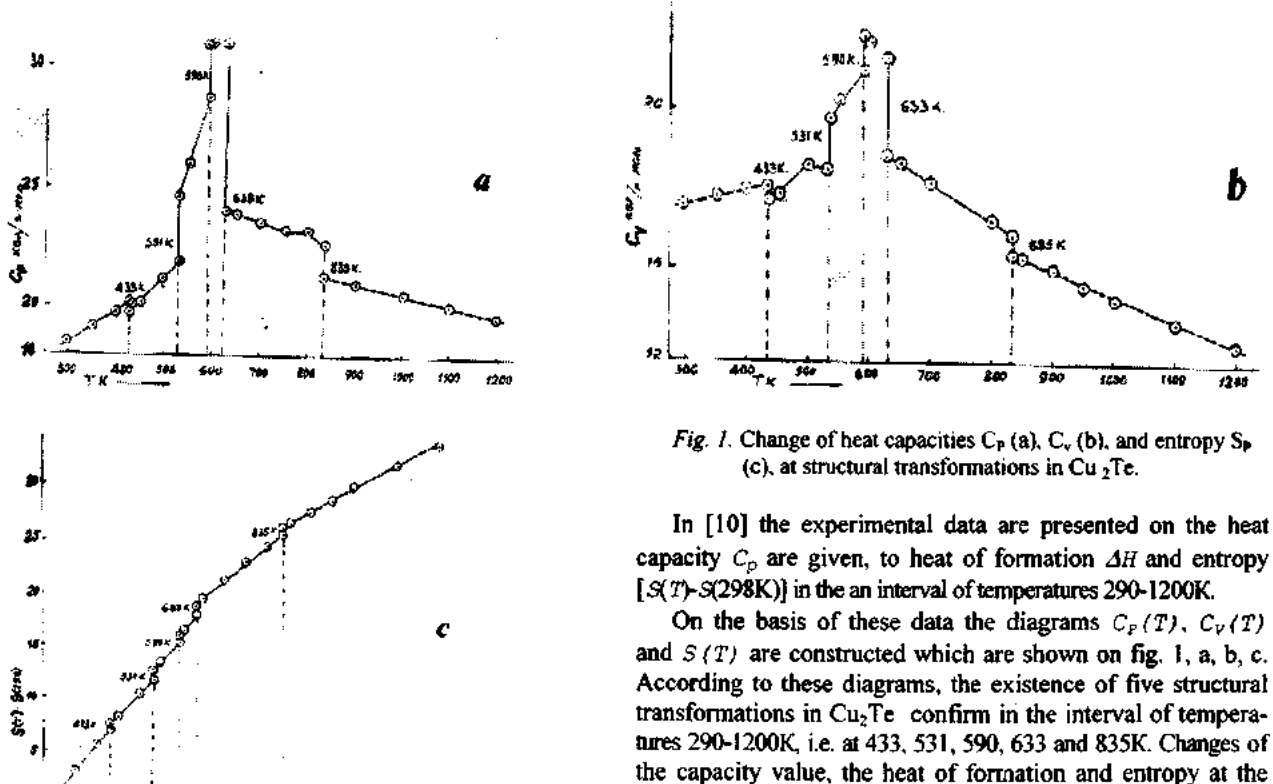

Fig. 1. Change of heat capacities C_P (a), C_v (b), and entropy S_P (c), at structural transformations in Cu_2Te.

In [10] the experimental data are presented on the heat capacity C_p are given, to heat of formation ΔH and entropy $[S(T)-S(298K)]$ in the an interval of temperatures 290-1200K.

On the basis of these data the diagrams $C_P(T)$, $C_V(T)$ and $S(T)$ are constructed which are shown on fig. 1, a, b, c. According to these diagrams, the existence of five structural transformations in Cu_2Te confirm in the interval of temperatures 290-1200K, i.e. at 433, 531, 590, 633 and 835K. Changes of the capacity value, the heat of formation and entropy at the transformation are presented in table 2.

Table 2.

Change of thermodynamic parameters at structural transformations of Cu_2Te

T k	$\Delta C_{P\ kal\ mol.k}$	$\Delta H_{Kkal\ mol}$	$\Delta S_{kal/mol}$
433	0.46	0.052	0.12
531	2.85	0.454	0.84
590	2.40	0.232	0.39
633	6.96	0.600	0.95
835	1.46	0.470	0.56

Thermodynamic parameters are not sufficient for the complete explanation of the mechanism of structural transformations in a solid state of substances. Therefore for the complete explanation of structural transformations, it is necessary to take into account also structural parameters of this phenomenon. These questions are successfully solved by the high-temperature roentgenography method. The research of structural transformations in the solid state of substances by this method enables also to establish the connection between general thermodynamic properties and concrete structural characteristics of separate modifications.

Temperature researches were carried out on the diffractometer "DRON-3M", with the prefix for adjustment of the temperature "URVT-2000". The experiments were carried out in vacuum 10^{-1} pa. A condition of the shooting resolution was approximately 0.°. Diffractogramm was written continuously, diffraction corners were determined by the method of measurements on the peak of intensity. The mistake of definition of reflection corners did not exceed the value $\Delta\Theta\pm$ 0.02° at experiments.

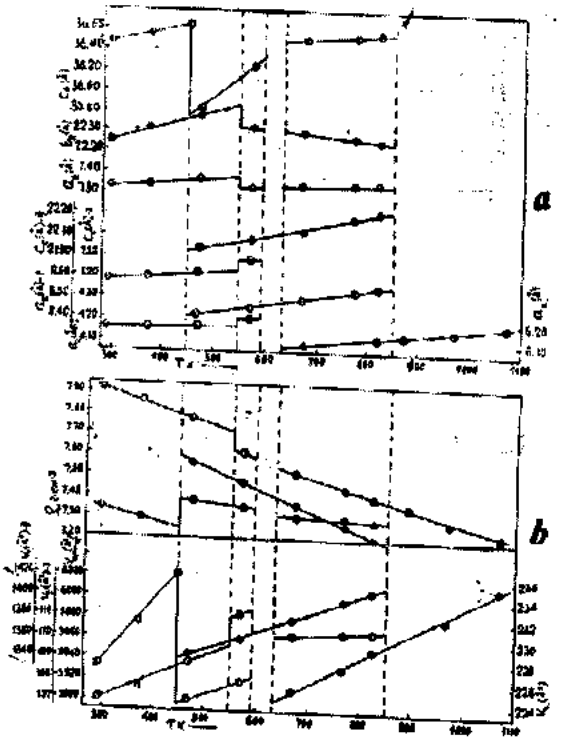

Fig. 2. Temperature dependence of parameters of a crystal lattice on volumes and density (б) of existing modification Cu_2Te.

◒◑◐-parameters of the lattice of the orthorhombic modification

⊙ - parameters of the lattice of the hexagonal-I modification

◐● - parameters of the lattice of the hexagonal -II modification

⊗ - parameters of the lattice of the FCC modification

Records of diffraction reflections from the natural surface of the monocrystal Cu_2Te, (with sizes 4X4X2mm), split on layers of soldering, were carried out in the interval of temperatures 290-1100K, in every 100K.

On the basis of received diffraction data the parameters of the crystal lattice were calculated. Temperature areas of existing modification and results are deduced in the table 3, and are presented on fig. 2. From fig. 2 we can see: a) crystals Cu_2Te in the interval of temperatures 290-418K are biphase and consist of orthorhombic and hexagonal modification, with parameters of lattice a=7.319, b=22.236, c=36.453A and a= 4,1418, c=7,1833A accordingly. b) At 448K the second hexagonal modification from a biphase sample with parameters of the lattice a=8.4191, c=21.8733A. According to fig. 2, formed second hexagonal modification does not influence on parameters of the first hexagonal modification. However at formation of this hexagonal is allocated modification the value of the parameter with the orthorhombic modification sharply reduces Δc=0,72A. It gives us the basis to make the conclusion, that the second hexagonal modification is formed at the expense of the orthorhombic modification. c) At 540K parameters a and c of the first hexagonal modification grow by jump, and parameters a and b of the orthorhombic modification decrease by jump. In this case, probably, cations shifts occur between modification. d) At 590K the orthorhombic and first hexagonal modification turn in to second hexagonal modification and the crystal Cu_2Te becomes single-phase. So far as parameters of the second hexagonal modification don't vary in this case, then it is possible to confirm, that in this process the second hexagonal modification plays a part of the epitaxy. Thus the crystal Cu_2Te becomes single-phase in the interval of temperatures 590-638K. At 638K, with appearance of the reflection from the plane (III) of the high-temperature FCC of modification, the orthorhombic modification restored again. At 848K the orthorhombic and the second hexagonal modification turn into the FCC modification with the parameter of lattice a=6.1140 A.

All above-stated transformations are invertible, and the crystal Cu_2Te comes back to the initial condition at cooling up to the room temperature.

On fig.2 changes of the density and volume of existing modification are shown versus the temperature. As it is seen from fig. 2, at 484K with the formation of the second hexagonal modification the volume of the lattice of the orthorhombic modification reduced on the value ΔV=-72,776A^3 in comparison with the volume at 290K; at 548K as a result of reduction of parameters a and b, volume of the lattice is reduced ΔV =-25,460A^3, and at transformations at 520, 633 and 835K the volume of the lattice of the orthorhombic modification grows by jump: 3,463; 32,886 and 36,378A^3 accordingly. Volume of the elementary cell of the I-hexagonal modification grows linearly up to 548K and at this temperature the sharp growth of parameters a and c occurs with the growth of the volume of the lattice ΔV=1,4A^3, and at 590K ΔV=0,4A^3. In this case the volume of the elementary cell of II-hexagonal modification grows linearly before the transformation in FCC modification (875K).

From dependence of parameters of the lattice of all modifications, thermal expansions on the main crystal directions are calculated, which are deduced in the table 4.

Table 3

Temperature dependences of lattice parameters of modification of the monocrystal Cu_2Te.

Texp. K	Type of lattice	Parameters of lattice			$Z_{элем.ячейки}$	$V(A^3)$	ρ_x gr.cm^{-3}
		a (A)	b (A)	C (A)			
290	Orthorhombic	7,319	22,236	36,458	103	5933,3676	7,336
	Hexagonal-I	4,1481		7,1833			
373	Orthorhombic	7,3294	22,305	36,551	103	5975,4403	7,285
	Hexagonal-I	4,1537		7,1939		107,4861	7,863
473	Orthorhombic	7,3621	22,3663	35,8287	103	5899,659	7,378
	Hexagonal-I	4,1704		7,2225		108,783	7,77
	Hexagonal-II	8,4191		21,8733	24	1342,6522	7,554
573	Orthorhombic	7,3188	22,3099	36,2493	103	5918,8472	7,354
	Hexagonal-I	4,2008		7,276		111,1923	7,601
	Hexagonal-II	8,459		21,9564	24	1357,9858	7,469
590	Hexagonal-II	8,4602		21,9314	24	1359,3945	7,461
673	Orthorhombic	7,3912	22,2831	36,504	103	5963,3614	7,299
	Hexagonal-II	8,4912		22,0623	24	1377,5482	7,256
	FCC	6,0821			4	224,9887	7,513
773	Orthorhombic	7,3421	22,2614	36,542	103	5972,6227	7,288
	Hexagonal-II	8,5342		22,1612	24	1397,7735	7,256
	FCC	6,1021			4	227,2155	7,44
821	Orthorhombic	7,3363	22,2497	36,5636	103	5968,2938	7,293
	Hexagonal-II	8,5533		22,2216		1407,8638	7,204
	FCC	6,1138			4	228,525	7,398
873	FCC	6,1221			4	229,457	7,368
973	FCC	6,1476			4	232,3362	7,277
1073	FCC	6,1731			4	235,2393	7,186

Table 4

Thermal expansions of modification of Cu_2Te crystals.

Cu_2Te	Temperature	$\alpha_{[100]}10^{-6}$degr^{-1}	$\alpha_{[010]}10^{-6}$degr^{-1}	$\alpha_{[001]}10^{-6}$ degr^{-1}	$\alpha=(2\alpha_{[100]}+\alpha_{[001]}10^{-6}$ degr$^{-1})/3$
I-hexagonal	290-373	34,62		17,78	16,77
	290-473	3473		29,59	29,53
	290-573	50,34		45,60	45,18
II- hexagonal	473-573	37,89		37,99	37,92
	473-673	39,52		39,52	39,50
	473-773	45,571		43,874	45,005
	473-821	45,80		45,76	45,77
Orthorhombic	290-373	17,12	37,39	30,73	28,41
	290-473	32,18	32,02	-94,32	-30,12
	290-573	-0,10	11,74	-20,18	-8,54
	290-773	6,54	2,36	4,77	4,56
	290-821	4,45	1,16	5,45	3,69
FCC	673-773	32,883			
	673-821	35,216			
	673-873	32,883			
	673-973	35,898			
	673-1073	37,405			

Coefficient of thermal expansion referred to 290K I-hexagonal modification Cu_2Te, have the certain anisotropy in the interval of temperatures 290 - 590K, whereas for the II-hexagonal modification formed at temperature 448K the anisotropy of thermal expansion (a [100] =a [001]) is absent.

Orthorhombic modification has the sharply expressed anisotropy of thermal expansions.

It is necessary to note, that change of the heat capacity, heat formation, entropy (Fig. 1, a, b, c and tab. 1), results of measurements of parameters of crystal lattices, value of the atomic volume, density (table, 3; fig. 2, a and, b) and coefficients of the thermal expansion of modification of the crystal Cu_2Te at temperatures 290 - 1100K, testify that all five polymorphic transformations are the phase transition of the sort I.

[1] *M. Hansen, K. Anderko.* Constitution of Binary allows. Mc Crow-Hill Book Co. New York, 1958, p.638

[2] *L.Patzak.* Uber die struktur und die Loge der phasen in system kupfertellur., Z.Metaak.47,418,1956

[3] *A.L. Stevels.* Phase transitions in nickel and cooper selenides and tellurides, Philips. Res. Repts, 24,124,1969

[4] *M.U. Tsypin and A.A. Chipizhenko.* The structure and property features of the lowest cuprouse telluride, Izv. AK NAUK, SSSR, Ser. Neorgan. Mater.10,1210,1974

[5] *P. Kubaschewski and I. Nolting.* Spezifische Warmen und thermische Fehlordning von kupferchalkakogeniden tiel 1; Cu_2Se and Cu_2Te bliangerahert stochiometriscer Zusammenzefzung, Ber. Bunsenges, Phys. Chem. 17. 70, 1973.

[6] *H. Gravemann and H. Wallbaura.* Zur kenntnis des Dreistoffsystems Kupfer-Blei-Tellur. Z.metallk., 47, 433, 1956.

[7] *F. Guastavino.* Lugueet and Bougnot, Etude du diagramme de phase du system Cu-Te dans le domaine de la solution solide Cu2-xTe ($0 < X < 16$). Mater. Res. Bull., 8.935,1956.

[8] *J. Bougnot, F. Guastavino, H. Laguet.* Sodini D., Etude du domaine d "existtence de laphase d" du Tellure cuivreux appartir de la conductive electrique/ Mater. Res. Bull. 5,763,1973.

[9] *N. Vouroutzis and Monolikas.* Phase transformations in cuprous telluride. Phis. Stat. Sol., (a), 111,491,1989.

[10] *P.H. Kubaschewski.* Thesis, University of Gottingen. 1969.

F.Y. Əsadov, A.İ. Mövlamverdiyeva, Ş.K. Kazımov, A.Q. Babayev

Cu_2Te MONOKRİSTALINDA QURULUŞ CEVRİLMƏLƏRİNİN TERMODİNAMİK VƏ QURULUŞ ASPEKTİ

Cu_2Te monokristalında 290-1190K temperatur intervalında yüksək temperatur rentgendifraktometrin üsulu ilə quruluş çevrilmələri öyrənilmişdir. Göstərilən temperatur intervalında Cu_2Te kristalında beş struktur çevrilməsi baş verir. Bəzi termodinamik və quruluş parametrlərindən istifadə etməklə quruluş çevrilməsinin mexanizmi aydınlaşdırılmışdır.

Ф.Ю. Асадов, А.И. Мовламвердиева, Ш.К. Казымов, А.Г. Бабаев

ТЕРМОДИНАМИЧЕСКИЕ И СТРУКТУРНЫЕ АСПЕКТЫ СТРУКТУРНЫХ ПРЕВРАЩЕНИЙ В МОНОКРИСТАЛЛЕ Cu_2Te

Высокотемпературным рентгенодифрактометрическим методом исследовались структурные превращения в монокристалле Cu2Te в интервале 290-1100К. В этом температурном интервале в кристалле происходит пять структурных превращений. Пользуясь литературными данными о теплоемкости, теплоте образования и энтропии связанными со структурными переходами и учитывая параметры структуры, выяснен механизм этих превращений.

Received:08.05.01

СОДЕРЖАНИЕ - *Ardu*

FШZШKA 2001 CШLD VII № 2

CONTENTS

CONTENTS - *Ardu*

FIIZIIKA 2001 CIIILD VII № 2